NUMERICAL SIMULATION OF GEYSERING IN NATURAL CIRCULATION LOOP USING DRIFT FLUX MODEL

By

Manas Ranjan Gartia

DEPARTMENT OF NUCLEAR ENGINEERING AND TECHNOLOGY

INDIAN INSTITUTE OF TECHNOLOGY KANPUR

AUGUST, 2003

NUMERICAL SIMULATION OF GEYSERING IN NATURAL CIRCULATION LOOP USING DRIFT FLUX MODEL

A Thesis Submitted

In Partial Fulfillment of the Requirements

for the Degree of

Master of Technology

by

Manas Ranjan Gartia

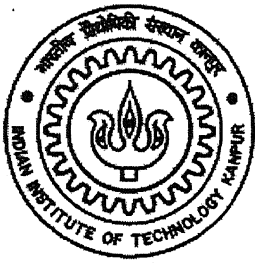

to the

DEPARTMENT OF NUCLEAR ENGINEERING AND TECHNOLOGY

INDIAN INSTITUTE OF TECHNOLOGY KANPUR

INDIA

August 2003

CERTIFICATE

It is certified that the work contained in the thesis entitled "**Numerical Simulation of Geysering in Natural Circulation Loop using Drift Flux Model**" , by Manas Ranjan Gartia, has been carried out under our supervision and that this work has not been submitted elsewhere for a degree.

Ashok Khanna

Dr. A. Khanna
Professor,
Department of Chemical Engineering
Indian Institute of Technology, Kanpur
India.

Dr. P. K. Vijayan
Scientific Officer 'H'
Reactor Engineering Division
Bhabha Atomic Research Centre, Mumbai
India.

Dedicated

to

The Vision of

A

Developed India.

ACKNOWLEDGEMENT

It gives me immense pleasure and satisfaction to express my deep gratitude to Prof. A. Khanna who inspired and encouraged me throughout the period of my M.Tech. thesis with his invaluable guidance and constructive suggestions. The long discussions with him not only enriched my knowledge but also widened my ways of thinking. He has been sympathetic and affectionate in moments of despair.

I would like to express my sincere gratitude to Dr. P. K. Vijayan for many invaluable suggestions, constant encouragement and generous help.

I would like to thank Dr. A. K. Nayak for his timely suggestions and generous help throughout the whole research.

I acknowledge my indebtedness to Mr. GSS Prasad Rao for providing me all experimental data required for the validation of the simulated results.

I am thankful to Prof. M. S. Kalra to help me choosing this particular topic and showing a right path for my future research.

I would like to thank all my NET friends, Vinay, Vivek, Amar, Amit, Rajneesh, Rajit, Sudesh and Suryaprakash for their pleasant company and creating a homely environment during my stay at IIT Kanpur.

I am thankful to all my friends especially Preeti, Ranjan bhai, Suraj bhai, Rajiv, Sachin, Saurabh, Rajat, Pradeep, Kamala for making my stay at IIT Kanpur enjoyable and memorable.

I must use this opportunity to acknowledge my indebtedness to my parents, my elder sister, my younger sister and my uncle who installed the motivation of higher studies and research in me.

Last but not the least I would like to thank BARC for giving me an opportunity to work in a premier research organization and also for providing me financial support during the whole span of my stay at IIT Kanpur.

Manas Ranjan Gartia

Abstract

Geysering is a type of unstable and periodic boiling occurring during start-up. It causes flow oscillations which change the void fractions and reactivity. This makes the nuclear reactor difficult to control. Hence bench-marking of geysering is required. In the present code, a four equation Drift-Flux model has been used for better numerical stability. Each component has been represented one dimensionally with variable cross-sectional area. The equations are solved by a partially implicit finite difference technique that can use different time steps in different components. The components are discretised using staggered mesh arrangements. In the finite difference approximation explicit updating of velocity has been done while pressure calculation has been done implicitly.

At onset of nucleate boiling (ONB), the bubble formation rate has been calculated from the evaporation heat consumed during growth and the latent heat of vaporization. The point at which the bubbles are first detached from the wall (this is OSV: onset of significant void) is determined by the sub cooling of the liquid which is dependent upon the thermal and hydrodynamic condition in the channel. The departure radius of the bubble at this point has been calculated using Unal's semi-empirical model. The growth and condensation behavior of small bubbles are inertia controlled and that of large bubbles are governed by heat transfer at the phase interface. Jacob number has been used to decide whether the flow is inertia dominant or controlled by heat transfer.

Inertia controlled condensation has been estimated by Hamit's correlation. Heat transfer controlled condensation has been calculated using Hainoun et al's model. The model incorporated in this work determines the void fraction in the sub cooled boiling regime. The simulation has been verified by comparing with the McMaster experiments on axial void distribution.

Finally the code has been run and validated for the experimental Apsara Loop at Bhabha Atomic Research Centre. The pressure drop in the single phase leg has been

satisfactorily matched with the experimental data. The simulated void fraction distribution in the two phase leg has been attempted to match with experimental results. But there are still some anomalies while choosing the thermal constraint for the energy equation. The assumptions like thermal equilibrium of the two phases or saturated condition of one of the phases, while considering mixture energy equation, are very crucial to the final solution. Above all a proper boundary condition, proper convergence criteria in the pressure iteration loop and a judicial setting of datum value of void fraction (α_c) is essential in getting a correct solution. The following important observations have been drawn from the present work:

1) The code can simulate the small break LOCA satisfactorily.
2) Inclusion of vapor generation and bubble condensation model was helpful in predicting the geysering phenomenon. The model has been validated with McMaster experimental test results on axial void distribution.
3) The usefulness of the code has been studied for validating the Apsara Loop experimental test data for void fraction in the two phase leg at two locations, pressure drop in the single phase leg and the temperature in the loop at different locations.

Contents

List of Figures

List of Tables

Nomenclature

General

A	Cross-sectional flow area of channel, m^2
a^2	Square of speed of sound for the liquid phase, $(m/s)^2$ [Equation (3.5)]
C	Coefficient of linear term in internal energy function, $kJ/kg\,°K$ [Equation (3.7) (3.8), (3.16), (3.19)]
C_1	Coefficient of quadratic term in internal energy function, $kJ/kg\,°K^2$ [Equation (3.7), (3.8)]
C_d	Drag coefficient in interfacial friction model, m^{-1} [Equation (3.24)]
c_p	Specific heat at constant pressure, $kJ/kg\,K$ [Equation (4.14), (4.15c), (4.22)]
d_h	Hydraulic diameter, m [Equation (2.14), (4.9), (4.13), (4.24)]
E	Constant in internal energy function, kJ/kg [Equation (3.7), (3.8)]
E_r	Heat flux ratio [Equation (4.18), (4.19)]
f	Friction coefficient [Equation (3.10), (3.11a)]
f_1	Local flow loss coefficient, m^{-1} [Equation (3.10)]
f_n	Detachment frequency, s^{-1} [Equation (3.16), (3.17), (3.18)]
f_{vis}	Distributed losses (Pipe wall friction and local losses due to sudden change in area), N/m^3 [Equation (2.3), (2.14), (2.21), (2.28), (2.29), (3.10), (4.3)]
g	Gravitational acceleration, m/s^2

h	Convective heat transfer coefficient, $W/m^2\,K$ [Equation (2.13)]
h_{evap}	Latent heat of vaporization, kJ/kg [Equation (3.13), (3.15), (3.16), (4.21a), (4.21b), (4.22)]
I	Specific internal energy, kJ/kg [Equation (2.4), (2.10), (2.12), (2.34), (2.35), (3.7), (3.8), (3.22), (4.4)]
Ja	Jacob number [Equation (4.22)]
j	Volumetric flux density of mixture, m/s [Equation (2.16)]
j_g	Volumetric flux density of vapor, m/s [Equation (2.18), (2.19)]
j_l	Volumetric flux density of liquid, m/s [Equation (2.17), (2.19)]
K	Momentum exchange function, $kg/m^3\,s$ [Equation (2.4), (2.34), (2.35), (4.4)]
k	Pipe wall roughness, m [Equation (3.11b), (3.11c), (3.11d)]
k_t	Thermal conductivity, $W/m°K$ [Equation (3.14), (3.15), (3.19), (4.9), (4.13), (4.15c)]
N	Number of bubbles per unit volume, m^{-3} [Equation (3.29), (3.30)]
n	Number of bubbles per unit area, m^{-2} [Equation (4.10)]
Nu	Nusselt number [Equation (4.23), (4.24), (4.25), (4.27)]
Pe	Peclet number [Equation (4.13), (4.14)]
Pr	Prandtl number [Equation (3.19), (4.9), (4.27)]
p	Mixture pressure, bar
Q	Heat source term per unit volume, W/m^3 [Equation (2.4), (2.13), (2.34), (2.35), (3.9), (4.4)]
q''	Wall heat flux, W/m^2 [Equation (3.13), (3.14), (4.7), (4.8), (4.16), (4.17), (4.20)]
Re	Reynolds number [Equation (3.17), (3.18), (4.9), (4.26)]
S	Surface area per unit volume of the bubbles, m^{-1} [Equation (3.13), (3.15), (3.27), (3.28)]
T	Temperature, ^0K
t	Time, s

U	Perimeter, m [Equation (4.21b)]
V	Velocity, m/s
V_{bd}	Bubble departure volume, m^3 [Equation (4.16)]
V_{gj}	Drift velocity of vapor, m/s [Equation (2.16), (2.19)]
V_{rs}	Relative speed taking into account turbulent fluctuations, m/s [Equation (3.31), (3.33)]
W_{vis}	Energy dissipation term, W/m^3 [Equation (2.4), (2.34), (2.35), (4.4)]
We_c	Critical Weber Number [Equation (3.31)]
y	Axial distance, m

Greek symbols

α	Void fraction
β	Weighting parameter in "weighted donor cell" difference scheme [Equation (2.45), (2.46), (2.47), (2.48)]
Δ	Change in variable or parameter
Γ_g	Vapor generation rate per unit area, $kg/m^3 s$ [Equation (2.2), (2.25), (3.13), (3.15), (4.1), (4.2), (4.21b)]
Γ_c	Vapor condensation rate per unit volume, $kg/m^3 s$ [Equation (4.1), (4.2), (4.23) (4.24), (4.29)]
γ	Ratio of specific heats, (C_p/C_v) [Equation (3.6)]
μ	Coefficient of dynamic viscosity, $kg/m\ s$ [Equation (1.6), (1.7a), (1.7b), (1.7c), (1.8), (1.9a), (1.9b), (1.9c)]
υ	Kinematic viscosity, m^2/s [Equation (3.24), (3.25), (3.26), (4.23), (4.24), (4.26)]
Φ	Phase

ρ	Mass density, kg/m^3
ψ	Relative velocity effect [Equation (3.12)]
σ	Interfacial Surface Tension, N/m [Equation (3.31)]
τ_c	Condensation time, s [Equation (4.30)]

Subscripts

a	Ambient condition
b	Bubble
bd	Bubble departure
c	Condensation
ch	Channel
eff	Effective
evap	Evaporation
GV	Generating void
g	Vapor
h	Hydraulic
he	Heated
l	Liquid
m	Mixture
nt	Nontranslating
0	Ambient condition
osv	Onset of significant void
r	Relative
recons	Reconstruction
s	Saturation
sub	Sub-cooling

sup	Superheating
TP	Two phase
t	Translating
w	Wall
y	Axial direction

Superscript

0	Pure quantities

Chapter 1

Introduction

1.1 Natural Circulation Loop

In a natural circulation loop the circulating fluid removes the heat from a heat source and transports it to heat sink, the fluid circulation being established due to the buoyancy force. The buoyancy force is the driving force. Buoyancy force is result of thermally induced density differences in a gravitational field. The heat sink is located at a higher elevation than the heat source. Such loops find application in many engineering fields such as, gas turbine blade cooling, solar water heater, geothermal systems, electrical machine rotor cooling, transformer cooling, nuclear reactor core cooling etc.

Present generation reactors like the Light Water Reactors (LWRs) and PHWR (Pressurized Heavy Water Reactors) utilize forced circulation loops for heat transfer from core to the steam generator. But this method has the following disadvantages:

1) Usage of pump is costly
2) If pump break down occurs then dissipation of fission heat is hampered. This results in tremendous accumulation of heat and may cause core melt down in the reactor. There are many examples of nuclear accidents due to core melt down like the Three Mile Island Unit-2 (1979) , Chernobyl (1986) and some less significant melting events like EBR-1 (National Reactor Testing Station, Idaho, USA, 1951), Windscale (now Sellafield, England, 1957), Lucens (Switzerland, 1969) and St. Laurent (France, 1969).
3) Back up safety measures have to be used.

Hence next generation of boiling water reactors should have natural circulation of primary coolant under normal operational situations. Figure1.1 shows the schematic diagram of a two-phase natural circulation loop. The loop essentially consists of a tubular heated section, a riser, a steam drum or a separator, a condenser, a down comer, and upper- lower horizontal sections. The steam collected in separator or steam drum goes to the condenser, where it is condensed and then sent back to the separator. This loop differs from forced circulation loop only by the absence of pump.

In a two-phase natural circulation loop since heat is removed by natural circulation, it is inherently safe. This method of cooling enhances passive safety.

Many proposed advanced designs of nuclear power reactors use two-phase natural circulation of primary coolants. However a major problem with these loops is the occurrence of flow instabilities. Flow instabilities are undesirable in boiling, condensing and other two-phase flow systems for several reasons.

1.2 Boussinesq Approximation

In natural convection flows, the basic driving force arises from the temperature or concentration field. The temperature variation results in a difference in density. This in turn results in a buoyancy force due to the presence of the body force field. For a gravitational field, the body force $\overline{F} = \rho\overline{g}$, where, $\overline{g}$ is the force per unit mass of the fluid. It is the variation of ρ that gives rise to the flow and if this variation were to be neglected, no flow would result. The temperature field (energy equation) is linked with the flow and all of the equations, mass balance, momentum balance and energy balance, are coupled through the variation of the density ρ. Therefore, these equations have to be solved simultaneously to give the distributions, in space and time, of the velocity, pressure and temperature fields. Due to this added complexity in the analysis of flow, several simplifying assumptions and approximations are made in natural convection, to allow a more convenient procedure for obtaining a solution to the Navier-Stokes equation.

In the momentum equation, the local static pressure p may be broken down into two terms, one due to hydrostatic pressure, p_a and the other due to the motion of the fluid, p_d. The former coupled with the body force acting on the fluid constitutes the driving mechanism for the flow.

$$p = p_a + p_d \tag{1.1}$$

The pressure p_a is the hydrostatic pressure in the ambient medium. Therefore, for a gravitational field, it is given as, $\nabla p_a = \rho_a \bar{g}$, where $\bar{g}$ is the force due to gravity per unit mass of the fluid and ρ_a is the density of the ambient fluid. Considering, for simplicity, an isothermal flat vertical surface at temperature T_S and immersed in an isothermal ambient medium T_a. The driving buoyancy force for the vertical flow arises due to the difference between the body force and the force due to the hydrostatic pressure gradient in the ambient medium. This implies that the driving force per unit volume of the fluid is $g(\rho_a - \rho)$. If this force acts over a vertical distance y and if the energy thus added is equated to the kinetic energy per unit volume, we have, $\frac{\rho V_y^{\,2}}{2} = gy(\rho_a - \rho)$

Since the viscous forces have been neglected here and only the driving force has been considered, the above estimate of V_y is the maximum value that may be expected in the flow. Considering an inviscid flow over the vertical surface, Bernoulli's equation may be applied to estimate the order of magnitude of the pressure difference in the flow. If p_a is the pressure in the ambient medium and p is the pressure at a location in the boundary layer, the value of $(p_a - p)$ may be determined, knowing that the velocity in the ambient medium is zero. Therefore,

$$p_a - p = \frac{\rho V_y^{\,2}}{2} \tag{1.2}$$

and $p_a - p \approx o[gy(\rho_a - \rho)]$

$$V_y \approx o\left[\sqrt{\frac{2gy}{\rho}(\rho_a - \rho)}\right] \tag{1.3}$$

Hence it is now necessary to determine the density difference in terms of the temperature and pressure in the flow.

If the density of the fluid ρ is a function of the pressure and temperature, the density at a given point in the flow, $\rho(p,T)$, may be written in terms of the density $\rho_a(p_a,T_a)$, in the ambient medium, as a double Taylor series expansion about the ambient conditions.
This may be given as follows:

$$\rho_a = \rho + \left(\frac{\partial\rho}{\partial T}\right)_P (T_a - T) + \frac{1}{2!}\left(\frac{\partial^2\rho}{\partial T^2}\right)_P (T_a - T)^2 + \ldots\ldots\ldots$$

$$+\left(\frac{\partial\rho}{\partial p}\right)_T (p_a - p) + \frac{1}{2!}\left(\frac{\partial^2\rho}{\partial p^2}\right)_T (p_a - p)^2 + \ldots\ldots\ldots$$

$$+\frac{\partial^2\rho}{\partial p\partial T}(p_a - p)(T_a - T) + \ldots\ldots\ldots \tag{1.4}$$

Now the coefficient of thermal volumetric expansion β is given by

$$\beta = -\frac{1}{\rho}\left(\frac{\partial\rho}{\partial T}\right)_P$$

and, $p_a - p \approx o[gy(\rho_a - \rho)]$ is the estimate of the maximum pressure difference. Therefore,

$$\rho_a - \rho = \rho\beta(T - T_a) + \frac{\rho\beta^2}{2!}(T - T_a)^2 + \ldots\ldots$$

$$+\left(\frac{\partial\rho}{\partial p}\right)_T [gy(\rho_a - \rho)] + \frac{1}{2!}\left(\frac{\partial^2\rho}{\partial p^2}\right)_T [gy(\rho_a - \rho)]^2 + \ldots\ldots$$

$$+\frac{\partial^2\rho}{\partial p\partial T}[gy(\rho_a - \rho)(T_a - T)] + \ldots\ldots \tag{1.5}$$

In the first series, the leading term is $\rho\beta(T - T_a)$

The second term is $\frac{\rho\beta^2}{2!}(T - T_a)^2$

Hence the nth term will be $\frac{\rho\beta^n}{n!}(T-T_a)^n$

The series will be convergent when $[\beta(T-T_a)]<1$ and if $[\beta(T-T_a)]<<1$, then only the first term of the series may be retained.

If $\left[\left(\frac{\partial\rho}{\partial p}\right)_T gy\right]<<1$, then the second series may be neglected. Similarly, $\left[\left(\frac{\partial\rho}{\partial p}\right)_T gy\right]$ and $[\beta(T-T_a)]$ must both be much less than unity to neglect the third series.

Therefore, if $[\beta(T-T_a)]<<1$ and $\left[\left(\frac{\partial\rho}{\partial p}\right)_T gy\right]<<1$ then the density difference may be estimated as: $\rho_a-\rho=\rho\beta(T-T_a)$

General momentum equation for natural convection:

$$\rho\frac{D\overline{V}}{Dt}=\overline{F}-\nabla p+\mu\nabla^2\overline{V}+\frac{\mu}{3}\nabla\left(\nabla\cdot\overline{V}\right) \tag{1.6}$$

where the operator $\frac{\mathbf{D}}{\mathbf{Dt}}$ represents the substantial or particle derivative and given by

$$\frac{D}{Dt}=\frac{\partial}{\partial t}+V_x\frac{\partial}{\partial x}+V_y\frac{\partial}{\partial y}+V_z\frac{\partial}{\partial z}$$

$\overline{\mathbf{V}}$ = Velocity vector = $iV_x+jV_y+kV_z$

$\overline{\mathbf{F}}$ = Body force per unit volume = $iF_x+jF_y+kF_z$

∇ = Vector Operator Del = $i\frac{\partial}{\partial x}+j\frac{\partial}{\partial y}+k\frac{\partial}{\partial z}$

μ = Coefficient of viscosity (dynamic viscosity) of the fluid

The shear stresses and normal stresses are related as follows:

$$\tau_{xy}=\mu\left(\frac{\partial V_x}{\partial y}+\frac{\partial V_y}{\partial x}\right)=\tau_{yx} \tag{1.7a}$$

$$\tau_{yz} = \mu\left(\frac{\partial V_y}{\partial z} + \frac{\partial V_z}{\partial y}\right) = \tau_{zy} \tag{1.7b}$$

$$\tau_{xz} = \mu\left(\frac{\partial V_x}{\partial z} + \frac{\partial V_z}{\partial x}\right) = \tau_{zx} \tag{1.7c}$$

$$\text{Normal stress}, \sigma_{xx} = -p + 2\mu\frac{\partial V_x}{\partial x} + \lambda\nabla\cdot\overline{V} \tag{1.8}$$

For an incompressible fluid, with constant density, $\nabla\cdot\overline{\mathbf{V}} = 0$ and therefore,

$$\sigma_{xx} = -p + 2\mu\frac{\partial V_x}{\partial x} \tag{1.9a}$$

$$\sigma_{yy} = -p + 2\mu\frac{\partial V_y}{\partial y} \tag{1.9b}$$

$$\sigma_{zz} = -p + 2\mu\frac{\partial V_z}{\partial z} \tag{1.9c}$$

λ is known as the second coefficient of viscosity and for variable density and monatomic gas it is given by, $\lambda = -\frac{2}{3}\mu$ .Here , $\mu\nabla^2\overline{\mathbf{V}} + \frac{\mu}{3}\nabla\left(\nabla\cdot\overline{\mathbf{V}}\right)$ represents the viscous dissipation term culminating from shear stresses and normal stresses.

Neglecting the viscous dissipation term, for a gravitational field, the body force $\overline{\mathbf{F}} = \rho\overline{g}$

Where $\overline{g}$ is the force per unit mass of the fluid (acceleration due to gravity).

Local static pressure $p = p_a + p_d$ (1.10)

p_a = Hydrostatic pressure in the ambient medium

p_d = Dynamic component of pressure due to the flow of fluid

For a gravitational field, $\nabla p_a = \rho_a\overline{g}$

$$\text{Or,} \qquad p_a = \rho_a g y \tag{1.11}$$

From the momentum equation:

$$\overline{\mathbf{F}} - \nabla p = \rho\overline{g} - \nabla\left(p_a + p_d\right)$$

$$= (\rho\bar{g} - \nabla p_a) - \nabla p_d$$

$$= (\rho\bar{g} - \rho_a\bar{g}) - \nabla p_d = (\rho - \rho_a)\bar{g} - \nabla p_d \quad (1.12)$$

If $\bar{g}$ is downwards and y-direction upwards, as is the generally case for vertical buoyant flows, $\bar{g} = -\hat{j}g$, and hence

$$\bar{\mathbf{F}} - \nabla p = (\rho_a - \rho)g\hat{j} - \nabla \tilde{p}_d \quad (1.13)$$

where $\hat{j}$ is the unit vector in y-direction and "g" is the magnitude of the gravitational force, per unit mass of the fluid (acceleration due to gravity). For $\bar{g}$ at an angle θ with the y-direction, the term, therefore, becomes $(\rho_a - \rho)g\cos\theta$ in the y-direction and $(\rho_a - \rho)g\sin\theta$ in the x, or horizontal direction.

In Cartesian co-ordinates it becomes: $-\rho g - \frac{\partial p}{\partial y} = (\rho_a - \rho)g - \frac{\partial p_d}{\partial y}$

$$= (\rho_a - \rho)g - \frac{\partial(p - p_a)}{\partial y} \quad (1.14)$$

But $\rho_a - \rho = \rho\beta(T - T_a)$ (1.15)

Hence, $-\rho g - \frac{\partial p}{\partial y} = \rho g\beta(T - T_a) - \frac{\partial(p - p_a)}{\partial y}$ (1.16)

1.3 Classification of Flow Instabilities

Flow instability phenomena can be classified on the basis of following definitions:
A steady flow is one in which the system parameters are functions of the space variables only. Practically, however, they undergo small fluctuations due to turbulence, nucleation, or slug flow. These fluctuations play a role in triggering several instability phenomena.

A flow is stable if, when momentarily disturbed, its new operating conditions tend asymptotically towards the initial ones. The various parameters that may affect the stability and can lead to instabilities are:
Geometry-which includes channel length, channel diameter, inlet and outlet restrictions, single or multiple channels,

Operating conditions- such as pressure, inlet sub cooling, mass velocity, power input, forced or natural circulation,

Boundary conditions- like axial heat flux distribution, pressure drop across the channels.

Boure *et al* [1973] divided these instabilities into two classes: static instability and dynamic instability.

Static instability is one where a small change in one of the independent variables leads to a large change in one of the dependent variables. A static instability can lead either to a different steady state condition or to a periodic behavior. Static instabilities can be described by steady state equilibrium also. Examples of static instability are listed below:

Flow regime transition: Cyclic flow pattern transitions and flow pattern variation occurs.

Boiling crisis: Bubbly flow has less void but higher pressure drop than that of annular flow characterized by the ineffective removal of heat from the heated surface, leads to wall temperature excursion and flow oscillation.

The Ledinegg instability or flow excursion instability: Flow undergoes sudden, large amplitude excursion to a new, stable operating condition, due to the internal pressure gradient being less than the external pressure gradient (imposed by the pump).

Geysering: an erratic boiling region exists, where the wall temperature moves between boiling and natural circulation in irregular cycles, due to the presence of gas; effect disappears at higher heat fluxes and higher pressures.

Dynamic instability: a flow is subjected to dynamic instability when inertia and other feedback effects have an essential part in the process. Examples of dynamic instabilities are listed below:

Density wave oscillations: Occur due to delay and feedback effects between flow rate, density and Δp.

Pressure drop oscillations: These oscillations occur due to dynamic interaction between channel and the compressible volume, which is initiated by flow excursions.

Acoustic oscillations: These are high frequency (10-100 Hz) oscillations related to time required for pressure wave propagation; occurs due to resonance of pressure waves.

Thermal oscillations: These oscillations occur in film boiling due to interaction of variable heat transfer coefficients with flow dynamics.

BWR instability: It is strong only for small fuel time constant and under low pressures; occurs due to interaction of void reactivity coupling with flow dynamics and heat transfer.
Parallel channel instability: there are various modes of flow redistribution; occurs due to interaction between small numbers of parallel channels.

The present work analyses geysering instability.

1.4 Geysering

1.4.1 A Brief Description

The concept of geysering has evolved from the natural geyser. The mechanism of geysering was first described by Bunsen [1958]. He described the mechanism as follows:

"If heat is added to a column of liquid which opens into a chamber of larger diameter, then it will ultimately rise to slightly above it's saturation temperature. When this occurs, bubbles will form. Due to this bubble formation remaining liquid in the column will experience a decrease in hydrostatic pressure at a virtually constant temperature. Consequently more bubbles will form, further reducing the pressure, and ultimately much of the liquid in the column will be blown out. This phenomenon of blowing out is known as geysering".

Griffith [1962] suggested that two mechanisms, rather than the one given by Bunsen, could lead to geysering. The two mechanisms proposed by him are as follows:
(1) Some amount of superheat in the liquid is required to nucleate a bubble. The superheat is often very large so that when a bubble forms, it grows very rapidly and often ejects most of the liquid which lies above it. In a nut shell, rapid growth of the bubbles is mainly responsible for geysering.
(2) The second theory says that, even when the liquid is in a local saturation state then also some amount of bubbles will form and eventually lead to geysering. But disturbance of any size will not lead to geysering. For example, if the bubble formed grows slowly enough (small disturbance) such that it rises out of the column before any other can get started, then geysering may not occur at all. In other words, the decrease in pressure due to the formation of bubble should be large enough to form another bubble to start geysering.

Earlier researchers mostly concentrated on superheated liquid and saturated liquid for geysering. But early nineties experiments show that geysering also occurs at low pressures and low flows condition. The concern for possibility of geysering or condensation induced instability during start up from low pressure and low flow conditions in a natural circulation plant like SBWR (Simplified Boiling Water Reactor) was first raised by Aritomi *et al.*,[1992]. Then researchers shifted their attention towards sub-cooled liquid. The mechanism of geysering has been modified as follows:

"Even though the bulk liquid is sub-cooled, the bubble at the vicinity of the fuel rod is superheated. Hence void will generate at some nucleating sites. At low flow rates and low pressure, the vapor bubbles produced in the heated channel will coalesce into a larger bubble. This will further grow due to decrease in hydrostatic pressure. This bubble will move towards the exit as its density is lower than the liquid. As the bulk liquid is still sub-cooled, the bubble will come in contact with the sub-cooled liquid and condense rapidly. Then due to collapse of bubble, pressure will drop suddenly. In order to balance this pressure drop, the sub-cooled liquid from the top will flow into the channel. Thus a flow reversal is induced. This process repeats periodically causing flow oscillation which is known as geysering". [Aritomi *et al.*, 1992]

1.4.2 Its Importance

Natural circulation systems require power to initiate the circulation through void generation. This means the natural circulation reactor would be heated by fission energy from the startup under low temperature and low pressure condition. Thermal hydraulic instabilities have been reported under low pressure conditions [Chiang *et al.*, 1994]. If thermal hydraulic instabilities were to occur at startup then the reactor would not continue operation during increase of power because the void fraction fluctuation in the reactor core would oscillate the reactivity. Therefore it is necessary to investigate and understand properly the role of reactivity during start up.

1.4.3 Interaction with Reactivity

Reactivity is defined as the relative departure of neutron production factor (K_∞) from unity,

that is, Reactivity $= \dfrac{Neutron\ Production\ Rate - Neutron\ Removal\ Rate}{Neutron\ Production\ Rate}$

$$\text{Mathematically, } \rho = \frac{K_\infty - 1}{K_\infty}$$

Neutron is required for the fission of nuclear fuel (say U^{235}). From every fission reaction, at an average 2.5 neutrons are evolved. If all the evolved neutrons react then the fission chain reaction will become uncontrollable. So we should allow only one neutron to react. That is we should make the reactor critical. But in actual practice the reactor is made slightly supercritical i.e. $\rho = 1.01$ to ensure that reactor remains critical, since in the reaction process some neutrons usually get lost. On the other hand if $\rho < 1$ then the number of neutrons available for the reaction will not be sufficient to move forward the chain reaction. Hence the reaction will die down and ultimately the reactor will stop.

Hence, in a way reactivity can be used to control the reactor. As reactivity depends upon temperature and there is a mutual dependence between temperature and void fraction, a slight variation in void fraction would oscillate the reactivity. This makes the reactor difficult to control.

1.4.4 Further Advances

Aritomi *et al.* [1992, 1993] and Chiang *et al.* [1992, 1994] have conducted extensive research in the area of geysering under natural circulation. Inada *et al.* [1992] and Masuhara *et al.* [1993] have also performed small scale experiments to demonstrate this phenomenon. These experiments illustrated that the geysering mode oscillation would occur at low pressures and low flow conditions.

Earlier attempts to model startup instabilities [Aritomi *et al.*, 1992] and [Paniagua *et al.*, 1996] indicate that, to predict the possible startup instabilities correctly, it is important to accurately predict the vapor generation rate. In the present code a four equation drift flux

model has been used which is numerically more stable than the five equation and six equation model. Moreover, most of the models are envisaged for system with high pressures (greater than 20 bars) and thus are unsuitable for the simulation of geysering owing to the great influence of pressure on the void content in the sub-cooled boiling regime. Finally in the existing models there is no conclusive and physically well-defined description of mass transfer rate between the vapor and liquid phase, an aspect which is of great significance for understanding the sub-cooled boiling regime. In the present code the effect of the bubble formation as well as the condensation rate has been considered.

1.5 Objective of the present work

To study the two-phase flow phenomena, one can use various models such as Homogeneous Equilibrium Model (HEM), Drift flux model or a six-equation (two-fluid) model. HEM model assumes both the phases are in thermodynamic and mechanical equilibrium, i.e. they have same velocity and temperature. But geysering is a highly non-equilibrium phenomena because it considers growth of bubble due to sub-cooled boiling and its condensation in sub-cooled water in riser. So a HEM model cannot address this problem. Also in homogeneous model relative velocity between vapor and liquid is not considered. However, in two-phase flow there is always a relative motion between the liquid and vapor phase.

The two-fluid models are the most robust and accurate. But their accuracies depend on the interfacial relationships for mass, energy and momentum transfer. The codes developed for these phenomenon, use empirical relationships which are not well established and they are continuously being upgraded with time. The second problem with two-fluid models is the use of single pressure for both the phases. This means that the velocity of sound in both the medium (liquid and vapor) will be equal. This makes the equations mathematically ill-posed. To avoid this problem, many codes use a numerical scheme to suppress the numerical instability. However, by this way, the codes miss the physical instability because the numerical scheme so used tries to damp the physical oscillation also.

The remaining possibility is the drift flux model. Its accuracy is better than a Homogeneous Equilibrium Model but lower than the two-fluid models. Because it considers the dynamic phasic slip between the phases by taking into account the vapor drift velocity (V_{gj}) in the two-phase region. Earlier some codes based on drift flux model have been developed [RETRAN, ATHLET]. But these codes are applicable to forced circulation loop only. Also ATHLET code uses a five equation system that uses separate mass and energy conservation equations for steam and water, and a single mixture momentum conservation equation.[A.Hainoun *et al.*,1996] This makes the system physically ill-posed as it has considered separate masses and velocities for steam and water, but still a single momentum for both the phases.

In the present work a four equation drift flux model has been considered. It is more stable than the five and six equation models as described before. Most of the times one uses a semi implicit-explicit scheme which is better than the explicit scheme so far as time step is concerned and implicit scheme so far as numerical oscillations are concerned. Further the equations are mathematically well posed. The objective of this thesis is to develop and validate a code based on four equation drift flux model incorporating natural circulation loop features and with the proper consideration of vapor generation and vapor condensation model.

1.6 Organisation of the present work

The thesis is organized as follows:

Chapter 1 gives a general introduction about the geysering phenomena and the literature survey.

Chapter 2 describes the basis of Drift Flux model formulation with discretization equations and the Boussinesq approximation for the natural circulation loop.

Chapter 3 deals with the simulation of small break LOCA using the two-phase code.

Chapter 4 presents void generation and condensation model along with the McMaster experiment validation results.

Chapter 5 deals with the validation of the code with the Apsara Loop experimental data obtained from Bhabha Atomic Research Centre (BARC), Mumbai.

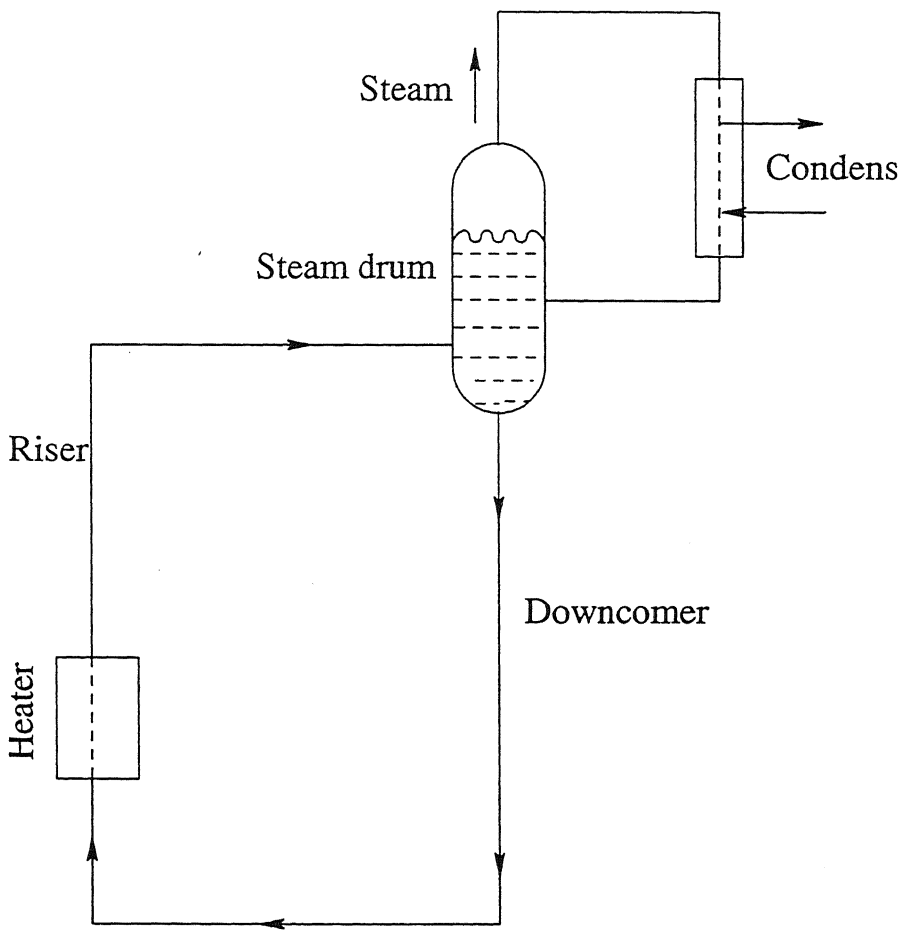

Figure 1.1: Schematic of Natural Circulation Loop.

Chapter 2

The Drift Flux Model

2.1 Drift Flux Formulation

2.1.1 Governing Equations

The Drift Flux model has been widely used for vertical flows in pipes and allows for slip between the phases and for a non-homogeneous distribution of the phases in a cross section. The basic model is due to Zuber and Findlay [1965] and contains elements of models by Wallis and by Bankoff [1960]. Its chief purpose is to provide a mechanistic framework for the calculation of the vapor void fraction α_g.

The drift-flux model for a two-phase mixture consists of two mass conservation equations, one momentum conservation equation, and one internal energy equation [Ishii, 1975]. Here the following form of these four partial differential equations has been used:

Total mass balance equation:

$$\frac{\partial \rho_m}{\partial t} + \frac{1}{A}\frac{\partial (A \rho_m V_m)}{\partial y} = 0 \tag{2.1}$$

Vapor mass balance equation:

$$\frac{\partial \rho_g}{\partial t} + \frac{1}{A}\frac{\partial}{\partial y} A\left(\rho_g V_m + \frac{\rho_g \rho_l}{\rho_m} V_r \right) = \Gamma_g \tag{2.2}$$

Mixture momentum balance equation:

$$\frac{\partial \rho_m V_m}{\partial t} + \frac{1}{A}\frac{\partial}{\partial y} A\left(\rho_m V_m^{\,2} + \frac{\rho_g \rho_l}{\rho_m} V_r^{\,2} \right) = -\frac{\partial p}{\partial y} + \rho_m g_y + f_{vis} \tag{2.3}$$

Mixture energy balance equation:

$$\frac{\partial \rho_m I_m}{\partial t} + \frac{1}{A}\frac{\partial}{\partial y} A\left[\rho_m I_m V_m + \frac{\rho_g \rho_l}{\rho_m}(I_g - I_l) V_r \right] = -\frac{p}{A}\frac{\partial}{\partial y} A\left[V_m + \frac{\rho_g \rho_l}{\rho_m}\left(\frac{1}{\rho_g^{\,0}} - \frac{1}{\rho_l^{\,0}} \right) V_r \right]$$

$$+ K V_r^{\,2} + W_{vis} + Q \tag{2.4}$$

The above four equations have been written using seventeen variables. The gravitational term g_y is a function of independent variable y only and does not depend on the state variables. Hence assuming that g_y is known from the geometrical configuration of the particular system under study, we must therefore specify twelve additional relationships among these variables. Two relationships may be obtained from basic definitions of mixture quantities. These definitions are:

1. Definition of ρ_m:

$$\rho_m = \alpha \rho_g^{\,0} + (1-\alpha)\rho_l^{\,0} = \rho_g + \rho_l \tag{2.5}$$

2. Definition of I_m:

$$I_m = \frac{\alpha \rho_g^{\,0} I_g + (1-\alpha)\rho_l^{\,0} I_l}{\rho_m} \tag{2.6}$$

2.1.2 Constitutive Equations

The ten additional relationships needed for the description of two phase system are referred to as constitutive equations. A general form of each of these equations is presented below:

1. *Thermal equation of state for the liquid:*

$$\rho_l = \rho_l(p, I_l) \tag{2.7}$$

This relationship must apply for a superheated as well as a sub-cooled liquid.

2. *Thermal equation of state for the vapor:*

$$\rho_g = \rho_g(p, I_g) \tag{2.8}$$

This relationship must apply for both superheated and sub-cooled vapor.

3. *Caloric equation of state for the liquid:*

$$T_l = T_l(p, I_l) \tag{2.9}$$

This has been assumed that this relationship can be inverted to obtain

$$I_l = I_l(p, T_l) \tag{2.10}$$

4. *Caloric equation of state for the vapor:*

$$T_g = T_g(p, I_g) \tag{2.11}$$

We again assume inversion is possible, yielding

$$I_g = I_g(p, T_g) \tag{2.12}$$

5. *Wall heat source:* The heat source term in the energy equation is assumed to be of the form

$$Q = hA_w(T_w - T_f) \tag{2.13}$$

where A_w is the wall area, T_w is the wall temperature, and T_f is the fluid temperature, possibly equals to T_l or T_g or some average temperature. The heat transfer coefficient h is obtained from correlations involving the fluid properties and the wall temperatures.

6. *Wall friction:*

$$f_{vis} = c\left(\frac{\rho_m V_m |V_m|}{2d_h}\right) \tag{2.14}$$

where d_h is the hydraulic diameter and c is a friction multiplier depending strongly upon the void fraction α and other fluid properties.

7. *Relative velocity correlation:* We assume the existence of a relationship specifying the relative velocity in terms of other state variables. This relationship will usually be strongly dependent on an assumed flow topology.

8. *Rate of phase change:* The rate of phase change Γ_g must be specified as a function of other variables. Various models employing equilibrium or non-equilibrium assumptions are possible.

9. *Saturation curve:* A saturation curve of the form

$$T_s = T_s(p) \tag{2.15}$$

must be specified. The saturation temperature provided by this curve enters the phase change expression above.

10. *A thermal constraint:* The drift-flux model equations provide only a single mixture energy equation for the two specific internal energies I_g and I_l. Hence, an additional thermal constraint is necessary to partition the mixture energy into the liquid and vapor phases. A variety of such constraints is possible, the simplest of which is thermal equilibrium between phases. Another possibility is the assumption that either the vapor or the liquid is at saturation, depending upon whether vaporization or condensation is occurring.

2.2 Drift Velocity

The vapor drift velocity (V_{gj}) is the velocity of the vapor phase with respect to the velocity of center of volume or volumetric flux density of mixture.

Mathematically,

$$V_{gj} = V_g - j \tag{2.16}$$

where j is the volumetric flux density of mixture.

The mean volumetric flux density, or the superficial velocity, of each phase is defined as the volumetric flow rate of that phase divided by the total cross-sectional flow area.

$$j_l = \frac{Q_l}{A_l + A_g} \quad \text{But} Q_l = A_l V_l, \quad j_l = \frac{A_l V_l}{A_l + A_g} = (1-\alpha)V_l \tag{2.17}$$

$$\text{Similarly } j_g = \frac{Q_g}{A_l + A_g} = \frac{A_g V_g}{A_l + A_g} = \alpha V_g \tag{2.18}$$

The mixture volumetric flux density will be given by:

$$j = j_l + j_g = (1-\alpha)V_l + \alpha V_g \tag{2.19}$$

Now, $V_{gj} = V_g - j = V_g - \{(1-\alpha)V_l + \alpha V_g\}$

$$= (1-\alpha)(V_g - V_l) = (1-\alpha)V_r \tag{2.20}$$

where V_r is the relative velocity of vapor with respect to the liquid phase.

2.3 The Finite Difference Scheme

The convective terms in equations (2.1)-(2.4) have been written in a divergence or conservation form. Because there are large sources and sinks of momentum in a nuclear reactor (pumps, orifice etc.), it has not been attempted to ensure that the difference scheme be rigorously conservative in the treatment of momentum convection. Therefore, equation (2.3) has been rewritten in a nonconservative form that is more convenient for our applications. Multiplying equation (2.1) by V_m and subtracting from equation (2.3) yields the equation

$$\frac{\partial V_m}{\partial t} + V_m \frac{\partial V_m}{\partial y} + \frac{1}{\rho_m A}\frac{\partial}{\partial y}\left(\frac{A\rho_g \rho_l}{\rho_m} V_r^{\,2}\right) = -\frac{1}{\rho_m}\frac{\partial p}{\partial y} + g_y + \frac{1}{\rho_m} f_{vis} \tag{2.21}$$

The advantage of using equation (2.21) over equation (2.3) is that V^{n+1} rather than $(\rho V)^{n+1}$, is calculated directly. Its disadvantage is that it is not in conservation form, so we do not get rigorous conservation of momentum in the difference approximation. However, when the percentage changes in dependent variables from one cell to the next cell are not large, the nonconservation form of the momentum equation should not cause any problems. Equations (2.1), (2.2), (2.4) and (2.21) have been used throughout the following analysis.

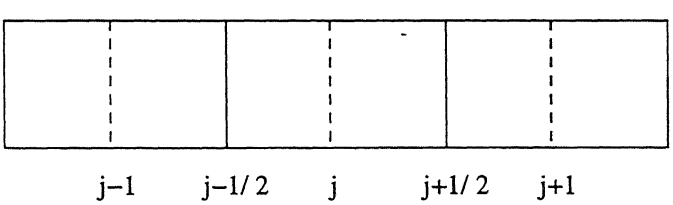

Figure 2.1: Mesh cell labeling convention.

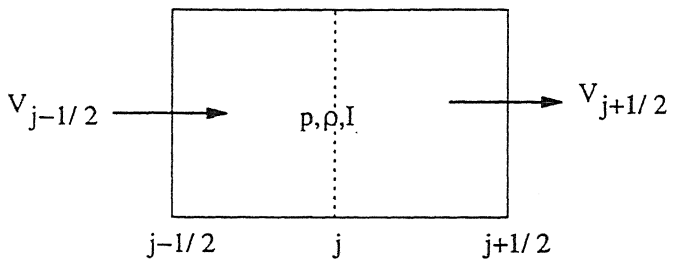

Figure 2.2: Mesh variables inside a computational cell.

The mesh cell configuration and the labeling conventions for cell edges and cell centers are depicted in the above figures. The mass and energy equations are differenced over the mesh cells indicated by solid lines in Figure 2.1; the momentum equation is differenced over the dashed mesh cells. This forms a staggered spatial difference scheme. For finding the relationships among the variables at the edges and center of mesh cells, a "weighted donor cell" difference scheme has been used. The resulting difference equations are given below.

From equation (2.1) the mixture density is updated as:

$$(\rho_m)_j^{n+1} = (\rho_m)_j^n - \frac{\Delta t}{A_j \Delta y_j}\left[A_{j+\frac{1}{2}}(\rho_m V_m)_{j+\frac{1}{2}} - A_{j-\frac{1}{2}}(\rho_m V_m)_{j-\frac{1}{2}}\right] \tag{2.22}$$

where

$$(\rho_m V_m)_{j+\frac{1}{2}} = \frac{1}{2}\left[(V_m)_j\{(\rho_m)_j + (\rho_m)_{j+1}\} + \beta\left|(V_m)_j\right|\{(\rho_m)_j - (\rho_m)_{j+1}\}\right] \tag{2.23}$$

$$(\rho_m V_m)_{j-\frac{1}{2}} = \frac{1}{2}\left[(V_m)_{j-1}\{(\rho_m)_{j-1} + (\rho_m)_j\} + \beta\left|(V_m)_{j-1}\right|\{(\rho_m)_{j-1} - (\rho_m)_j\}\right] \tag{2.24}$$

Quantities on the right hand side of equation (2.22) are evaluated using n level values for ρ_m and the available $n+1$ level values of V_m.

Vapor density is updated from equation (2.2) as given below:

$$(\rho_g)_j^{n+1} = (\rho_g)_j^n + \Delta t\left\{-\frac{1}{A_j \Delta y_j}\left[A_{j+\frac{1}{2}}(\rho_g V_g)_{j+\frac{1}{2}} - A_{j-\frac{1}{2}}(\rho_g V_g)_{j-\frac{1}{2}}\right] + (\Gamma_g)_j\right\} \tag{2.25}$$

where

$$(\rho_g V_g)_{j+\frac{1}{2}} = \frac{1}{2}\left[(V_g)_j\{(\rho_g)_j + (\rho_g)_{j+1}\} + \beta\left|(V_g)_j\right|\{(\rho_g)_j - (\rho_g)_{j+1}\}\right] \tag{2.26}$$

$$(\rho_g V_g)_{j-\frac{1}{2}} = \frac{1}{2}\left[(V_g)_{j-1}\{(\rho_g)_{j-1} + (\rho_g)_j\} + \beta\left|(V_g)_{j-1}\right|\{(\rho_g)_{j-1} - (\rho_g)_j\}\right] \tag{2.27}$$

Quantities on the right hand side of equation (2.25) are updated using n level values of $(\rho_g)_j$ and the available $n+1$ level values of $(V_g)_j$.

The finite difference equation used to approximate equation (2.21) is

$$\frac{(V_m)^{n+1}_{j+\frac{1}{2}} - (V_m)^n_{j+\frac{1}{2}}}{\Delta t} + (V_m)^n_{j+\frac{1}{2}}\left[\frac{(V_m)^n_{j+1} - (V_m)^n_j}{\Delta y}\right]$$

$$+ \frac{1}{(\rho_m)^n_{j+\frac{1}{2}} A_{j+\frac{1}{2}} \Delta y}\left\{\left[\frac{A\rho_g\rho_l V_r^2}{\rho_m}\right]^n_{j+1} - \left[\frac{A\rho_g\rho_l V_r^2}{\rho_m}\right]^n_j\right\}$$

$$= -\frac{1}{(\rho_m)^n_{j+\frac{1}{2}}}\left(\frac{p^{n+1}_{j+1} - p^{n+1}_j}{\Delta y}\right) + (g_y)_{j+\frac{1}{2}} + \left(\frac{f_{vis}}{\rho_m}\right)_{j+\frac{1}{2}} \tag{2.28}$$

$$(\tilde{V}_m)_j = (V_m)_j + \Delta t\left[-CFLUX - DFLUX + \frac{2(p_j - p_{j+1})}{\rho_{j+\frac{1}{2}}(\Delta y_j + \Delta y_{j+1})} + g_y + \left(\frac{f_{vis}}{\rho_m}\right)_j\right] \tag{2.29}$$

$(\tilde{V}_m)_j$ is the explicit estimate of $(V_m)^{n+1}_j$.

where

$$(\rho_m)_{j+\frac{1}{2}} = \frac{\Delta y_{j+1}\rho_j + \Delta y_j \rho_{j+1}}{\Delta y_j + \Delta y_{j+1}} \tag{2.30}$$

$$CFLUX = V_m \frac{\partial V_m}{\partial y} = \frac{1}{2}\left\{(V_m)_j\left[\frac{(V_m)_j - (V_m)_{j-1}}{\Delta y_j} + \frac{(V_m)_{j+1} - (V_m)_j}{\Delta y_{j+1}}\right]\right.$$
$$\left. + \beta\left|(V_m)_j\right|\left[\frac{(V_m)_j - (V_m)_{j-1}}{\Delta y_j} - \frac{(V_m)_{j+1} - (V_m)_j}{\Delta y_{j+1}}\right]\right\} \tag{2.31}$$

$$DFLUX = \frac{1}{\rho_m A}\frac{\partial}{\partial y}\left(\frac{A\rho_g\rho_l}{\rho_m}V_r^2\right)$$
$$= \frac{1}{\rho_{j+\frac{1}{2}}(A_j + A_{j+1})(\Delta y_j + \Delta y_{j+1})}\left(A_{j+1}\left(\frac{\rho_g\rho_l}{\rho_m}\right)_{j+1}\left\{\left[(V_r)_j + (V_r)_{j+1}\right]^2\right.\right.$$
$$\left. + \beta\left|(V_r)_j + (V_r)_{j+1}\right|\left[(V_r)_j - (V_r)_{j+1}\right]\right\} - A_j\left(\frac{\rho_g\rho_l}{\rho_m}\right)_j\left\{\left[(V_r)_{j-1} + (V_r)_j\right]^2\right.$$
$$\left.\left. + \beta\left|(V_r)_{j-1} + (V_r)_j\right|\left[(V_r)_{j-1} - (V_r)_j\right]\right\}\right) \tag{2.32}$$

Finally,

$$(V_m)_j^{n+1} = \left(\tilde{V}_m\right)_j - \frac{2\Delta t}{\rho_{j+\frac{1}{2}}(\Delta y_j + \Delta y_{j+1})}\left(p_{j+1} - p_{j+1}^n - p_j + p_j^n\right) \tag{2.33}$$

The energy equation (2.4) is finite differenced as:

$$\frac{(\rho_m I_m)_j^{n+1} - (\rho_m I_m)_j^n}{\Delta t} + \frac{A_{j+\frac{1}{2}}(\rho_m I_m V_m)_{j+\frac{1}{2}} - A_{j-\frac{1}{2}}(\rho_m I_m V_m)_{j-\frac{1}{2}}}{A_j \Delta y_j}$$

$$+ \frac{1}{A_j \Delta y_j}\left\{\left[\frac{\rho_l\rho_g(I_g - I_l)}{\rho_m}V_r\right]_{j+\frac{1}{2}}^n - \left[\frac{\rho_l\rho_g(I_g - I_l)}{\rho_m}V_r\right]_{j-\frac{1}{2}}^n\right\}$$

$$= -\frac{p_j^{n+1}}{A_j}\left[\frac{A_{j+\frac{1}{2}}(V_m)^{n+1}_{j+\frac{1}{2}} - A_{j-\frac{1}{2}}(V_m)^{n+1}_{j-\frac{1}{2}}}{\Delta y_j}\right]$$

$$-\frac{p_j^n}{A_j \Delta y_j}\left\{\left[\frac{A\rho_g\rho_l}{\rho_m}\left(\frac{1}{\rho_g^0}-\frac{1}{\rho_l^0}\right)V_r\right]^n_{j+\frac{1}{2}} - \left[\frac{A\rho_g\rho_l}{\rho_m}\left(\frac{1}{\rho_g^0}-\frac{1}{\rho_l^0}\right)V_r\right]^n_{j-\frac{1}{2}}\right\}$$

$$+\left[KV_r^2\right]_j^n + \left[W_{vis}\right]_j^n + Q_j^n \qquad (2.34)$$

Mixture energy equation (2.34) is rearranged as

$$(I_m)_j^{n+1} = \frac{1}{(\rho_m)_j^{n+1}}\left[(\rho_m)_j (I_m)_j + \Delta t\left\{-FLUXG - FLUXL - PWK\right.\right.$$

$$\left.\left. + \frac{1}{4}K_j\left((V_r)_j + (V_r)_{j-1}\right)^2 + (W_{vis})_j + Q_j\right\}\right] \qquad (2.35)$$

where

$$FLUXG = \frac{1}{A_j \Delta y_j}\left[A_{j+\frac{1}{2}}(\rho_g I_g V_g)_{j+\frac{1}{2}} - A_{j-\frac{1}{2}}(\rho_g I_g V_g)_{j-\frac{1}{2}}\right] \qquad (2.36)$$

$$FLUXL = \frac{1}{A_j \Delta y_j}\left[A_{j+\frac{1}{2}}(\rho_l I_l V_l)_{j+\frac{1}{2}} - A_{j-\frac{1}{2}}(\rho_l I_l V_l)_{j-\frac{1}{2}}\right] \qquad (2.37)$$

The convective energy flux terms are given by

$$(\rho_g I_g V_g)_{j+\frac{1}{2}} = \frac{1}{2}\left\{(V_g)_j\left[(\rho_g I_g)_j + (\rho_g I_g)_{j+1}\right] + \beta|V_g|\left[(\rho_g I_g)_j - (\rho_g I_g)_{j+1}\right]\right\} \qquad (2.38)$$

$$(\rho_g I_g V_g)_{j-\frac{1}{2}} = \frac{1}{2}\left\{(V_g)_{j-1}\left[(\rho_g I_g)_{j-1} + (\rho_g I_g)_j\right] + \beta|V_g|\left[(\rho_g I_g)_{j-1} - (\rho_g I_g)_j\right]\right\} \qquad (2.39)$$

$$(\rho_l I_l V_l)_{j+\frac{1}{2}} = \frac{1}{2}\left\{(V_l)_j\left[(\rho_l I_l)_j + (\rho_l I_l)_{j+1}\right] + \beta|V_l|\left[(\rho_l I_l)_j - (\rho_l I_l)_{j+1}\right]\right\} \qquad (2.40)$$

$$(\rho_l I_l V_l)_{j-\frac{1}{2}} = \frac{1}{2}\left\{(V_l)_{j-1}\left[(\rho_l I_l)_{j-1} + (\rho_l I_l)_j\right] + \beta|V_l|\left[(\rho_l I_l)_{j-1} - (\rho_l I_l)_j\right]\right\} \qquad (2.41)$$

The vapor and liquid velocities used in these expressions are defined as

$$\left(V_g\right)_j = \left(V_m\right)_j + \left(\rho_l\right)_{j+\frac{1}{2}} \frac{\left(V_r\right)_j}{\left(\rho_m\right)_{j+\frac{1}{2}}} \tag{2.42}$$

$$\left(V_l\right)_j = \left(V_m\right)_j - \left(\rho_g\right)_{j+\frac{1}{2}} \frac{\left(V_r\right)_j}{\left(\rho_m\right)_{j+\frac{1}{2}}} \tag{2.43}$$

The pressure work term is approximated as

$$PWK = \frac{p_j}{A_j \Delta y_j}\left(A_{j+\frac{1}{2}}\left\{\left(V_m\right)_j + \left[\frac{\left(\rho_g\right)_{j+\frac{1}{2}} - \left(\rho_m\right)_{j+\frac{1}{2}} + \rho_l^0}{\rho_l^0} - \frac{\left(\rho_g\right)_{j+\frac{1}{2}}}{\left(\rho_m\right)_{j+\frac{1}{2}}}\right]\left(V_r\right)_j\right\}\right.$$
$$\left. - A_{j-\frac{1}{2}}\left\{\left(V_m\right)_{j-1} + \left[\frac{\left(\rho_g\right)_{j-\frac{1}{2}} - \left(\rho_m\right)_{j-\frac{1}{2}} + \rho_l^0}{\rho_l^0} - \frac{\left(\rho_g\right)_{j-\frac{1}{2}}}{\left(\rho_m\right)_{j-\frac{1}{2}}}\right]\left(V_r\right)_{j-1}\right\}\right) \tag{2.44}$$

Quantities on the right hand side of the energy equation (2.35) are evaluated using n level values for ρ_m, ρ_g and I_m, whereas $n+1$ level values are used for $\left(V_m\right)_j, p_j$ and the overall divisor $\left(\rho_m\right)_j$. These difference equations have been supplemented by additional relationships among variables at the edges and center of mesh cells. The "weighted donor cell" difference scheme that has been used above is given by:

$$\rho_{j+\frac{1}{2}} = \left(\frac{1+\beta}{2}\right)\rho_j + \left(\frac{1-\beta}{2}\right)\rho_{j+1} \tag{2.45}$$

$$\alpha_{j+\frac{1}{2}} = \left(\frac{1+\beta}{2}\right)\alpha_j + \left(\frac{1-\beta}{2}\right)\alpha_{j+1} \tag{2.46}$$

$$I_{j+\frac{1}{2}} = \left(\frac{1+\beta}{2}\right)I_j + \left(\frac{1-\beta}{2}\right)I_{j+1} \tag{2.47}$$

$$V_j = \left(\frac{1+\beta}{2}\right) V_{j-\frac{1}{2}} + \left(\frac{1-\beta}{2}\right) V_{j+\frac{1}{2}} \tag{2.48}$$

where β is the weighting parameter. It varies between -1 and +1. It can be chosen in various ways. For example,

$\beta = 0$ yields more accurate but less stable central difference technique.

$\beta = V_{j+\frac{1}{2}} \Big/ \left| V_{j+\frac{1}{2}} \right| = \pm 1$ gives full donor cell difference or fully upstream or fully upwind difference scheme. This scheme is stable provided fluid does not convect through more than one mesh cell in one time step. Though this technique is stable, it is first order accurate.

2.4 The Solution Procedure

The numerical scheme that has been developed is based on SIMPLE (Semi-Implicit Method for Pressure Linked Equations) algorithm formulated by Patankar [1980]. Primitive variables p, V, and I (ultimately it will lead to temperature T) are used in a staggered grid system. The computation domain is divided into rectangular control volumes with one grid point located at the center of the control volume that forms the basic cell. Pressure p and temperature T are calculated at the center of the cell. Velocity V is calculated for points that lie on the face of these basic cells. A typical basic cell with mesh cell labeling convention is shown in the following figure.

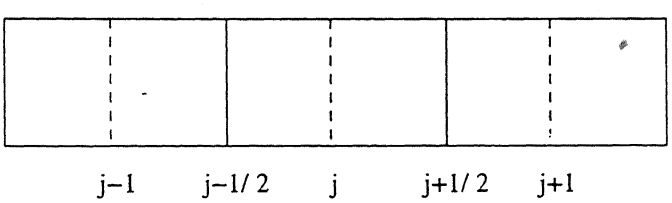

The basic philosophy of the pressure correction method used in SIMPLE algorithm is as follows:

1. Start the iterative process by guessing the pressure field. Denote the guessed pressure by p_0.
2. Use the value of p_0 to solve for the velocity V in the momentum equation. Since this velocity is associated with the values of p_0, denote this by V_0.
3. Since the velocity is obtained from guessed value of pressure p_0, the velocity V_0, when substituted into the continuity equation, will not necessarily satisfy that equation. Hence, using the continuity equation, construct a pressure correction p' which when added to p_0 will bring the velocity field more into agreement with the continuity equation. That is, the "corrected" pressure p is

$$p = p_0 + p'$$

Corresponding velocity correction V' can be obtained from p' such that

$$V = V_0 + V'$$

4. Designate the new value p as the new value of p_0. Return to *STEP-2*, and repeat the process until a velocity field is found that *does* satisfy the continuity equation. When this is achieved, the correct flow field is at hand.

2.5 Stability

One has to use a proper time step and grid size to avoid the problem of numerical diffusion. Numerical diffusion means as we discretise a differential equation by FDM (finite difference method), normally we neglect the higher order terms. Suppose they diffuse from one calculation to the other and the error keeps on building, then it may cause numerical error. As we know from Von-Neumann stability criteria that explicit method is conditionally stable and has got a stringent time step limitation. Using a smaller time step means number of iterations to reach at the solution is more. This adds to the round off error. On the other hand, implicit methods are unconditionally stable. But it uses the advanced time step value to proceed to the

next cycles, which are generally not known. Hence a semi implicit-explicit scheme has been used which is better than the explicit scheme as far as time step is concerned and implicit scheme so far numerical oscillation are concerned. Basically the iterative explicit treatment of pressure, equation of state term makes this technique applicable at all flow speeds (sonic as well as sub sonic).

The necessary condition for stability is that the fluid should move less than one mesh cell per iteration. This is known as effective Courant number criteria. Hence the stability of the numerical scheme can be assured only for the time step sizes below the effective Courant number as given by:

$$\frac{V_m \Delta t}{\Delta y} < 1$$

Also, stability is expected when the upwinding weighting parameter β is chosen such that

$$\beta > max\left[\frac{V_m \Delta t}{\Delta y}, \frac{\rho_g \rho_l V_r \Delta t}{\rho_m^{\ 2} \Delta y}\right]$$

In the present work effective Courant number has been taken less than 0.25. Also the grid size should be chosen so that it is larger than the bubble radius. Otherwise there may be instability due do sudden change in state in two adjacent cells due to the presence of bubble in one cell and liquid in the next cell. On the other hand, too large a grid size will make the truncation error prominent.

2.6 Closure

In this chapter, formulation of Drift flux equation is described along with the finite difference discretized form for these governing equations. The solution procedure for solving the system of equation has been described. This chapter also presents the general concept of stability criterion.

Chapter 3

Simulation of Small LOCA

3.1 Motivation: The Three Mile Island accident

The motivation behind choosing this problem is to illustrate how a small break LOCA can trigger to a large scale accident. In March 1979, an event occurred at the Three Mile Island Unit 2 (TMI-2) that resulted in the first case of melted fuel in a full scale commercial nuclear reactor power plant. The initial phase of this accident involved a loss of steam generator feed water that led to depletion (boil-off) of the liquid inventory on the steam generator secondary side. The resulting loss of heat removal caused heat-up and expansion of the primary coolant. The pressure rose in the reactor primary cooling system until the reactor shutdown. This led to the actuation of the pressurizer relief valve. This valve failed to close when it was supposed to-after pressure dropped below the set point for closure. This initial stage of the incident does not call for sophisticated analysis, and the models employed in the plant simulators for operator training could have addressed it adequately.

That, however, was not the case due to the occurrence of the subsequent small break LOCA. The simulators available at that time did not include provisions to account for the presence of two-phase flow within the primary coolant system. Any void (steam) generated anywhere in the system was thought to end up, without delay, in the upper portion of the pressurizer. The simulators therefore taught the operators to concentrate on keeping the pressurizer liquid level within prescribed limit; a liquid-full pressurizer was regarded as an indication of a liquid-full primary coolant system.

Lack of heat removal combined with loss of pressure caused by discharge of coolant through the stuck-open relief valve, eventually caused liquid flashing in parts of the reactor vessel and accumulation of steam within its upper regions. The liquid displaced by the steam was pushed into the pressurizer, giving the high water level indication and causing operator to turn off the emergency water injection pump. This ultimately leads to excessive fuel heating and fuel melt down

.

3.2 Problem Statement

A schematic of the problem geometry is shown in Figure 3.1 A constant pressure pump (p =75 bar) induces flow of a liquid (water) at a temperature of 500°K through a single branching system into a pressurized vessel at a pressure of 70 bar. The flow is calculated until steady state is achieved. A guillotine break is then made in one of the line branches at its vessel connection and the transient output is then calculated. Figure 3.2 shows the dimensions and computational zone for the pipe system, which contains three components and one junction. The bottom end of the component (pipe) 1, which is connected to the vessel, is treated as an isolated end with a constant pressure outflow boundary condition. At the time of the break the boundary condition of bottom end of pipe 1 will be changed to ambient condition (p =1bar) to reflect the pipe's separation from the vessel. The top end of the pipe 1 and the bottom end of the pipe 2 and pipe3 are connected to the junction. The top end of the pipe 2 remains connected to the vessel during the entire calculation and is described by an isolated constant pressure outflow boundary. The top end of pipe 3 is treated as an isolated constant pressure inflow boundary to simulate the pump.

3.2.1 Geometry

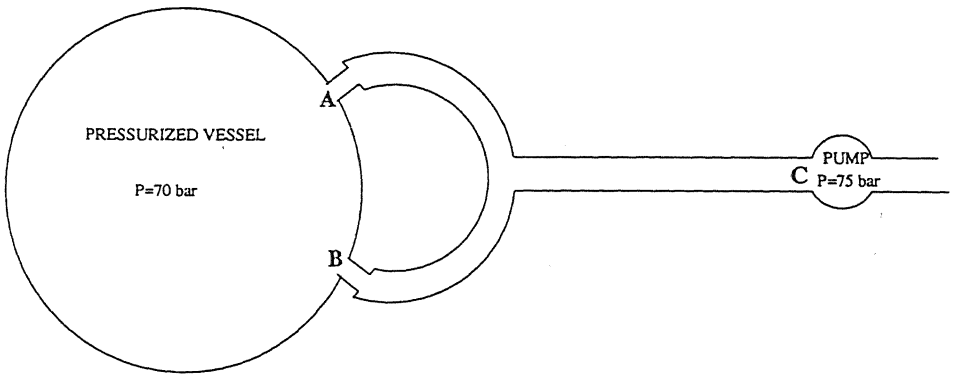

Figure 3.1: Single loop system geometry for the test problem.

3.2.2 Computational Domain

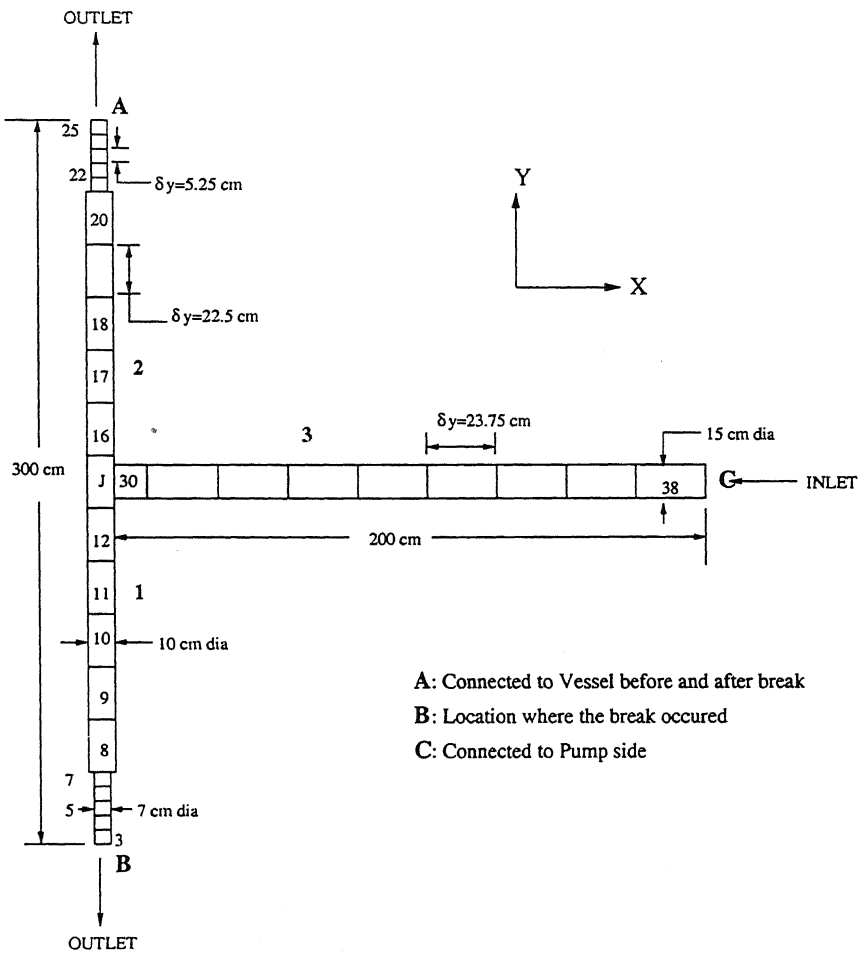

Figure 3.2 : Structure of the computing mesh for the test problem.

3.3 Constitutive Relations

Basic definitions of mixture quantities are as follows:

$$\rho_g = \alpha \rho_g^{\,0} \tag{3.1}$$

$$\rho_l = (1-\alpha)\rho_l^{\,0} \tag{3.2}$$

$$\rho_m = \rho_g + \rho_l = \alpha \rho_g^{\,0} + (1-\alpha)\rho_l^{\,0} \tag{3.3}$$

$$\alpha = \frac{\rho_l^{\,0} - \rho_m + \rho_g}{\rho_l^{\,0}} \tag{3.4}$$

1. *Thermal equation of state for the liquid:*

$$p = p_0 + a^2\left(\rho - \rho_l^{\,0}\right) \quad for \alpha \le \alpha_c \tag{3.5}$$

2. *Thermal equation of state for the vapor:*

$$p = (\gamma - 1)\rho_g^{\,0} I_g \quad for \alpha > \alpha_c \tag{3.6}$$

3. *Caloric equation of state for the liquid:*

$$I_l = E_l + C_l(T_l - T_0) - C_{l1}(T_l - T_0)^2 \tag{3.7}$$

4. *Caloric equation of state for the vapor:*

$$I_g = E_g + C_g(T_g - T_0) - C_{g1}(T_g - T_0)^2 \tag{3.8}$$

5. *Wall heat source:*

$$Q = Heat\ \ flux\ density = \frac{Power}{\pi R_i^{\,2} \times Length\ of\ \ heated\ \ section} \tag{3.9}$$

6. *Wall friction:*

The distributed losses (pipe wall friction and local losses that occur due to sudden change in area) can be given as:

$$f_{vis} = -\frac{f}{R_h}\left[\frac{\rho_m}{\rho_l^0}(1-\psi)\phi_{TP}\right]^2 \rho_l{}^0 V_m{}^2 - \frac{f_1}{2}\rho_l{}^0 V_m{}^2 \qquad (3.10)$$

Using Govier and Aziz [1972] correlation, the friction coefficient f is given by:

$$f = a + \frac{b}{\mathrm{Re}^c} \qquad (3.11a)$$

where,

$$a = 0.026(k/2R_h)^{0.225} + 0.133(k/2R_h) \qquad (3.11b)$$

$$b = 22.0(k/2R_h)^{0.44} \qquad (3.11c)$$

$$c = 1.62(k/2R_h)^{0.134} \qquad (3.11d)$$

R_h = Hydraulic radius

ϕ_{TP} = Two-phase friction multiplier

$\phi_{TP} = (1-\alpha)^{-1.75}$

The coefficient f_1 relates to the local losses and is given by

$f_1 = \dfrac{f(L/2R_h)}{\Delta y}$ Where $(L/2R_h)$ is the hydraulic diameter of an equivalent straight channel and Δy is the segment length over which the loss occurs.

7. *Relative velocity correlation:*

ψ accounts for the relative velocity effects and is given by:

$$\psi = \rho_g\left[1+(\rho_m-\rho_g)\frac{V_r}{\rho_m V_m}\right]^2 \Big/ \rho_m \qquad (3.12)$$

8. *Rate of phase change:*

The vapor generation rate is calculated as follows;

$$\Gamma_g = \frac{q''S}{h_{evap}}$$

q'' = Interfacial heat flux

h_{evap} = Latent heat of vaporization (3.13)

$$q'' = \frac{k_{tl}(T_l - T_s)}{l} \tag{3.14}$$

Hence,

$$\Gamma_g = \frac{k_{tl}(T_l - T_s)S}{h_{evap} l} \tag{3.15}$$

Where, l = Thickness of thermal boundary layer over which the liquid temperature changes from its interior bulk temperature T_l to the value T_s

Theofanous *et al.* [1975] had given the value of $l = l_{nt}$ for a single, nontranslating bubble growing in an infinite fluid region as:

$$l_{nt} = r\left[\frac{6}{\pi}\frac{\rho_l^{\,0}}{\rho_g^{\,0}}\frac{C_l|T_l - T_s|}{h_{evap}}\right]^{-1} \tag{3.16}$$

Moalem and Sideman [1973] had given the value of $l = l_t$ for bubbles which are translating with respect to surrounding liquid with speed V, as

$$l_t = r\left(\frac{\pi}{Re_b Pr}\right)^{1/2} \tag{3.17}$$

Where, $Re_b = \frac{2rV\rho_l^{\,0}}{\mu_l}$ = Bubble Reynolds number (3.18)

$$Pr = \frac{C_l \mu_l}{k_{tl}} = \text{Liquid Prandtl number} \tag{3.19}$$

Combining both of these effects,

$$\frac{1}{l} = \frac{1}{l_{nt}} + \frac{1}{l_t} \tag{3.20}$$

9. *Saturation curve:*

$$T_s = 255.2 + 117.8p^{0.223} \tag{3.21}$$

10. *Thermal constraint:*

For equal-phase temperatures, the mixture temperature can be computed from the mixture internal energy as the solution of a quadratic equation

$$\rho_m I_m = \rho_g I_g + \rho_l I_l \tag{3.22}$$

When the vapor is considered to be saturated, its temperature is determined from the mixture pressure by the relation

$$T_g = 255.2 + 117.8 p^{0.223} \tag{3.23}$$

The Momentum exchange function:

$$K = \frac{\rho S}{8\alpha_1}\left(C_d |V_r| + \frac{12\nu}{r_0} \right) \tag{3.24}$$

Where,

$$\alpha_1 = \alpha, \qquad \nu = \nu_l (1-\alpha)^{-2.5} \qquad for \alpha \le 0.5 \tag{3.25}$$

$$\alpha_1 = 1-\alpha, \quad \nu = \nu_g \alpha^{-2.5} \qquad for \alpha > 0.5 \tag{3.26}$$

The surface area per unit volume of bubbles with mean radius r_0 is given by:

$$S = \frac{3\alpha}{r_0} for \alpha \le 0.5 \tag{3.27}$$

$$S = \frac{3(1-\alpha)}{r_0} for \alpha > 0.5 \tag{3.28}$$

The *mean bubble radius* is given by:

$$r_0 = \left(\frac{3\alpha}{4\pi N} \right)^{1/3} \qquad for \alpha \le 0.5 \tag{3.29}$$

$$r_0 = \left[\frac{3(1-\alpha)}{4\pi N} \right]^{1/3} \qquad for \alpha > 0.5 \tag{3.30}$$

The *maximum stable bubble radius* in terms of critical Weber number and σ, the interfacial surface tension is,

$$r_w = \frac{\sigma We_c}{2\rho_l {}^0 V_{rs}{}^2} \tag{3.31}$$

$$r = Min(r_0, r_w) \tag{3.32}$$

Relative speed V_{rs} used in equation (3.31) is given by,

$$V_{rs} = |\underline{V_r}| + \beta_t |\underline{V_m}| \tag{3.33}$$

$\underline{V_m}$ = Mass averaged mixture velocity $= \frac{1}{2}\left| \left[(V_m)_j + (V_m)_{j-1}\right] \right|$

$\underline{V_r}$ = Average relative velocity $= \frac{1}{2}\left| \left[(V_r)_j + (V_r)_{j-1}\right] \right|$

β_t = Parameter accounting for turbulent fluctuation = 0.1

3.4 Mesh Construction

3.4.1 Mesh construction for the components

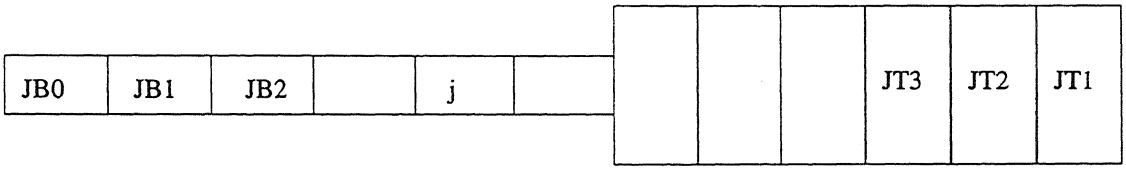

Figure 3.3: Arrangement of fictitious cells at the bottom and top of the component 'I'.

Referring to Figure 3.3

I: denotes component (pipe)

J: denotes cell

JB0: denotes first fictitious bottom cell

JB1: denotes second fictitious bottom cell

JB2: denotes first real bottom cell

JT1: denotes last fictitious top cell

JT2: denotes last real top cell

Component can be divided into different segments.

Assumption: All cells in a segment has identical properties.

If necessary, we can define different properties for every cell by making each cell a segment. The first two bottom cells JB0 and JB1 and last top cell JT1 in the component are "dummy" or "fictitious" cells used to set boundary conditions and accomplish coupling of components. Two cells are needed at the beginning of a component to set the boundary conditions because a staggered mesh arrangement has been used, where velocities are located at the cell boundaries. All other dependent variables are located at the cell centers.

3.4.2 Mesh Construction for a Junction Cell

A junction cell is a three-dimensional rectangular control volume that can join up to four components in a plane. In the present case flow in the third dimension is restricted. This restriction allows the use of a two-dimensional rather than a three-dimensional solution algorithm for the junction cell.

A one-dimensional component may be attached perpendicular to any of the four faces of the junction as shown in the Figure 3.4 and Figure 3.5. For simplicity only one component is allowed per face and components opposite to one another must have the same cross-sectional area at the junction. If no components are attached to a given junction face, it is treated as a rigid wall boundary.

The coupling of a junction cell and two or more component is accomplished by making the junction cell the neighboring cell to the JB2 (first bottom real cell) or JT2 (last top real cell) cells that belong to the adjoining ends of the components. The JB1 or JT1 fictitious cells at the adjoining ends overlap the junction cell. The centers of the overlapping cells coincide with the center of the junction cell so that cell centered quantities in the junction cell and cells JB1 and JT1 are identical. Furthermore, the boundaries of the overlapping cells on which velocities are stored coincide with the boundaries of the junction cell so that velocities on the common boundaries are identical.

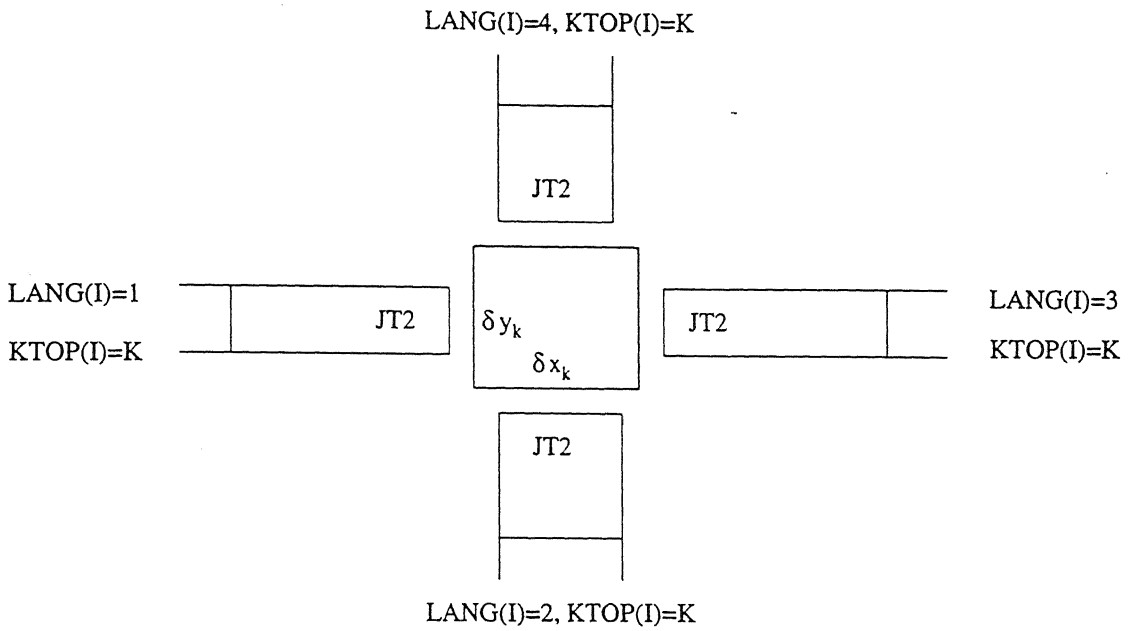

Figure 3.4: Junction cell orientation for component coupling connecting from the top.

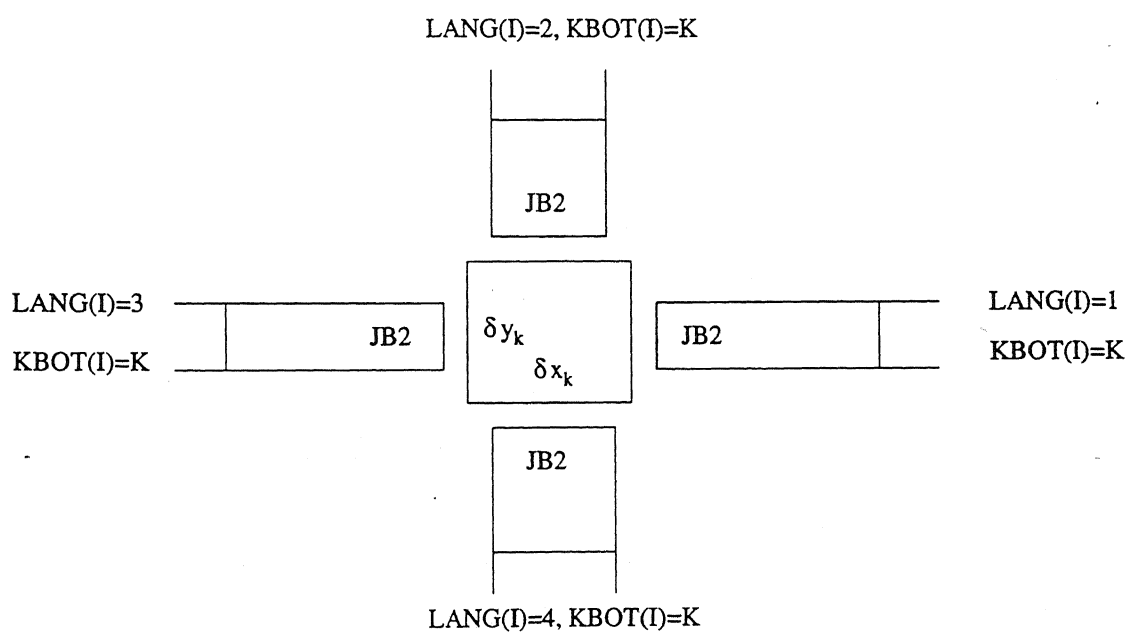

Figure 3.5: Junction cell orientation for component coupling connecting from the bottom.

3.5 Component Boundary Conditions

Various types of boundary conditions may be used at the ends of the one-dimensional component meshes. The following is the list of boundary conditions that are available in the present code.

1. **Prescribed Zero Velocity.** A prescribed zero velocity can be set as boundary condition in the component.
   Example: $V(JB0)=0$
2. **Prescribed Non-zero Velocity.** A nonzero or time varying prescription can be set as boundary condition in the component. While setting nonzero velocity, one must also specify the pressure, void fraction and temperature at the boundary.
   Example: $V(JB0)=constant$ or $f(t)$
3. **Uniform Outflow.** A uniform or gradient free outflow boundary condition at the ends of the component can be specified by setting the velocity at a particular cell equals to the velocity at the previous cell. Use of this boundary condition also requires the additional specification of pressure, void fraction and temperature at the boundary.
   Example: $V(JB1)=V(JB1-1)=V(JB0)$
4. **Periodic Coupling.** The top and bottom boundaries of component can be joined together through the periodic boundary condition.
   Example: $V(JB0)=V(JT2)$
5. **Prescribed Pressure.** When pressure is prescribed at the JB0 end, it must be set for the cell JB1. The velocity $V(JB0)$ should be set equal to $V(JB1)$ so that fluid can flow freely into or out of the specified pressure region. The values for pressure, void fraction and temperature at the boundary also need to be specified.

Initial and boundary conditions: The initial and boundary conditions used in the present work are given below.

I.C.: at $t=0$, T = specified, p = specified, $\alpha=0$ for all cells.

For $t > 0$, **B.C. 1:** at **A, B, C** in Figure 3.2 T = specified

B.C. 2: at **A, B, C** in Figure 3.2 p = specified

B.C. 3: at **A, B, C** in Figure 3.2 α = specified

3.6 Solution Algorithm

3.6.1 Solution Algorithm for Components

A calculation cycle has been broken down into four tasks. First, the momentum equation is advanced explicitly using the previous cycle values. Next, iteration is made to replace the pressure used in the first task with advanced time values. Iteration is needed because the advanced pressures depend on the velocities being calculated. This part of the cycle contains the main implicitness of the numerical scheme. The third task in a cycle is to update all other dependent variables. Finally, the fourth task consists of data output and time step control.

3.6.2 Solution Algorithm for a Junction Cell

Junction cell values are calculated using the two-dimensional analogues of the one dimensional equations of motion [equation 3.1- equation 3.4]. The difference equations for junction cells are the two-dimensional counterparts of the one-dimensional finite difference equations. In the cross convection of momentum two-dimensionality is not maintained, because a one-dimensional component can have momentum only in the axial direction. This means, momentum entering the right or left side of a junction is not allowed to convect into components connected to the top or bottom of the junction. To ensure the coincidence between the junction and fictitious cell centers and boundaries, an additional segment is added automatically to the end of the component that adjoins the junction cell. This additional segment contains the required one or two fictitious cells, depending on which end of the component it is added to, and one real cell. Inclusion of this real cell, however, slightly increases the overall length of the component. But a better approximation of the actual length

can be obtained by specifying input data that are one cell short of the desired length (two cells short if junctions exist at both ends of the components).

3.7 Numerical Scheme

The numerical scheme that has been developed is based on SIMPLE (Semi-Implicit Method for Pressure Linked Equations) algorithm formulated by Patankar [1980]. Primitive variables p, V, and I (ultimately it will lead to temperature T) are used in a staggered grid system. The computation domain is divided into rectangular control volumes with one grid point located at the center of the control volume that forms the basic cell. Pressure p and temperature T are calculated at the center of the cell. Velocity V is calculated for points that lie on the face of these basic cells. A typical basic cell with mesh cell labeling convention is shown in the following figure.

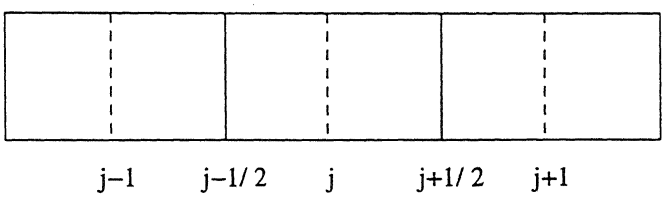

The following is a brief description of the numerical procedure:

1. Set or estimate the initial values of dependent variables: V_0, p_0 *and* T_0
2. Advance in time $(t + \Delta t)$
3. Evaluate the pseudo velocities from the momentum equation using the V_0, p_0 *and* T_0 value at n^{th} time.
4. Use the pseudo velocities in continuity equation to find the updated density $\tilde{\rho}$ and $\tilde{\alpha}$. Also using this pseudo velocity, calculate the correction in continuity equation "D". Our aim is to calculate such velocities for which "D" equals to zero. Actually D is an approximation to cell volume change per unit volume. This is given by,

$$D = \frac{\Delta t}{A}\frac{\partial}{\partial y}AV_m \approx \frac{1}{A_j}\frac{\Delta}{\Delta y_j}\left(A_{j+\frac{1}{2}}(V_m)_j - A_{j-\frac{1}{2}}(V_m)_{j-1} \right)$$

5. If "D" is not zero, then using this D solve the pressure correction equation.

$$\Delta p = -\frac{F}{\left(\frac{\partial F}{\partial p}\right)_j}$$

where, $F = p - f\left(\bar{\rho}_m, \bar{\rho}_g, \bar{I}_m\right) = 0$.

The equation of state $f\left(\bar{\rho}_m, \bar{\rho}_g, \bar{I}_m\right)$ is evaluated using

$$\bar{\rho}_m = (\rho_m)^n/(1+D)$$

$$\bar{\rho}_g = (\rho_g)^n/(1+D)$$

and $$\bar{I}_m = (I_m)^n - \frac{p^n}{(\rho_m)^n}D$$

6. Using this Δp solve the pressure field and velocity field as follows:

$$\tilde{p} = p_0 + \Delta p$$

$$V_j = V_j + \frac{2\Delta t \cdot \Delta p}{\rho_{j+\frac{1}{2}}\left(\Delta y_j + \Delta y_{j+1}\right)}$$

$$V_{j-1} = V_{j-1} - \frac{2\Delta t \cdot \Delta p}{\rho_{j-\frac{1}{2}}\left(\Delta y_{j-1} + \Delta y_j\right)}$$

7. Return to step-3. Solve the momentum equation based on new pressure field $\tilde{p}$ and continue updating values until the correction in continuity equation "D" satisfies a predetermined convergence criteria.

   The general form of convergence criteria is given by:

$$\left|\frac{p - f\left(\bar{\rho}_m, \bar{\rho}_g, \bar{I}_m\right)}{p + f\left(\bar{\rho}_m, \bar{\rho}_g, \bar{I}_m\right)}\right| < \varepsilon$$; Here ε is taken to be 0.001.

8. Solve for the new temperature field using new velocity field values.
9. When the convergence criterion for "D" is satisfied, we will have the value of primitive variable for the next time step i.e. $V^{n+1}, p^{n+1}, T^{n+1}$
10. Return to step-2 and continue till steady state is reached.

3.8 Variable Time Steps and Subcycling

One of the advanced features of the current code is the use of variable time steps and subcycling during calculations. This is due to the reason that network systems often contain low speed flow with slowly varying properties in one region and high speed flow or flow that requires a finely detailed description in another region. The variable time stepping and subcycling provisions in this code are designed specifically for such systems to provide efficient and accurate calculations. The time steps are determined by numerical stability requirements.

For numerical stability the time step in each component and junction is limited by the Courant stability criterion, which is given by $\frac{V_m \Delta t}{\Delta y(\Delta x)} \leq \frac{1}{4}$. The time steps determined according to this criterion are then increased or decreased by 1%. The direction of adjustment is determined by the relative ease of the previous time integration of the system. If fewer than five system iterations were required, the time steps are increased; otherwise, they are decreased. The time step for the system is related to the maximum time step determined for the components and junctions. The system time step is not a computational time step, but rather provides a time level toward which all the components and junctions are integrated simultaneously. The system time step is increased or decreased by 1%, based on relative ease of the previous system integration and the number of subcycles used. The system time step is increased if the number of subcycles is less than a specified number of subcycles, otherwise it is decreased.

3.9 Results

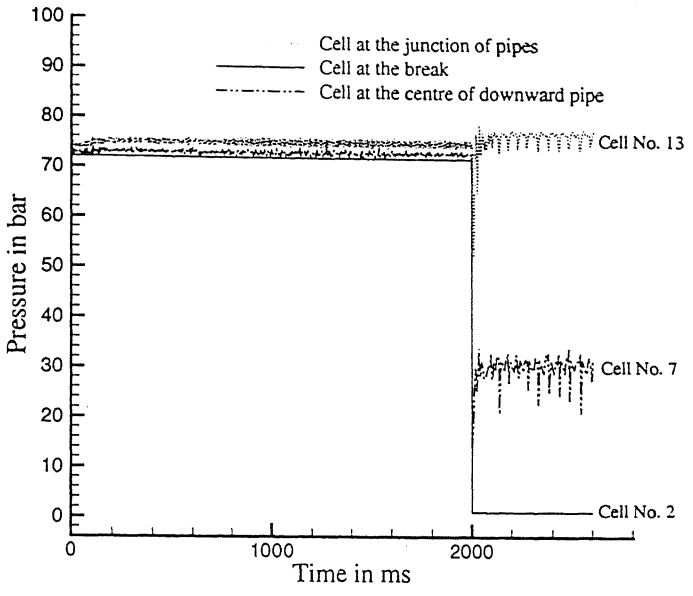

Figure 3.6: Time Variation of Pressure at different cells (break at 2000 ms).

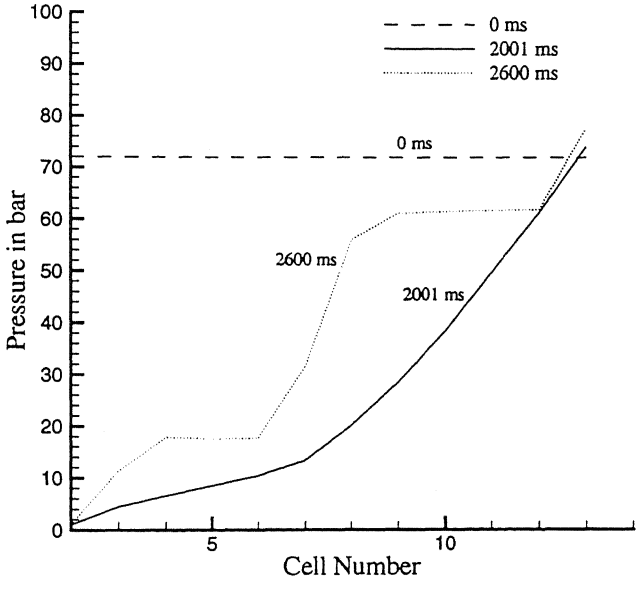

Figure 3.7: Time Variation of Pressure in the first pipe.

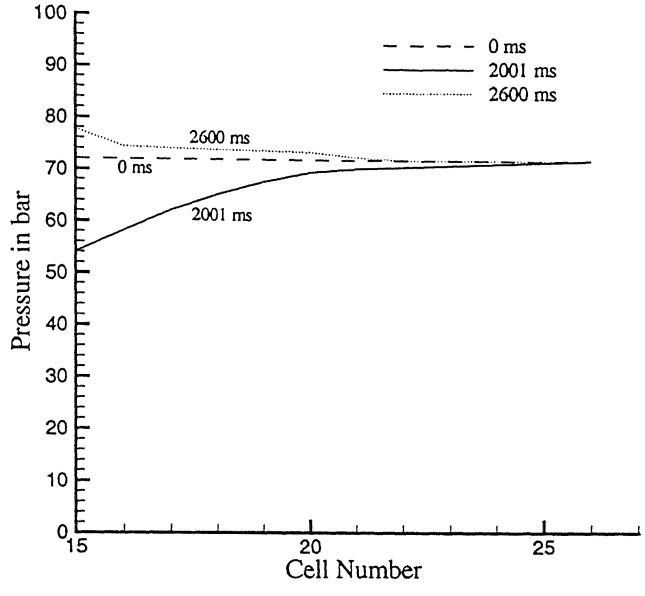

Figure 3.8: Time Variation of Pressure in the second pipe.

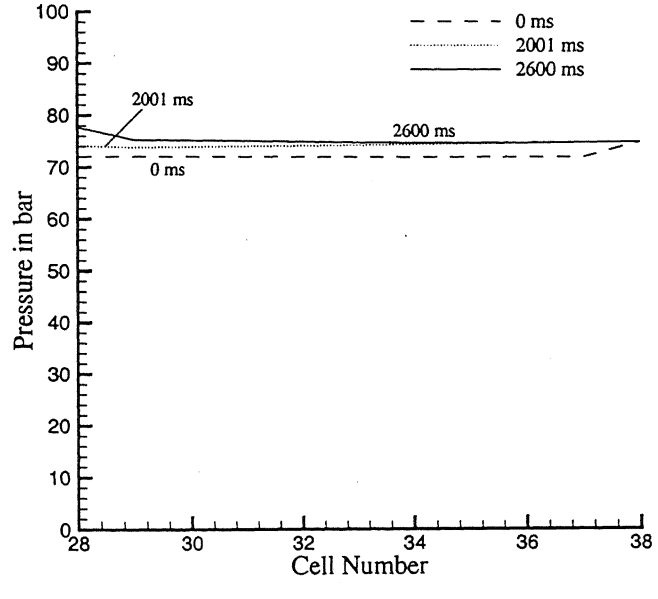

Figure 3.9: Time Variation of Pressure in the third pipe.

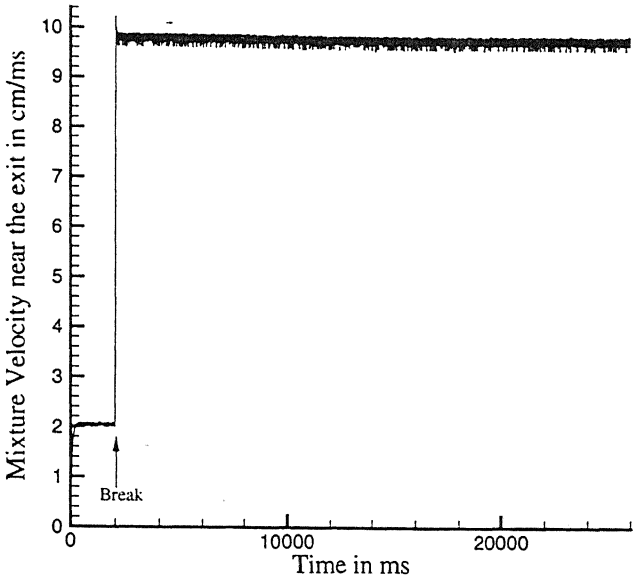

Figure 3.10: Time Variation of Velocity near the break.

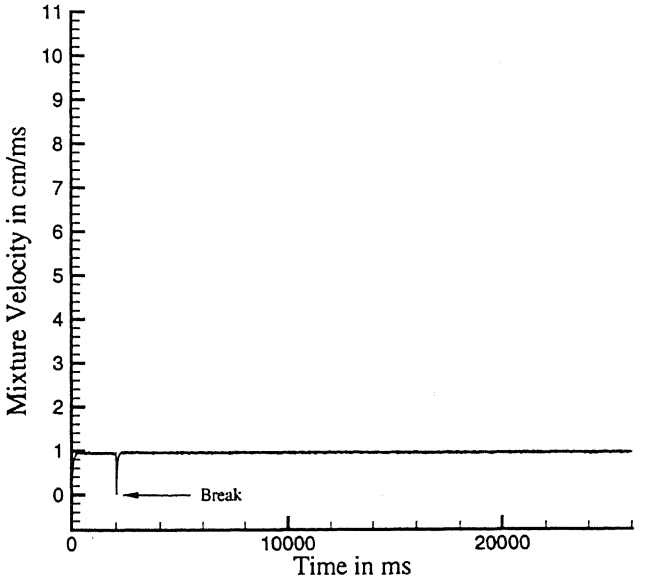

Figure 3.11: Time Variation of Velocity just above the tee-junction.

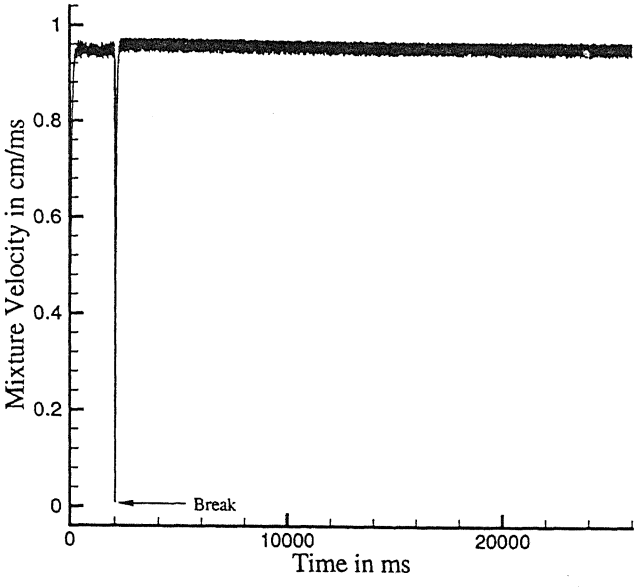

Figure 3.12: Enlarged View of Time Variation of Velocity just above the tee-junction.

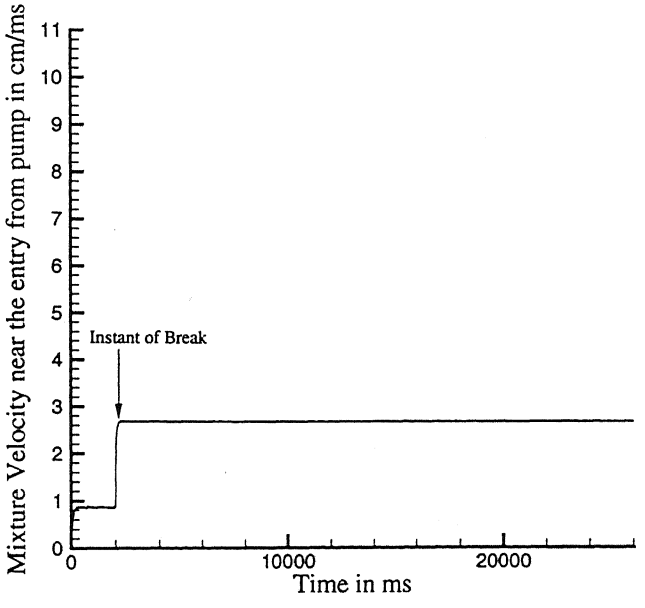

Figure 3.13: Time Variation of Velocity near the entry from the pump.

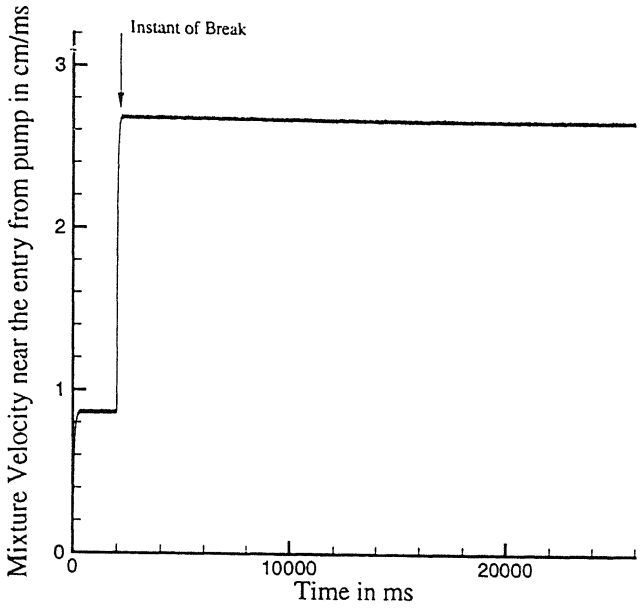

Figure 3.14: Enlarged View of Time Variation of Velocity near the entry from the pump.

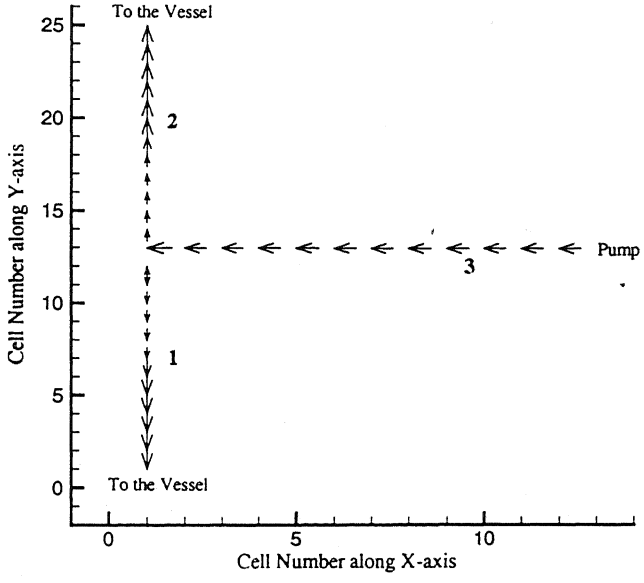

Figure 3.15: Velocity vector before the introduction of break

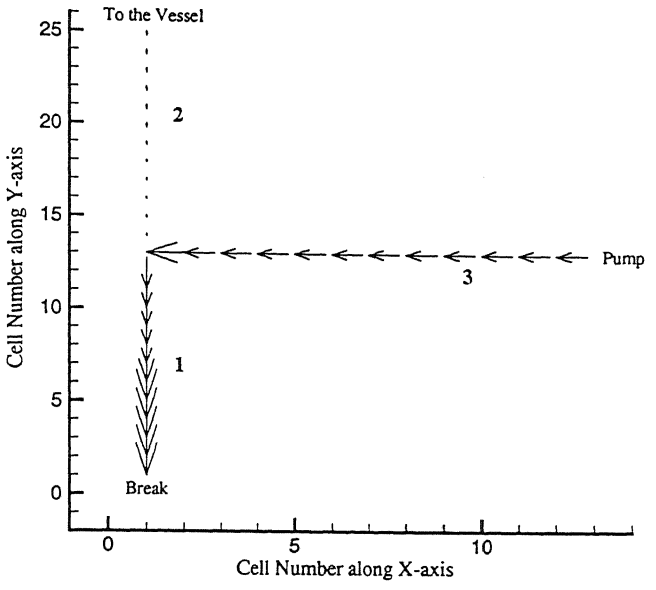

Figure 3.16: Velocity vector after the introduction of break.

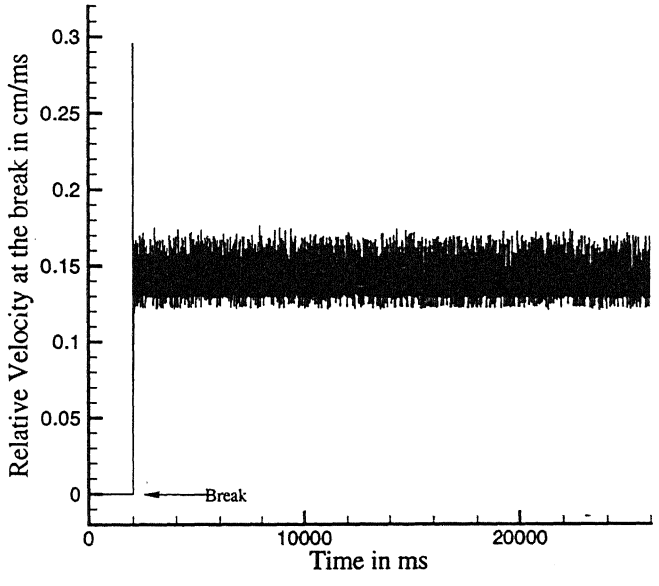

Figure 3.17: Time Variation of Relative velocity at the break.

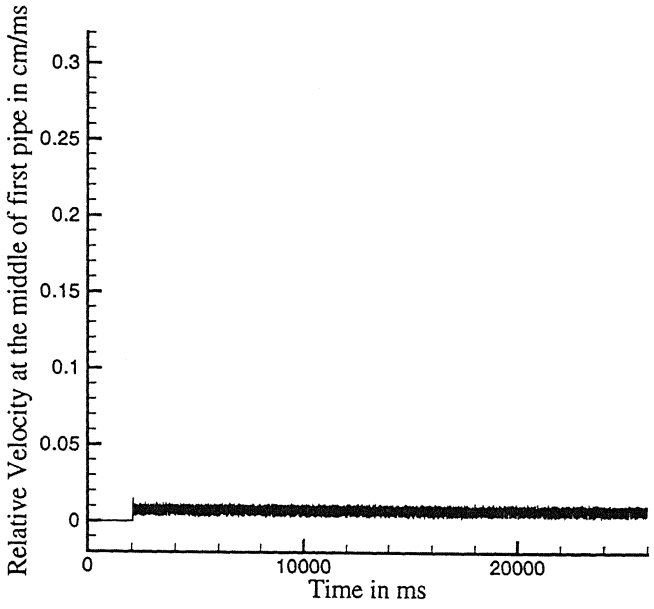

Figure 3.18: Time Variation of Relative velocity at the middle of the first pipe.

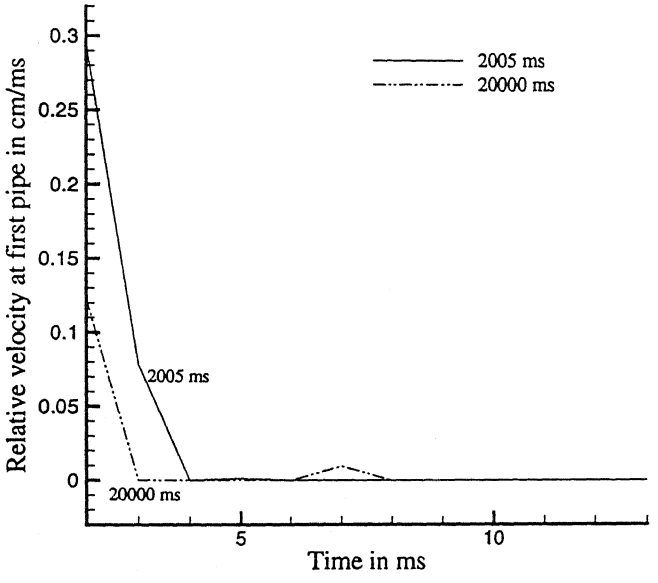

Figure 3.19: Comparison of Relative velocity in the first pipe just after and long after the break.

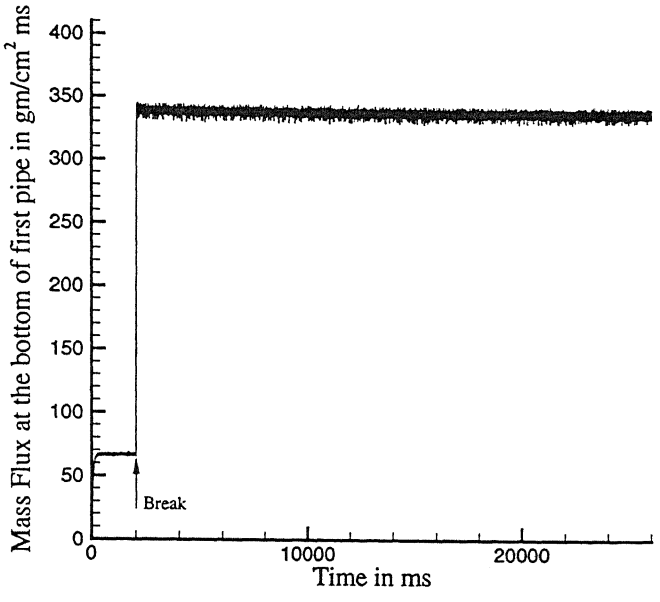

Figure 3.20: Time Variation of Mass Flux at the bottom end of the first pipe.

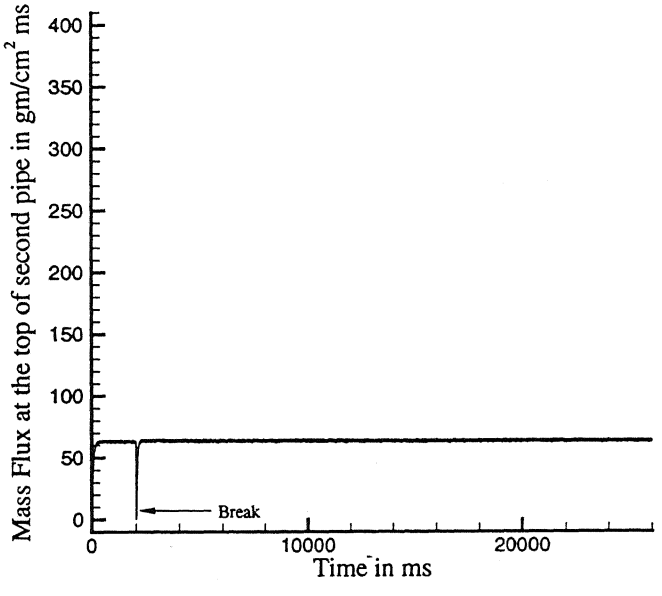

Figure 3.21: Time Variation of Mass Flux at the top end of the second pipe.

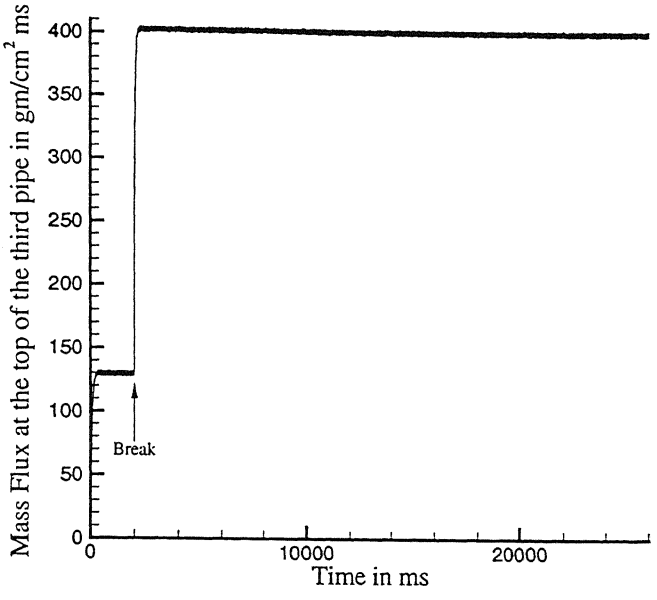

Figure 3.22: Time Variation of Mass Flux at the top end of the third pipe.

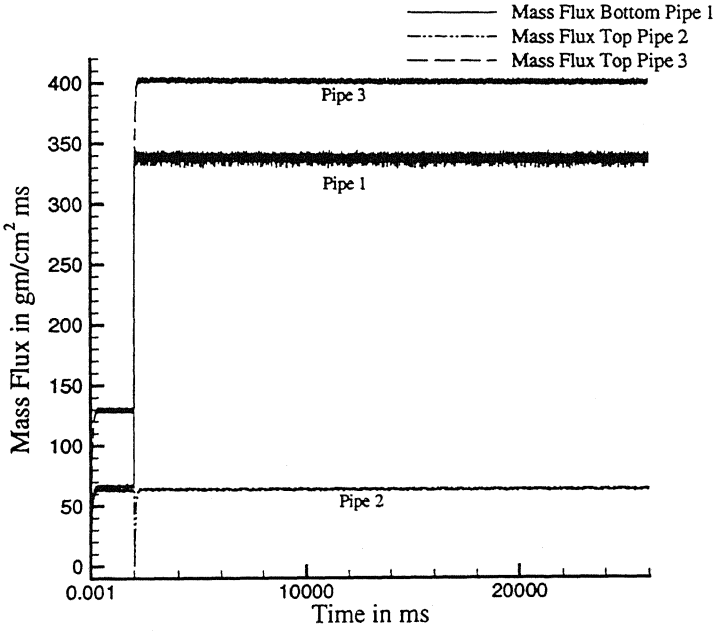

Figure 3.23: Time Variation of Mass Flux in the whole system.

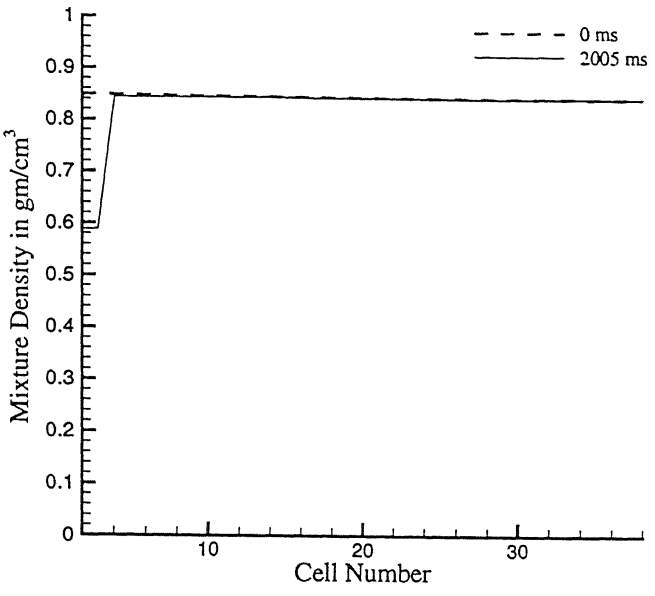

Figure 3.24: Time Variation of Density before and just after break calculated with single precision accuracy.

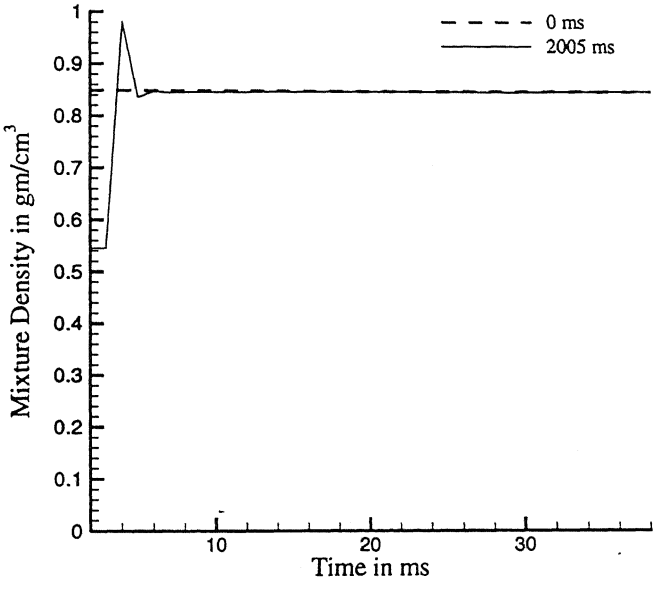

Figure 3.25: Time Variation of Density before and just after break calculated with double precision accuracy.

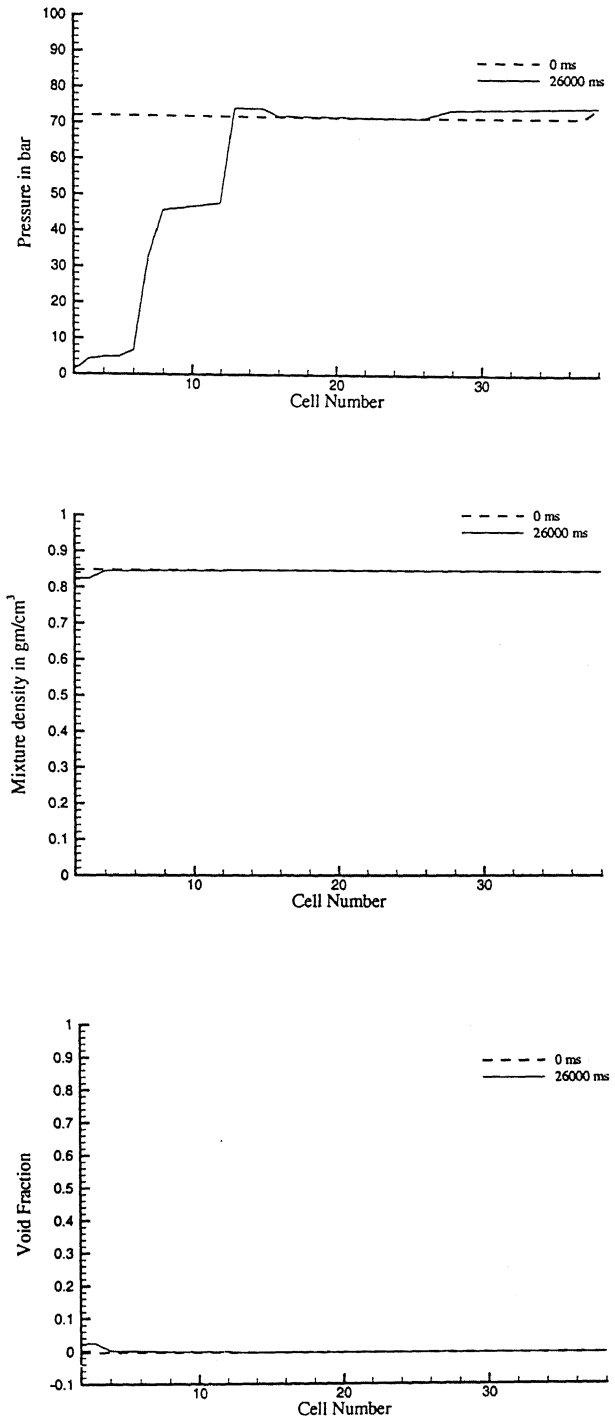

Figure 3.26: Time Variation of Pressure, Mixture Density and Void Fraction before and long after break calculated with single precision accuracy.

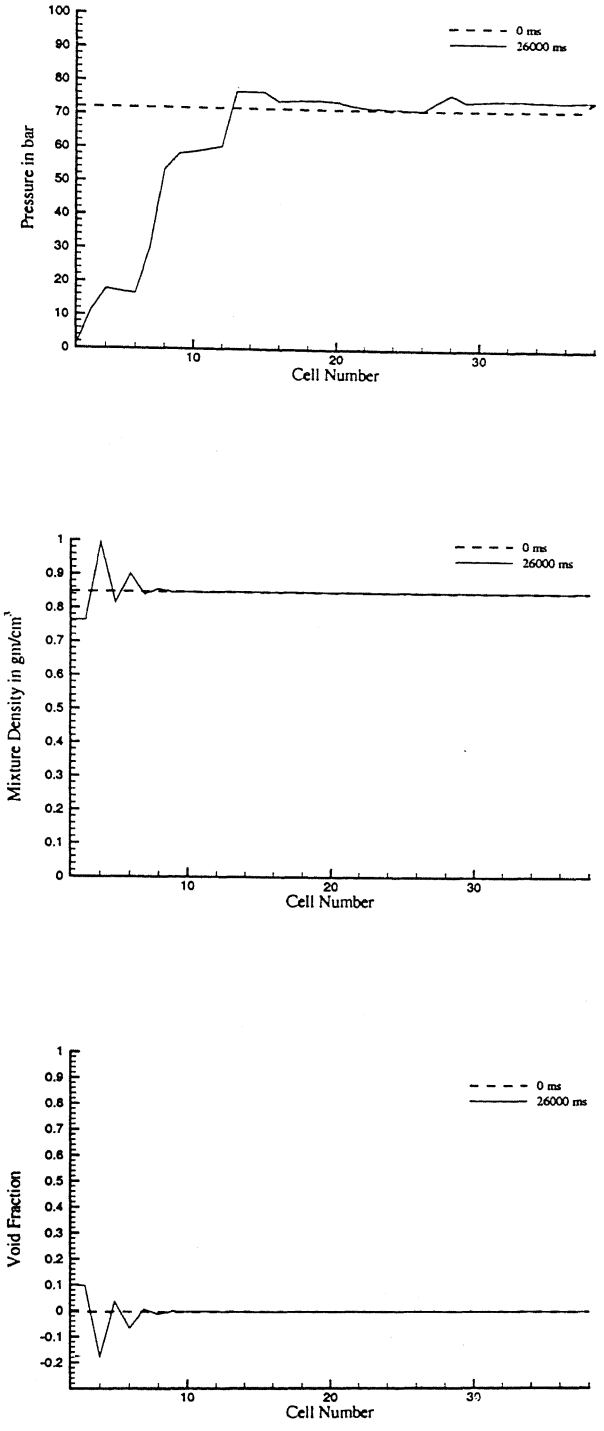

Figure 3.27: Time Variation of Pressure, Mixture Density and Void Fraction before and long after break calculated with double precision accuracy.

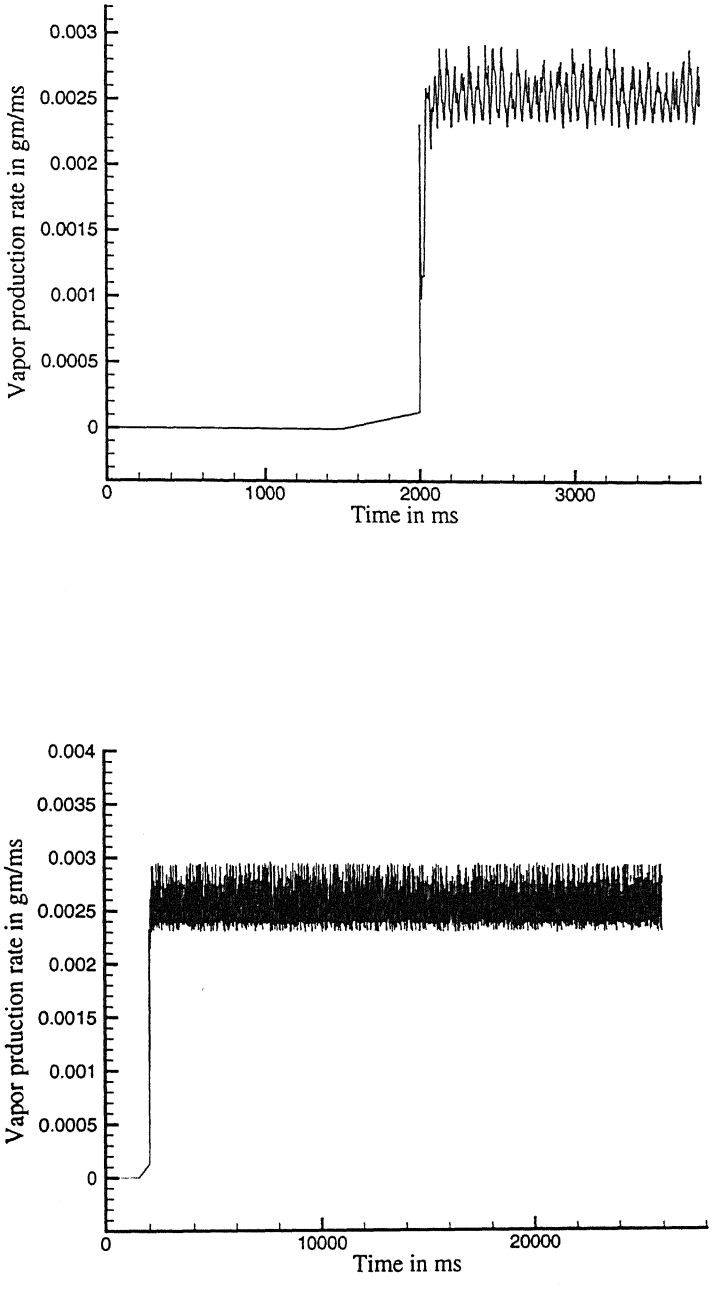

Figure 3.28: Time Variation of Vapor production rate near the break.

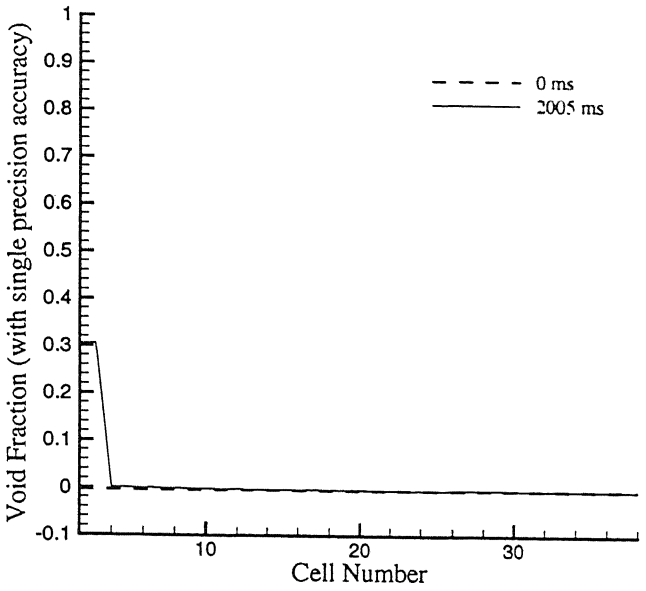

Figure 3.29: Time Variation of Void fraction before and just after break calculated with single precision accuracy.

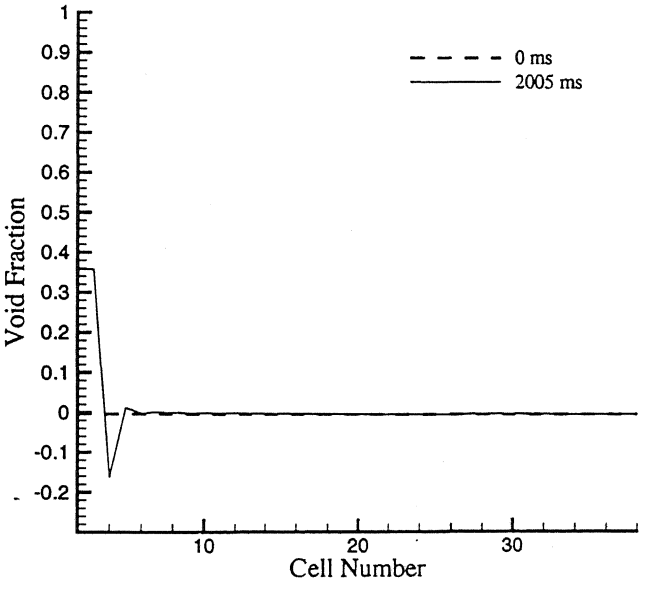

Figure 3.30: Time Variation of Void fraction before and just after break calculated with double precision accuracy.

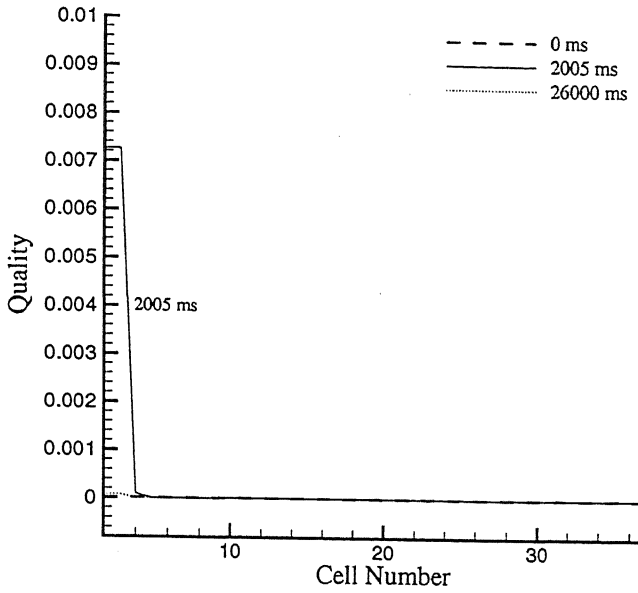

Figure 3.31: Time Variation of Quality before and after the break calculated with single precision accuracy.

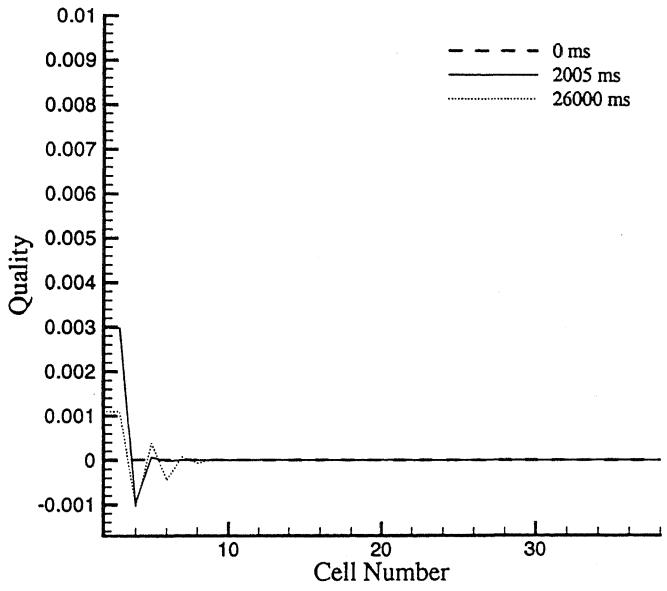

Figure 3.32: Time Variation of Quality before and after the break calculated with double precision accuracy.

3.10 Discussions

The variation of pressure at different cell of the component with respect to time has been plotted in the Figure 3.6. The flow is calculated up to 2000 ms where steady state is achieved. At this instant a guillotine break is made in one of the pipe at the vessel connection. The plot shows an instant fall in pressure at the first cell (Cell No. 2) of the broken pipe. After this point the pressure in the pipe fluctuate with time as expected. This is because the pressure at the cell suddenly reduces to a lower value (from 72 bar to 1 bar) and due to which flashing of steam starts. Due to production of bubble the pressure in the cell rises, which in turn reduces the number of bubble being produced. Hence again the pressure falls due to lack of bubble production and this process repeats.

Figure 3.7 shows the variation of pressure in the first component at a particular time. In the present case pipe break is made at the lower vertical pipe. Hence the variation of pressure, before and after the introduction of break, is more in the vertical pipes than the horizontal pipe. Figure 3.8 and Figure 3.9 shows the variation of pressure in the second and in the third component respectively. The variations of mixture velocity with respect to time at different cells are shown in Figure 3.10 – Figure 3.14. The square of sonic velocity in the liquid at this particular pressure (1bar) is nearly $12340(m/s)^2$. That means the sonic velocity is around $\approx 111 m/s$. Referring to the Figure 3.10 the velocity near the break is $\approx 10 cm/ms$ which equals to near sonic velocity. The fluctuation of velocity is due to the fluctuation of pressure governed by Bernoulli's equation. Figure 3.15 and Figure 3.16 gives the vectorial representation of velocities in the component before and after the introduction of break. The variation of relative velocity after introducing break is given by Figure 3.17. The variation of relative velocity in the first pipe is shown in Figure 3.18 and Figure 3.19. This confirms that voids are created only after break is made. Figure 3.20, Figure 3.21 and Figure 3.22 gives the mass flux variation with respect to time in first, second and third pipe respectively (Refer Figure 3.2 for the pipe number notation). Figure 3.23 shows the mass flux variation in the whole system. The area under each curve in Figure 3.23 represents the mass flux in gm/cm^2

from each of the component. The mass flux coming from pipe 3 goes to pipe 1 and pipe 2 and this can be verified in Figure 3.23. The effect of single precision and double precision accuracy calculation on the mixture density before and just after the break has been shown in Figure 3.24 and Figure 3.25. Here double precision calculation tends to give an erroneous result as the mixture density at one of the cell is even more than the single phase density. This may be due to numerical diffusion occurring in double precision calculation. The time variation of pressure, mixture density and mixture void calculated with single precision and double precision accuracy has been shown in Figure 3.26 and Figure 3.27. Figure 3.28 shows the time variation of vapor production rate after the introduction of break. The void fraction variation calculated with single precision accuracy and double precision accuracy has been shown in Figure 3.29 and Figure 3.30 respectively. Figure 3.29 and Figure 3.30 shows that the void fraction variation occurs only after the break and the fluctuation is more prominent in the cells of the broken pipe. The fluctuation of pressure changes the saturation temperature of liquid in that particular cell. This in turn varies the density of fluid in the cell and finally the density is responsible for varying the void fraction. Finally the variation of quality in the entire system at different time has been shown in the Figure 3.31 and Figure 3.32.

3.11 Closure

The simulation of small break LOCA on a test problem has been performed successfully and the various results that have been derived are quite encouraging. It was the motivating factor to include the void generation and condensation model in the present code, to be applied to sub-cooled boiling, which is described in the next chapter.

Chapter 4

Application of Generation and Condensation Models in Sub-cooled Boiling

4.1 McMaster Experimental Set-up

This experimental project was jointly funded by NSERC (National Science and Engineering Research Council, Canada) and AECL (Atomic Energy of Canada Limited).The objective of this project was to obtain detailed measurements of void generation and collapse, void profiles of different bubble size and condensation rates during low-pressure sub-cooled boiling. The test section was divided into two parts: a heated section followed by an unheated section. Measurements were taken in both areas. In the heated section, the void results from the net effect of generation and condensation, whereas in the subsequent section, condensation has been studied as a separate effect.

The test section was installed in a low pressure loop. A pump had been used to circulate the water to the loop through a preheater, which controls temperature to the test section. The test section was a vertical concentric annulus with measurements shown in the Figure 4.1. The annular channel consisted of an inner and an outer tube. Heat was generated uniformly in the test section by direct heating from a 55 kW stabilized direct current (dc) power supply. The heat was uniformly input via the inner tube (diameter 12.70 mm). The width of the annular channel was 6.15 mm. The test section had upward flow and consisted of a heated lower section 300 mm in length and a subsequent unheated upper section 120 mm in length. Flow was measured by a rotameter and void fraction by a traveling gamma

densitometer. In addition, high-speed photography was used to capture bubble action in the generation and condensation regions. The details of experimental procedure and void profile results, together with error estimation, were given by Donevski and Shoukri [1989]. The experimental parameters have been given in Table 4.1.

	Case					
	1	2	3	4	5	6
Heat flux ($W.m^{-2}$)	714403	586420	594136	576132	481482	732700
Pressure (kPa)	165.9	211.4	173.5	168.7	154.2	152
Mass flux (kg/m^2s)	367.5	315.1	420.0	429.1	392.1	450
Inlet temperature(^0C)	85.0	98.1	95.5	95.2	93.8	85.8
Inlet subcooling(^0C)	29.2	23.8	20.2	19.6	18.6	26.3

Table 4-1: Experimental parameters used in McMaster experiment

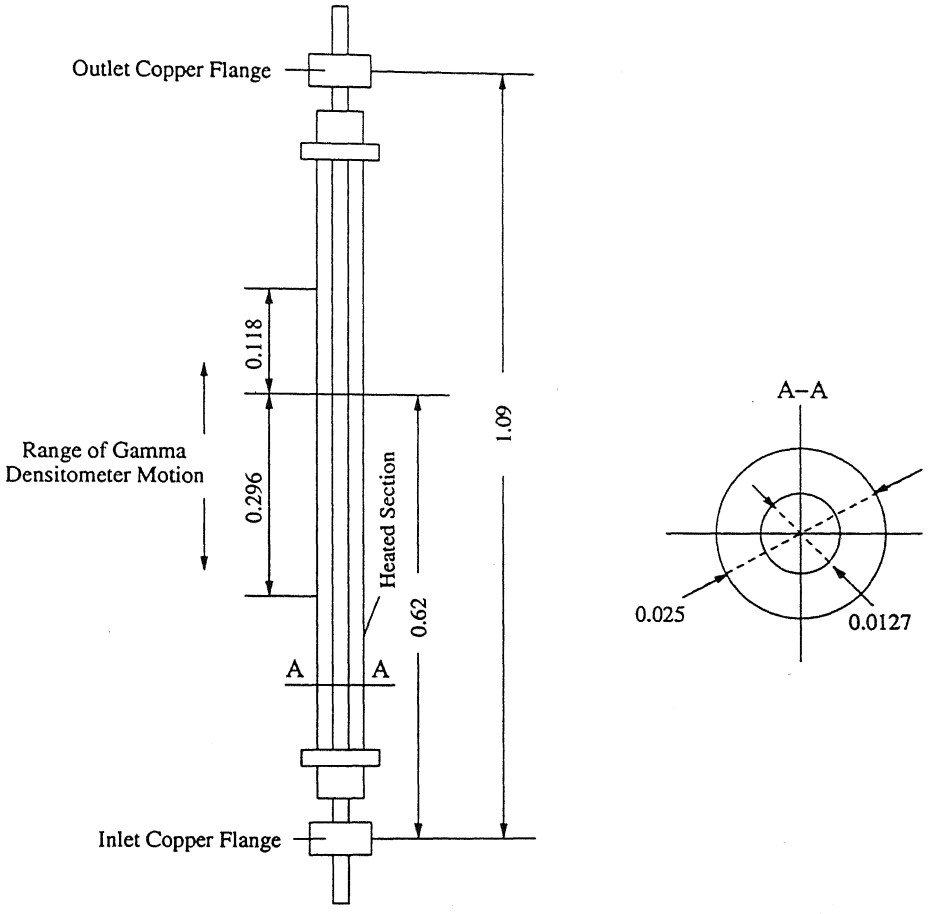

Figure 4.1: Geometry of the McMaster experimental test section.

4.2 Mathematical Formulation

Liquid mass balance:

$$\frac{\partial}{\partial t}\left((1-\alpha)\rho_l^0\right)+\frac{\partial}{\partial y}\left((1-\alpha)\rho_l^0 V_l\right)=\Gamma_c-\Gamma_g \tag{4.1}$$

Vapor mass balance:

$$\frac{\partial}{\partial t}\left(\alpha\rho_g^0\right)+\frac{\partial}{\partial y}\left(\alpha\rho_g^0 V_g\right)=-\Gamma_c+\Gamma_g \tag{4.2}$$

Mixture momentum balance:

$$\frac{\partial}{\partial t}\left(\rho_m V_m\right)+\frac{\partial}{\partial y}\left(\alpha\rho_g^0 V_g^2+(1-\alpha)\rho_l^0 V_l^2\right)=-\frac{\partial p}{\partial y}+\rho_m g_y+f_{vis} \tag{4.3}$$

Mixture energy balance:

$$\frac{\partial}{\partial t}\left(\rho_m I_m\right)+\frac{\partial}{\partial y}\left(\alpha\rho_g^0 h_g V_g+(1-\alpha)\rho_l^0 h_l V_l\right)=KV_r^2+W_{vis}+Q \tag{4.4}$$

4.3 Modeling of Void Formation in the Sub-cooled Boiling Regime

In the sub-cooled boiling regime, boiling occurs at the liquid cooled heating surfaces due to high heat flow densities, although the fluid has on average not yet reached the saturation temperature associated with the system pressure. In accordance with a suggestion by Griffith (Griffith *et al.*, 1958) four zones of heat transport and flow activity can be differentiated along

a channel axis until saturation boiling has been reached. Zone I is referred to as single phase heat transfer zone, Zone II is onset of nucleate boiling (ONB) zone, Zone III is onset of significant Void (OSV) and Zone IV is the saturated core flow region. A visual of all these four zones is given in Figure 4.2. The equation of the following effect must be formulated in order to determine the void content in the sub-cooled boiling regime: (1) on set of nucleate boiling (ONB). (2) bubble formation and bubble growth (bubble generation rate) at the heating surface (3) onset of significant void (OSV) and bubble departure diameter (4) bubble condensation in the sub-cooled core flow.

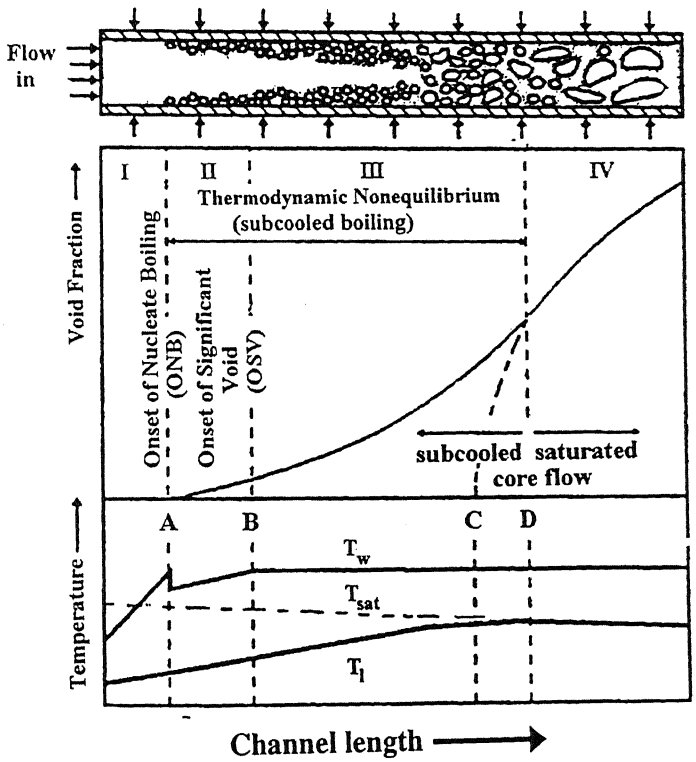

Figure 4.2: Temperature and Void fraction variation in sub-cooled and bulk boiling regions.

4.3.1 Onset of Nucleate Boiling (ONB)

It describes the point at which first boiling nuclei are activated at the boiling surface. A correlation by Bergels *et al.* [1981] and Rohsenow has been used to determine the wall superheating at which ONB will be activated.

$$\Delta T_{sup} = \frac{5}{9}\left(\frac{q''}{1100}p^{-1.156}\right)^{0.463p^{0.0234}} \tag{4.5}$$

$$T_W = T_S + \frac{5}{9}\left(\frac{q''}{1100}p^{-1.156}\right)^{0.463p^{0.0234}} \tag{4.6}$$

The range of validity of the correlation is: channel diameter 2.4 and 4.6mm; flow velocity: 3-7ms^{-1}.Pressure: 1-36 bar.

4.3.2 Onset of Significant Void (OSV)

A schematic description of heat transfer mechanism in sub-cooled boiling is given in Figure 4.3. Assuming that the sub-cooled boiling occurs, the total heat Q supplied to the fluid from the heating surface per unit area can be arbitrarily partitioned into two fractions- single phase convection and heat required for growth of bubbles:

$$Q = Q_{1\Phi} + Q_{GV}$$

Heat required to generate void is composed of: $Q_{GV} = Q_{evap} + Q_c$

The above two expressions are combined to give the heat flux as:

$$q'' = q''_{1\Phi} + q''_{evap} + q''_c \tag{4.7}$$

The heat flux associated with the single phase liquid convection from the heating surface is given as:

$$q''_{1\Phi} = B_{1\Phi} h_{1\Phi} (T_w - T_l) \tag{4.8}$$

Where T_w and T_l are the wall and liquid temperature respectively and $h_{1\Phi}$ is the heat transfer coefficient of the single phase liquid flow, which can be determined from the Dittus-Bolter correlation as:

$$h_{1\phi} = 0.023 \frac{(k_t)_l}{d_h} Re^{0.8} Pr^{0.4} \tag{4.9}$$

The factor $B_{1\Phi}$ is dependent on the void and is intended to take into consideration the fact that with increasing wall superheating, the number of bubbles formed will increase. $B_{1\Phi}$ describes the heating surface fraction in direct contact with the sub-cooled liquid.

$$B_{1\phi} = \frac{A_{eff}}{A_{he}} = \frac{A_{he} - A_b}{A_{he}} = 1 - \pi \sum_{i=1}^{I} n_i R_{i,b}^2$$

$$= 1 - n\pi \bar{R}_b^2 \tag{4.10}$$

Where A_b is the surface covered by bubbles, A_{he} is the heated surface, n is the number of bubbles per unit area and $\pi \bar{R}_b^2$ is the projection area of a bubble on the heated surface.

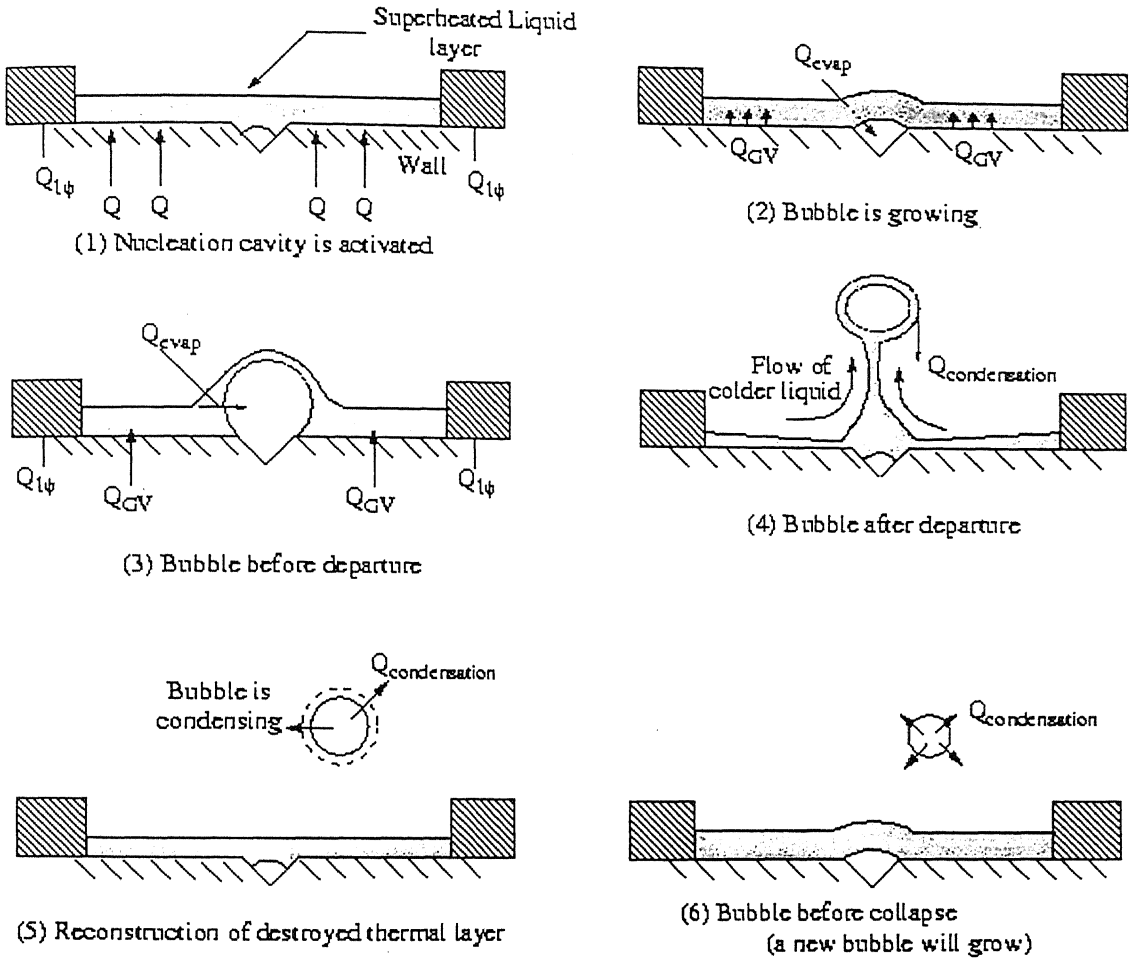

Figure 4.3: Schematic description of heat transfer mechanism by growth and condensation of steam bubbles in sub-cooled boiling regime.

Although the bubbles have statistically different radii, the calculation has been carried out with average radius $\overline{R_b}$ for the sake of simplicity.

Hainoun [1994] has proposed $B_{1\Phi}$ as:

$$B_{1\Phi} \approx 1 - \frac{\pi}{16}\frac{\alpha}{\alpha_{osv}} \quad for\ \alpha \le \frac{16\alpha_{osv}}{\pi} \tag{4.11}$$

$$B_{1\Phi} \approx 0 \quad for\ \alpha \ge \frac{16\alpha_{osv}}{\pi} \tag{4.12}$$

where α_{osv} is the void fraction at the point when the bubbles become detached from the heating surface(OSV).Experimental data shows that α_{osv} may be about 5%-10%(Rogers *et al.*,1987).

Subcooling at OSV: The bubble will be detached from the wall only when the drag and buoyancy forces are greater than the holding force. The point at which the bubbles are first detached from the wall (this is OSV: Onset of Significant Void) is determined by the sub cooling of the liquid at this location. The sub cooling has been calculated using Saha and Zuber's model [Saha and Zuber, 1974] as follows:

$$\Delta T_{sub} = 0.0022 q'' \frac{d_h}{(k_t)_l} \quad Pe \le 70000 \tag{4.13}$$

$$\Delta T_{sub} = 153.8 \frac{q''}{V_l \rho_l c_{p,l}} \quad Pe \ge 70000 \tag{4.14}$$

Where Peclet number is defined as $Pe = Re * Pr$.

Validity of the correlation:

$p = 0.1\text{-}13.8$ MPa, $m = 95\text{-}2760$ kg.m^{-2}s^{-1}, $q'' = 0.28\text{-}1.9$MWm^{-2}.

Bubble Departure Radius: The radius at which the bubbles are detached from the wall after reaching their critical size and required subcooling is called the bubble departure radius. Bubble departure radius has been calculated using Unal's semi empirical model [Unal, 1976].

$$R_{bd} = 1.21 \times 10^{-5} \frac{p^{0.709} S}{\sqrt{b\Phi}} \tag{4.15}$$

where

$$b = \frac{T_s - T_l}{2}\left(1 - \frac{\rho_g^0}{\rho_l^0}\right) \tag{4.15a}$$

$$\Phi = \left(\frac{V_l}{0.61}\right)^{0.47} \qquad for \quad V_l > 0.61 ms^{-1}$$

$$= 1 \qquad for \quad V_l < 0.61 ms^{-1} \tag{4.15b}$$

$$S = \frac{T_w - T_s}{2\rho_g^0 h_{evap}}\left(\frac{(k_t)_w \rho_w c_{p,w}}{\pi}\right)^{1/2} \tag{4.15c}$$

The range of validity of the correlation:

Pressure: 0.1-17.7 MPa, Heat flux: 0.47-10.64 MWm^{-2}, Velocity: 0.08-9.15 ms^{-1}, and ΔT_{sub} =3-86 K

4.3.3 Bubble Formation Rate

The heat flux required for evaporation which is transferred from superheated boundary layer into the bubble can be calculated by:

$$q''_{evap} = n f_n V_{bd} \rho_g^0 h_{evap} \tag{4.16}$$

f_n is the detachment frequency of the nucleation center at which bubbles are formed and n is the number of bubble nucleation center per unit area of heating surface. The heat flux required to reconstruct the superheated thermal boundary layer is given by:

$$q''_{GV} = n f_n Q_{recons} \tag{4.17}$$

Q_{recons} is the quantity of heat per nucleation centre withdrawn from the superheated wall to reconstruct the thermal boundary layer. To eliminate the unknown product *nf*, *a* parameter E is being defined as:

$$E_r = \frac{q''_{GV}}{q''_{evap}} = \frac{n f_n Q_{recons}}{n f_n V_{bd} \rho_g^0 h_{evap}} = \frac{q'' - q''_{1\phi}}{q''_{evap}}$$

Hence, $q''_{evap} = \frac{q'' - q''_{1\phi}}{E_r}$ (4.18)

Also from Meister's consideration for thermal boundary layer [Meister, 1979], the parameter E has been calculated as:

$$\frac{1}{E_r} = 2C_{evap}\left(\frac{T_w - T_s}{T_w - T_l}\right)^2 \quad (4.19)$$

C_{evap} = Evaporation parameter

≈ 0.5

Finally, evaporation heat flux is given by:

$$q''_{evap} = 2(q'' - q''_{1\Phi})C_{evap}\left(\frac{T_w - T_s}{T_w - T_l}\right)^2 \quad (4.20)$$

Bubble formation rate:

The bubble formation rate per unit area is given by:

$$\Gamma_g^* = \frac{q''_{evap}}{h_{evap}} \quad (4.21a)$$

Hence the bubble formation rate per unit volume can be calculated as:

$$\Gamma_g = \Gamma_g^* * \frac{U_{he}}{A} = \Gamma_g^* * \frac{q''_{evap}}{h_{evap}} \quad (4.21b)$$

4.3.4 Bubble Condensation Rate

The condensation of bubble in a sub cooled liquid is governed by two effects: (1) heat transfer at the phase interface; (2) inertia of the surrounding liquid. In the case of a large bubble formed with low sub cooling and low flow rate, condensation proceeds very slowly. Hence the inertia of liquid surrounding the bubble can be neglected. In this case condensation is mainly governed by heat transfer at the phase interface. On the other hand, small bubbles, resulting in the case of considerable sub-cooling and high flow rate, condense very rapidly. Owing to the inertia of condensation, the surrounding fluid cannot flow fast enough to fill the space vacated by the condensed bubble. Hence it cannot compensate for the resulting under-pressure. So, a large local pressure fluctuation may arise; this is termed as cavitations effect [Hamit, 1980]. Mayinger and Nordman [1976] have shown that the pressure fluctuations in the vicinity of condensed bubbles increases greatly above Jacob number 100. This is an indication that condensation is predominantly controlled by inertia above Jacob number 100. Chen [1986] has demonstrated by measurements on bubble condensation with the aid of holographic interferometry that a thermal boundary layer exists in the vicinity of condensed bubble, up to Jacob number of 60-80. Up to this boundary, the pressure fluctuations at the end of condensation are slight, which is an indication of heat transfer controlled condensation. Thus Jacob number can be used to differentiate different condensation regions. The Jacob number indicates the ratio between the energy that the liquid requires to reach the saturation state and the heat stored in the steam at the same volume.

$$Ja = \frac{\rho_l^0 c_{p,l}(T_s - T_l)}{\rho_g^0 h_{evap}} \tag{4.22}$$

(1) $Ja \leq 80$: condensation is largely determined by heat transfer at the phase boundary.

(2) $80 < Ja < 100$: transition region. Both the heat transfer and inertia effects are significant.

(3) $Ja \geq 100$: inertia effect is dominant.

Heat transfer controlled condensation

Heat transfer controlled condensation rate has been calculated using Hainoun *et al's* model [1996] as:

$$\Gamma_c = C_c\, 3.6 \frac{\alpha}{d_{bd}^2} \rho_g^0\, \upsilon_l\, Nu_1\, Ja \qquad for\ Re_{ch} < 10^4 \tag{4.23}$$

$$\Gamma_c = C_c\, 3.6 \frac{\alpha}{d_{bd} d_h} \rho_g^0\, \upsilon_l\, Nu_2\, Ja \quad for\ Re_{ch} > 3\times 10^4 \tag{4.24}$$

Here Re_{ch} is the channel Reynolds's number.

For $10^4 < Re_{ch} < 3\times 10^4$, Γ_c is interpolated between the two regions.

C_c is the condensation parameter and equal to 0.16. Nu_1 is given by Hewitt *et al* [1990] as :

$$Nu_1 = 0.185 Re_B^{0.7} Pr^{0.5} \tag{4.25}$$

Re_B is the Bubble Reynolds's number given by: $Re_B = \dfrac{V_r d_{bd}}{\upsilon_l}$ (4.26)

$$Nu_2 = 0.228 Re_{ch}^{0.7} Pr^{0.5} A_v^{0.25} \tag{4.27}$$

. A_v has been introduced by Avdeev [1986] which can be found from the correlation:

$$A_v = 1 \quad for\ \alpha \le 5\%\ ,\ A_v = (1-\alpha)^{-2.53}\ for\ \alpha > 5\% \tag{4.28}$$

Inertia controlled condensation

Inertia controlled condensation has been estimated by Hamit's correlation [1980] as follows:

$$\Gamma_c = C_c \rho_g^0 \frac{\alpha}{\tau_c} \tag{4.29}$$

τ_c is the condensation time [Hamit, 1980] which is given by:

$$\tau_c = 0.458 d_{bd} \left(\frac{\rho_l^0}{p_l} \right)^{\frac{1}{2}} \tag{4.30}$$

Now the expressions for the evaporation rate Γ_g in $kgm^{-3}s^{-1}$ [equation (4.21b)] and condensation rates Γ_c in $kgm^{-3}s^{-1}$ [equations (4.23), (4.24) and (4.29)] have been calculated. Finally Γ_g and Γ_c are put in the vapor mass balance equation [equation (4.2)] to find out the void fraction.

4.4 Results and Discussions

The comparison of simulated results with McMaster test data on axial void distribution has been given in Figure 4.4. The simulated results are matching quite satisfactorily with the test data. The length of heated section is 300 mm. Hence the void fraction keeps rising in between the length 100mm to 400mm as expected. As the rest of the section of the test pipe is unheated the void fraction is decreasing after the heated section. Figure 4.5 shows the channel pressure variation with respect to time at a low system pressure (1.542 bar). Figure 4.6 shows the channel pressure with respect to time at a high system pressure (72 bar). The average void distribution in the channel at low pressure and at high pressure is given in Figure 4.7 and Figure 4.8 respectively.

The possible explanation for the void fluctuation at low pressure may be described as follows. For the same quality, void fraction is larger at high pressure as compared to low pressure. This is because, the latent heat of vaporization decreases with increase of pressure. So, a slight change in quality causes a large change in void fraction at low pressure than at

high pressure. Hence, there is a greater chance that void will oscillate at lower pressure than at higher pressure.

The reason for pressure fluctuation at low system pressure may be attributed to the sudden collapse of bubbles in sub cooled water above the heated section (riser). At high system pressure there is a less possibility of sub cooled boiling to occur. Hence the pressure remains constant at high system pressure.

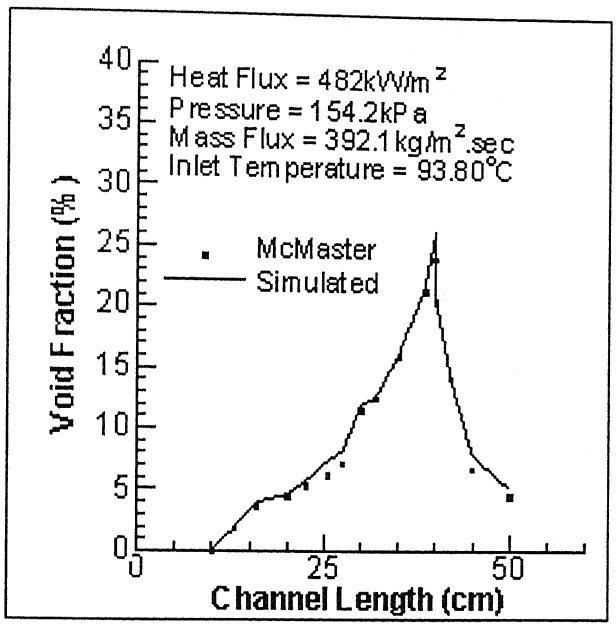

Figure 4.4: Comparison of simulated results with McMaster test data for axial void distribution.

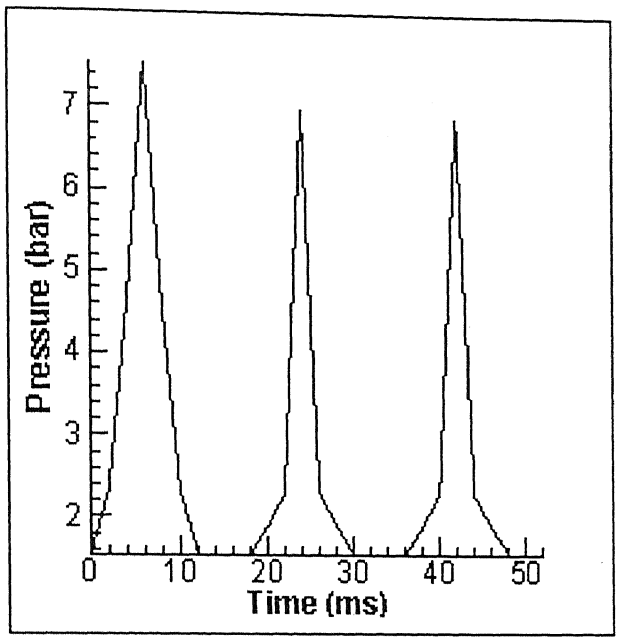

Figure 4.5: Channel pressure variation with respect to time with initial pressure of 1.542 bar

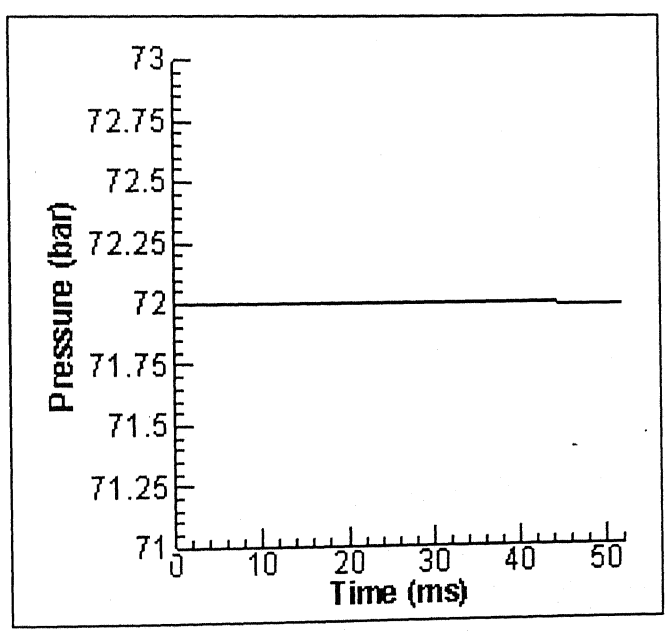

Figure 4.6: Channel pressure variation with respect to time with initial pressure of 72bar.

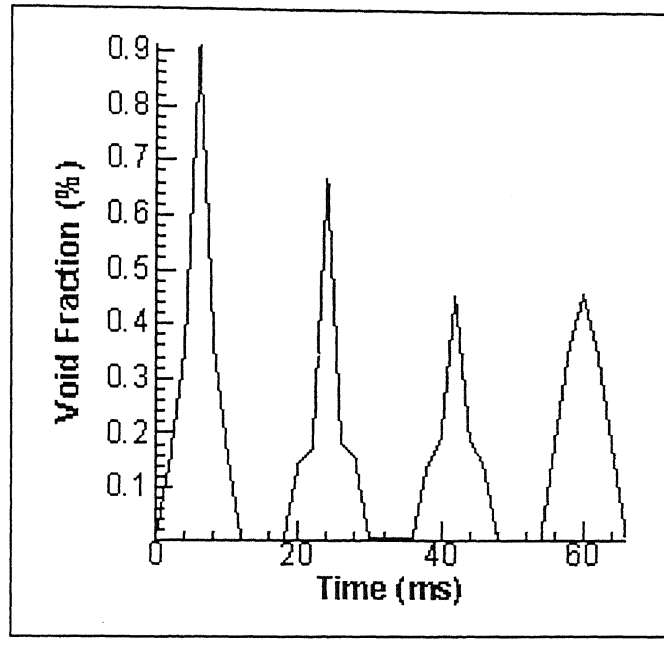

Figure 4.7: Channel average void distribution with respect to time with initial pressure of 1.542 bar.

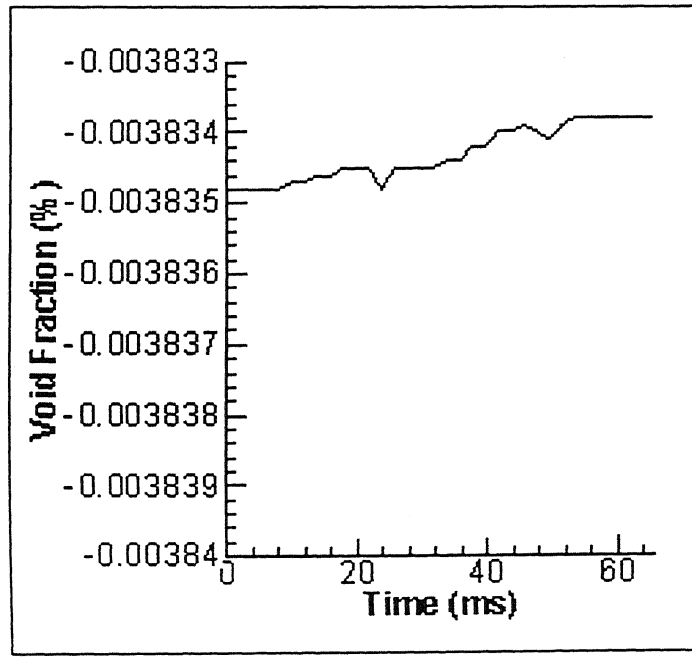

Figure 4.8: Channel average void distribution with respect to time with initial pressure of 72 bar.

4.5 Closure

A model for vapor generation and vapor condensation has been presented in this Chapter. The validity of the model has been checked successfully by validating the results with that of McMaster test data. The model is then used to simulate the geysering phenomenon at start up. In order to gain more confidence in the model, the code has been validated with the Apsara loop experimental test data, which is being done at Bhabha Atomic Research Centre (BARC), Mumbai. This has been described in the next chapter.

Chapter 5

Model Validation

5.1 Apsara Experimental Loop

5.1.1 Introduction

Apsara reactor is a swimming pool type research reactor. It uses enriched uranium-aluminium alloy as its fuel material. It uses light water as moderator and coolant. Cadmium is used as control rod in this reactor. The core size of this reactor is 8.5 m (L) x 3.0 m (W) x 8.2 m (H). The maximum reactor power is 1 MW.

Apsara loop experiment is being carried out at the Apsara reactor site. The neutron source required for the flow visualization is provided by the Apsara reactor. The objective of the experiment is to generate data for the validation of flow pattern transition criteria and developing correlations for flow pattern specific pressure drop. The experiment is being carried out jointly by Reactor Engineering Division (RED), High Pressure Physics Division (HPPD), and Solid State Physics Division (SSPD). HPPD has provided the expertise for the visualization of flow, recording of flow pattern and measurement of void fraction. SSPD has provided the support for neutron radiography. RED is responsible for the design, fabrication, safety and data acquisition. Installation at site and commissioning has been done by RED with on site help from SSPD and ROD.

5.1.2 Experimental Procedure

First the total system is filled with water with the help of hand pump and vented out any stranded air inside the water. Some amount of water is drained out to maintain a certain level in the steam drum. Also pressurized nitrogen gas has to be supplied to bring the loop to the desired pressure level. The usual practice is to keep the pressure up to 4 bars higher than the desired system pressure for taking into account the leakage and dissolution of nitrogen with water. Once it is assured that the system is devoid of air bubble, the power is supplied to the system from heater and temperature is raised to the saturation temperature corresponding to the system pressure. Initially low power is supplied to the system. Later on as the temperature of the heated section as well as the fluid temperature stabilizes, power is increased. This raise in power is done in steps of 150W to 200W at a time. Maximum power to the heated test section depends on at what pressure the experiment is being carried out. After some time the system natural circulation starts, which becomes evident from the Δp readings. But two-phase will not be initiated as the actual pressure is still higher than the system pressure. To have two-phase natural circulation, some amount of pressure from the system is needed to be released. This is done through the vent valve provided at the top of the heat exchanger. Once the fluid temperature crosses the saturation temperature corresponding to the experimental pressure, it can be said that two-phase flow has been established. The experiment has been carried out for various tube sizes. The loop inventory corresponding to that tube size is given in the following Table 5.1.

Test section(dia.)	Inventory with condenser(liters)	Inventory without condenser(liters)
3/8" (7.035 mm)	3.75	2.072
1/2" (10.21 mm)	4.14	2.460
3/4" (15.74 mm)	5.16	3.490
1" (19.86 mm)	6.24	4.560

Table 5-1: Loop inventory corresponding to various pipe sizes

Maximum operating temperature and pressure of the system are 315 ^{0}C and 125 bar respectively. But in the present loop, the experiments were carried out at low pressure and temperature. Experimental set up is shown in the Figure 5.1.

TEST LOOP FOR FLOW PATTERN TRANSITION STUDIES

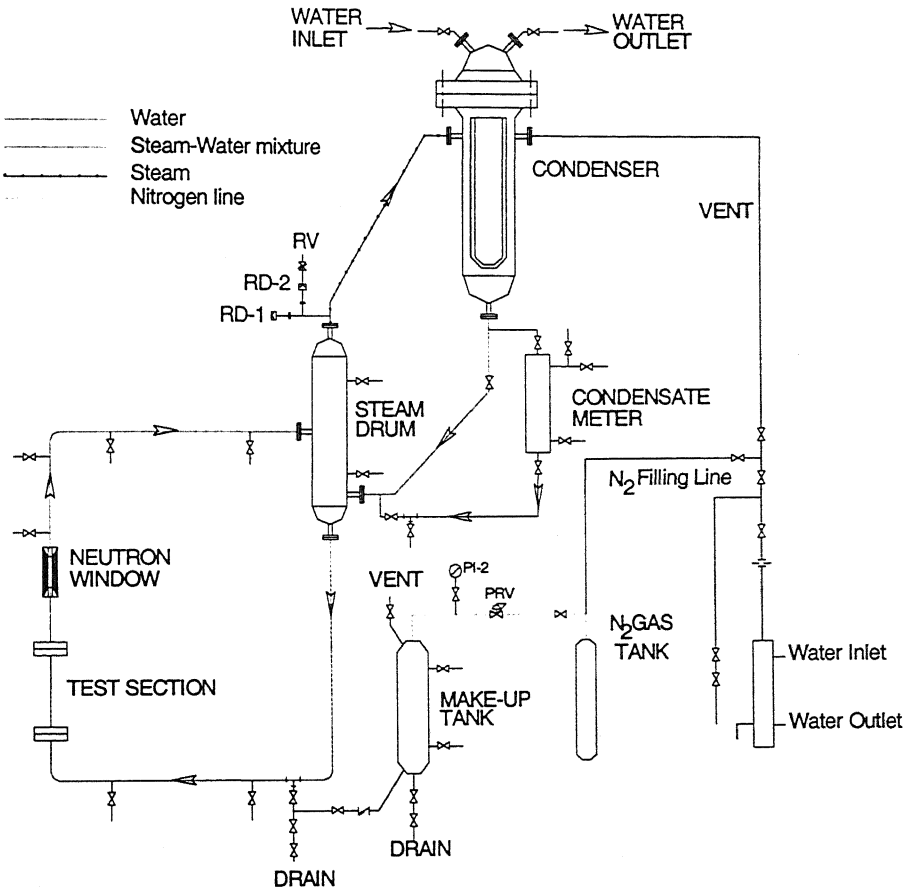

SIMPLIFIED FLOW SHEET

DESIGN PARAMETERS

pressure : 125 bar

Temperature : 315 °C

Power : 10 kW

Location : Apsara Reactor Hall

Figure 5.1: The Apsara experimental loop.

5.2 Void Fraction Measurement Techniques

Visualization of flow pattern and measurement of void fraction are very important to the study of two-phase flow. Observations of flow pattern are necessary to understand the physics of two-phase flow and to validate the flow pattern transition criterion. Conventionally optical method using glass tubes supplemented by X-ray, gamma rays and conductance probe methods are used for flow visualization. In the present work neutron radiography and conductance probe has been used.

5.2.1 Neutron Radiography

Most of the real life application in industry and particularly nuclear industry demands that flow pattern must be studied inside metallic pipe and that too under high pressure, temperature and heat flux. Conventional optical methods for flow visualization cannot be applied in such cases. X-ray or Gamma ray probe though easy to use, are not suitable for the simple reason that attenuation of these rays due to metallic wall of pipe is much more than that due to the water steam mixture. Also this technique is much less sensitive to the changes in the composition of the water-steam mixture.

In the present neutron radiography thermal neutron has been used. It's because thermal neutron can easily penetrate most of the metals used for pipes and have quite high sensitivity. Experimental set up of neutron radiography is shown in the Figure 5.2. The neutrons are absorbed by the water layers but passes through the voids. These unabsorbed neutrons are converted into light by the converter and it falls on the mirror where it gets reflected to another mirror. This is then viewed by the high sensitivity camera. Images are stored in image recorder and signals are passed to the data logger.

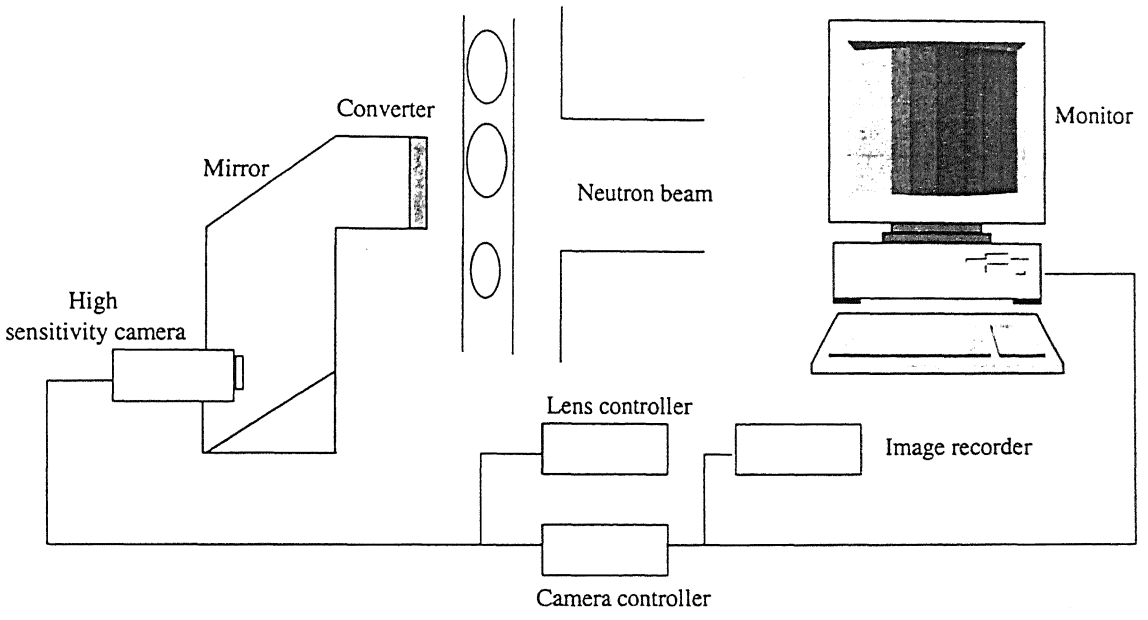

Figure 5.2: Schematic of void fraction measurement by neutron radiography.

5.2.2 Conductance Probe

The schematic of conductance probe is shown in the Figure 5.3. It works on the principle of change of resistance with change in flow pattern. Working principle of the conductance probe is shown in the Figure 5.4 and Figure 5.5. Conductance probe is supplied with DC power supply, voltmeter and a resistance. When there is no void in the flow across the probe then the voltage measured is due to the resistance R_1. But when there is change in flow pattern i.e. voids in the flow, there is a large resistance across the probe than R_1. This means that the voltage across R_1 is less than the former case. Conductance probe assembly is connected to the PC for data acquisition and processing. The void fraction is measured with the help of following formula,

$$\text{Void fraction} = \frac{\text{Time elapsed between the changes of resistance}}{\text{Total time}} = \frac{T_1}{\text{Time}}$$

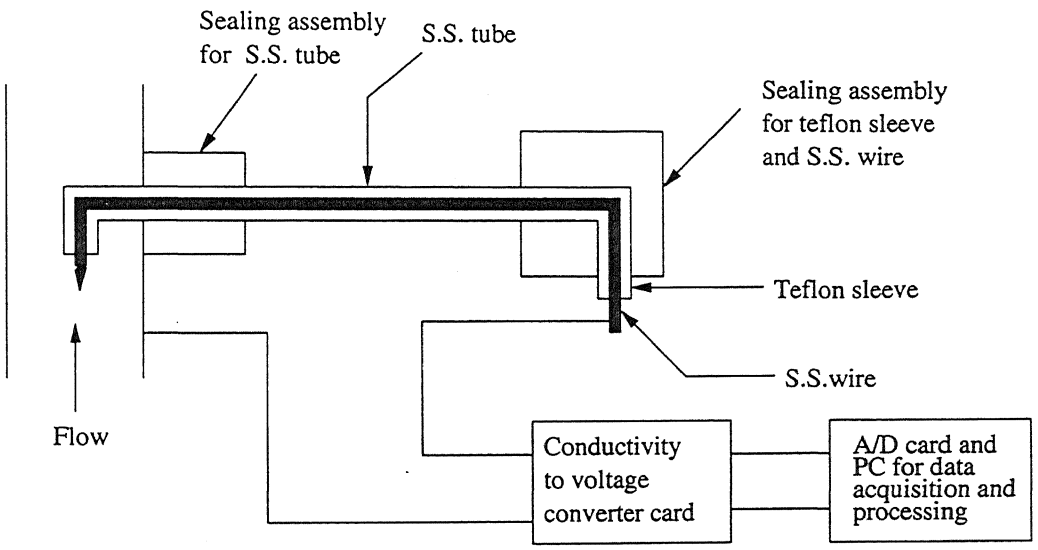

Figure 5.3: Schematic of Single point conductance probe.

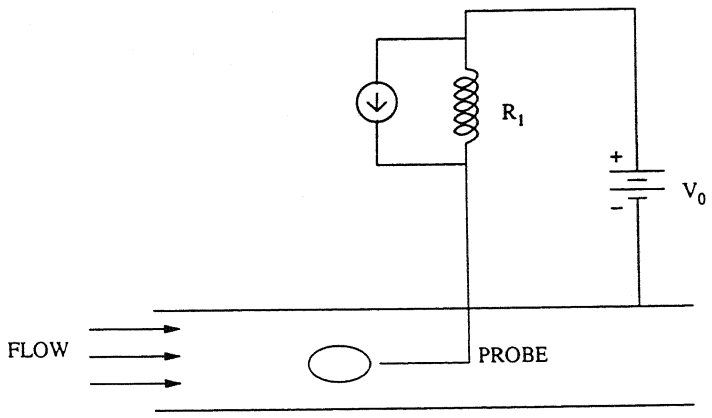

Figure 5.4: Electrical circuitry of a Single point conductance probe.

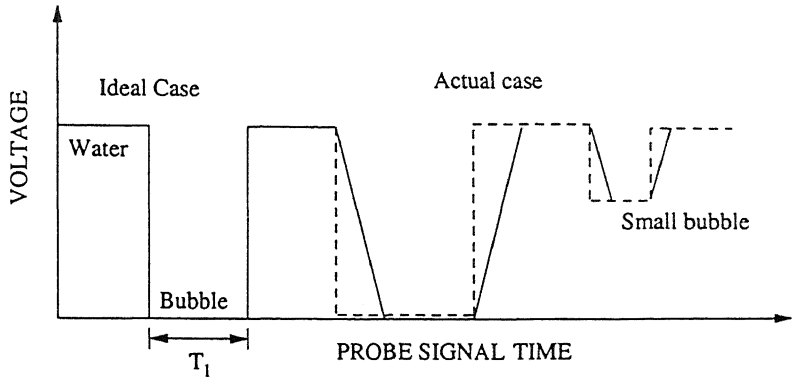

Figure 5.5: Voltage signal from the probe.

5.3 Results and Discussions

The simulated results have been compared with the experimental data. The experimental as well as the simulated results have been reported below.

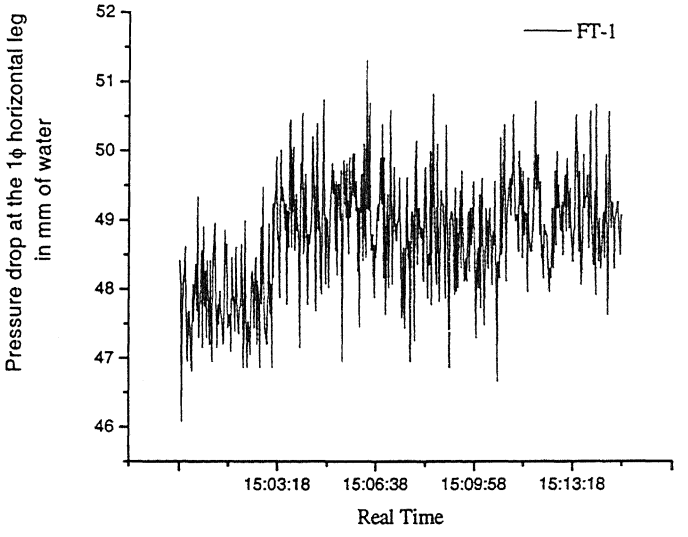

Figure 5.6: Experimental single phase pressure drop in the horizontal leg of Apsara Loop.

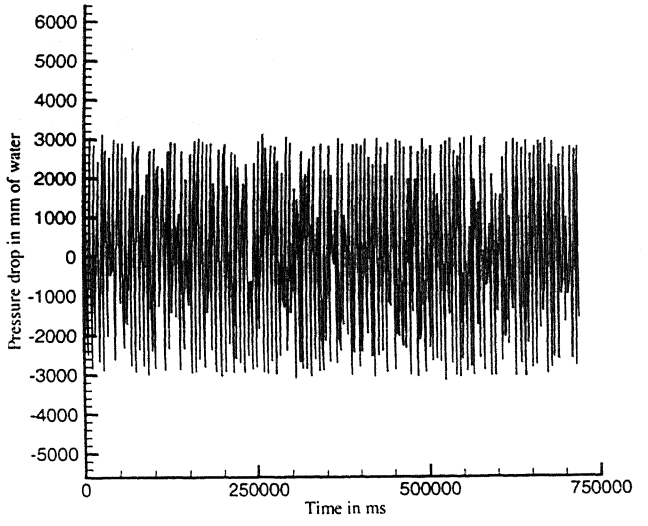

Figure 5.7: Simulated single phase pressure drop in the horizontal leg.

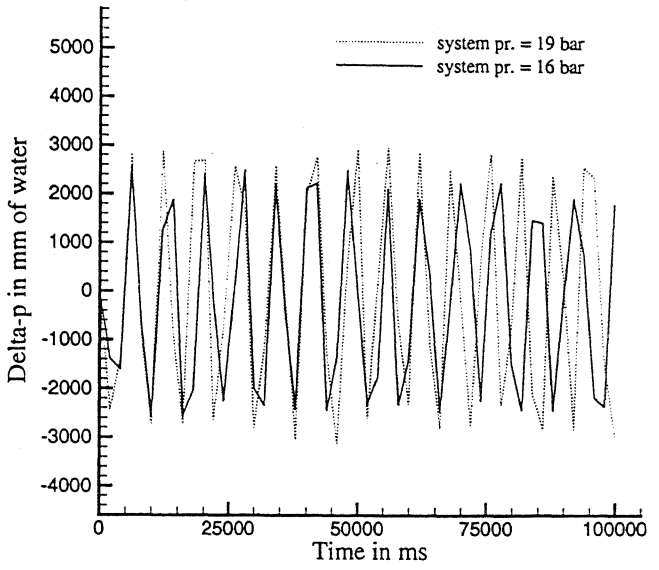

Figure 5.8: Variation in simulated single phase pressure drop with change in system pressure.

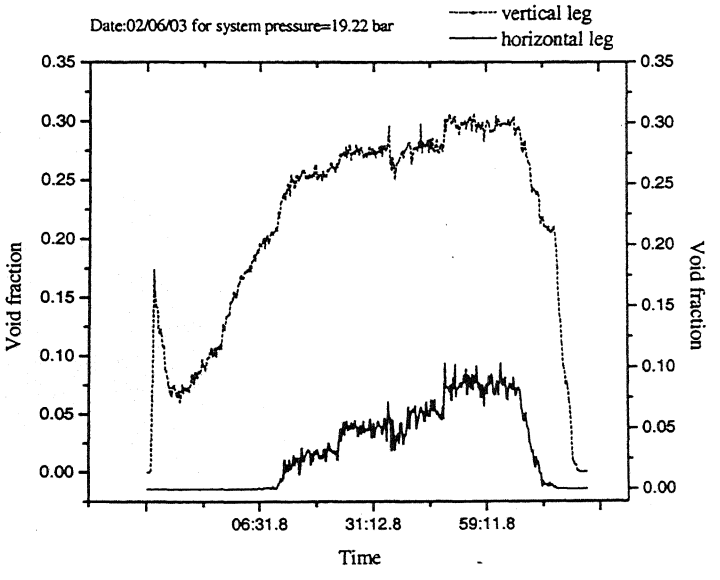

Figure 5.9: Experimental Void fractions measured in Conductance probe.

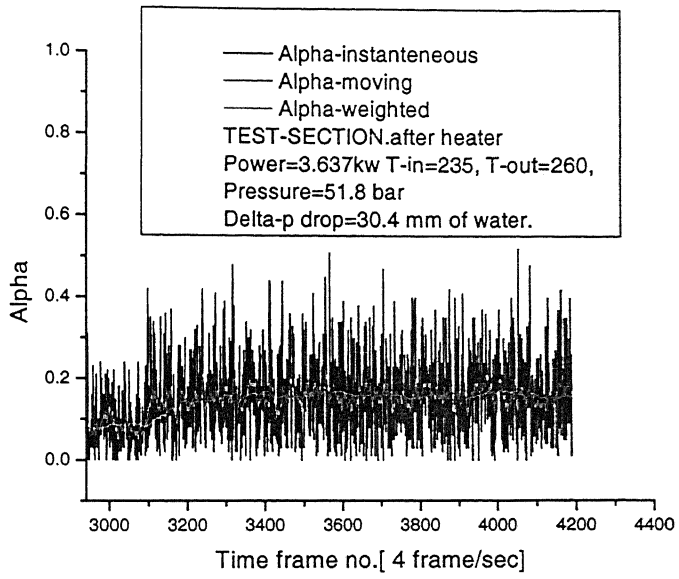

Figure 5.10: Experimental Void fraction measured by Neutron Radiography.

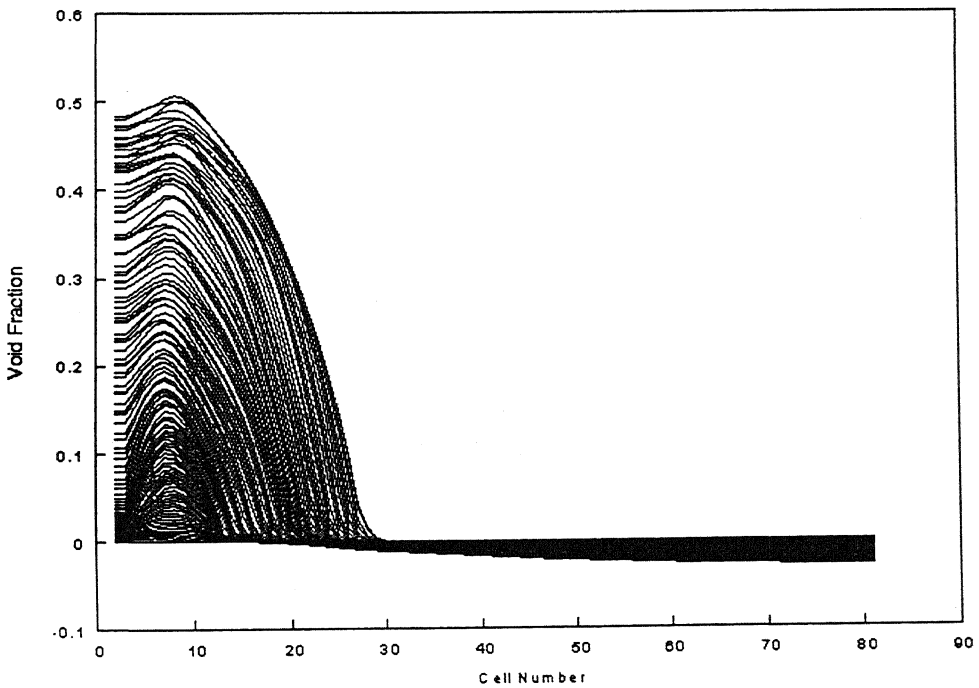

Figure 5.11: Simulated Void fraction in the two phase leg at system pressure 19.22 bar.

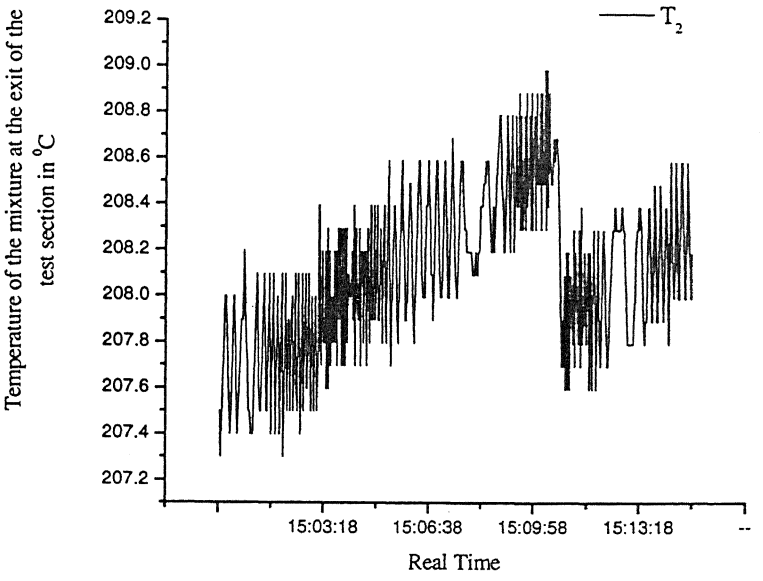

Figure 5.12: Experimental Temperature variation at the exit of the test section.

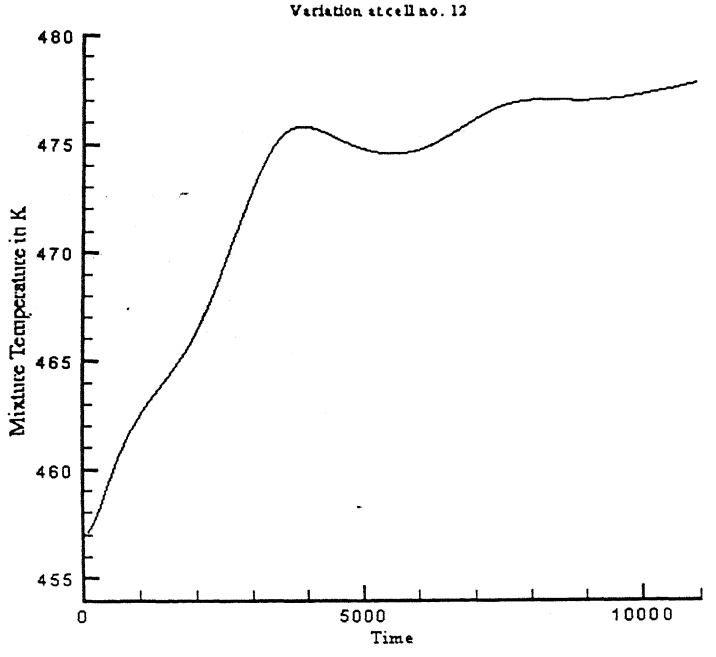

Figure 5.13: Simulated Temperature variation at the exit of the test section.

5.4 Code Tuning Parameters

5.4.1 Numerical Stability

The following parameters are essential in fine tuning the code.

i) Upstream differencing parameter β :

Convection Dominance:

(a) A value of 0.2-0.3 for β gives good results with LOCA conditions and at high pressure simulation.

(b) $\beta = 1$ gives full up streaming or forward differencing.

$\beta = 0$ gives central differencing.

The order of accuracy of central difference scheme is $o(h^2)$ whereas the order of accuracy of forward and backward difference scheme are $o(h)$. Therefore $\beta = 0$ will give a more accurate result; but this poses a problem in the stability of the numerical scheme. This is discussed in the following paragraph.

$$Pe = Re_{2\phi} * Pr_{2\phi} = \frac{V_m d}{\alpha_{2\phi}} \tag{5.1}$$

where $\alpha_{2\phi}$ is thermal diffusivity and Pe number indicates the strength of convection and diffusion in two phase flow. Hence, the condition $Pe >> 1$ indicates that convection is more dominant. The qualitative temperature distributions T vs x (with Pe as parameter) are indicated in Figure 5.14.

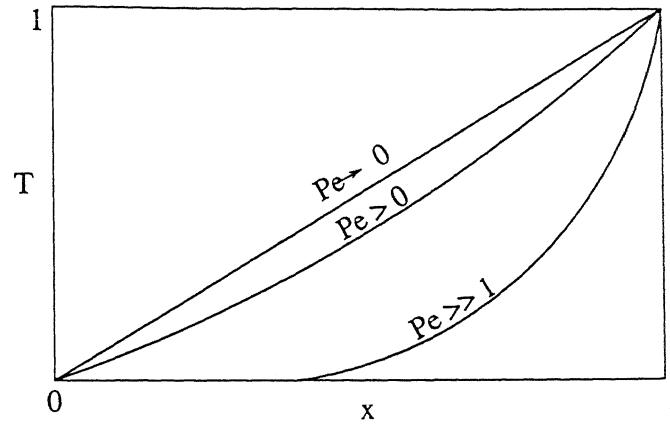

Figure 5.14: The fluid temperature profile as a function of Peclet number.

From the above figure it can be inferred that when convection is more dominant then upstream differencing scheme is more realistic as it uses backward difference for the convection term. In the present study, the convection term is more dominant as $Pe >> 1$. Hence $\beta \approx 0.8 - 0.9$ is suggested; since β more close to 1 means proximity to upstream differencing.

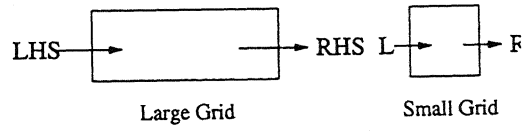

Figure 5.15: Grid Size

When using smaller grid size upwinding is more realistic as RHS value will clearly depend upon LHS. On the other hand, central differencing is suggested when using larger grid size. As the difference in values at LHS and RHS is large, an average of both the values will fit as the value of the entire cell.

ii) Time Step Δt

Apart from calculating the effective Courant number Δt can be utilized to choose a proper method out of Pure-implicit, Implicit-explicit (semi implicit) and explicit schemes. Courant number is defined as $V_m \Delta t/\Delta y$.

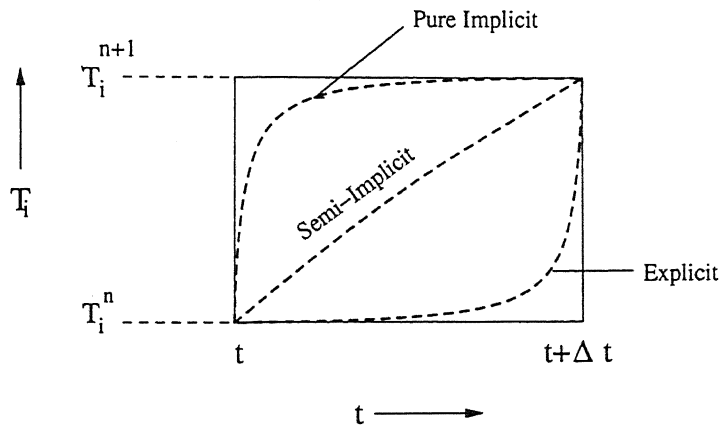

Figure 5.16: Physical representation of various numerical schemes.

Hence if Δt is large, then pure implicit is more realistic whereas for small Δt semi-implicit is more realistic.

iii) Stability Control Parameter.

It is used to set the effective Courant number for stability of the numerical scheme as

$$\frac{(V_m)_{max}\Delta t}{\Delta y} \leq \frac{1}{STABC} = \frac{1}{4} \qquad (5.2)$$

The purpose of viscosity in viscous stress term is to damp the high frequency oscillations that can not be resolved or would lead to numerical instability. But the magnitude of υ_s (Specified Kinematic viscosity coefficient) must not be so large as to appreciably damp the larger scale flow instabilities of physical interest.

Let, $\frac{(V_m)_{max}\Delta t}{\Delta y} = f$

υ_s is calculated using Hirt's[C.W. Hirt, 1968] results as:

$$\upsilon_s \approx \frac{(V_m)_{max}\Delta y}{2}\left[\frac{1}{2}+\frac{(V_m)_{max}\Delta t}{\Delta y}\right]$$

$$=\frac{(V_m)_{max}\Delta y}{2}\frac{\Delta y}{\Delta y}\frac{\Delta t}{\Delta t}\left[\frac{1}{2}+\frac{(V_m)_{max}\Delta t}{\Delta y}\right]$$

$$=\frac{(V_m)_{max}\Delta t}{\Delta y}\left[\frac{1}{2}+\frac{(V_m)_{max}\Delta t}{\Delta y}\right]*\frac{(\Delta y)^2}{2\Delta t}$$

$$=f\left(\frac{1}{2}+f\right)\frac{(\Delta y)^2}{2\Delta t} \qquad (5.3)$$

To avoid diffusion instability, we also require

$$4\upsilon_s\Delta t < (\Delta y)^2 \text{ with } \upsilon_s = \frac{\mu_{2\phi}}{\rho_{2\phi}}.$$

This is automatically satisfied provided $f < 1/2$.

$f = 1/4$ provides a better solution, which simultaneously ensures sufficiently small fluid motion per cycle and adequate dissipation, while precluding diffusion instability and excessive damping.

iv) Pressure Convergence Rate Parameter.

This is the relaxation parameter $\Omega(OMG)$ for the calculation of Δp in the pressure iteration. This variable affects the rate of convergence. A value of $OMG = 1.7$ often improves the rate of convergence for low Mach number flows. For high Mach number flows (Supersonic), $OMG = 1.0$ or near to 1 is suggested. Two phase flow under natural convection is at Mach number less than unity.

v) Convergence Criteria.

While working with low pressure more stringent $(\varepsilon \cong 10^{-5})$ convergence criteria can be set. Also while working with double precision, a strict convergence criteria $(\varepsilon \cong 10^{-8})$ is expected. For single precision, generally the convergence criterion is of the order of $(\varepsilon \cong 10^{-3})$. However, more strict criteria lead to more CPU time for running the code.

A **sensitivity analysis** has been carried out in double precision to study the effect of ε on the results and on the number of iterations to converge.

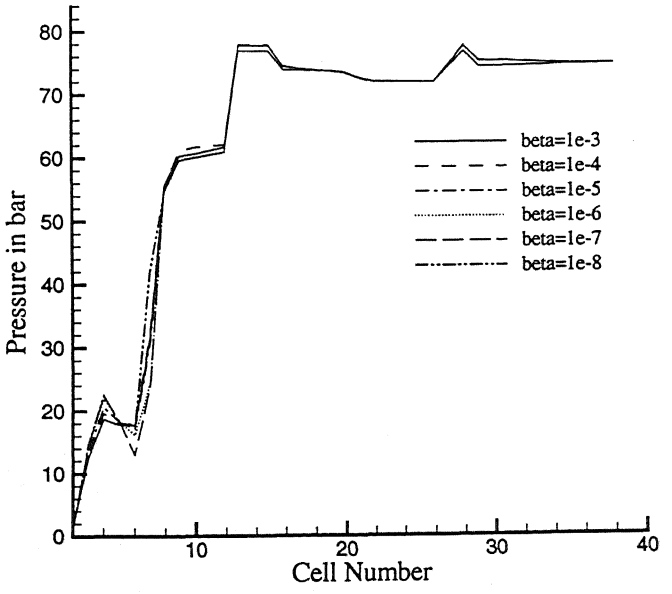

Figure 5.17: Pressure Variation with ε as a parameter.

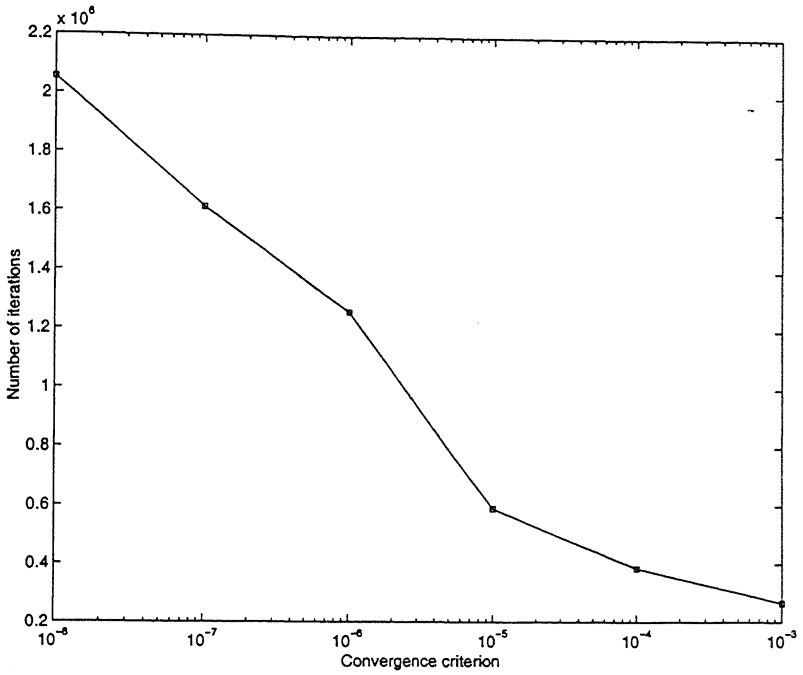

Figure 5.18: Variation of Number of Iterations with ε.

From the sensitivity analysis it is concluded that applying a stricter convergence criterion does not refine the results. On the contrary it increases the number of iterations for convergence; thereby increasing the CPU time.

vi) Subcycle Parameter.

This specifies the desired number of sub cycles in the code. A large network system often contain low speed flow (Low Mach Number) with slowly varying properties in one region and high speed flow or flow that requires a finely detailed description in another region. Hence a provision is made in the present work that allows the use of different time steps for integration in each component and junction cell in the network. It's because the time step can be significantly different in the various components; that is one component may have to be integrated several time steps to keep pace with one time integration in another component. This subcycling feature enables accurate time integration.

5.4.2 Heat Transfer

i) Heat Flux and Wall Temperature.

(a) Q_{flux}: It can be calculated directly from the power supplied to the test section. As the power that is supplied has to be distributed uniformly in the test section volume, the heat flux per unit volume is given by

$$Q_{flux} = \frac{Power}{\pi * r_i^2 * Height\ of\ the Test\ section}$$

(b) T_{wall}: The second option may be to calculate the Q_{flux} from the given wall temperature of the test section.

$$Q_{flux} = h_i A_i \Delta T_i \tag{5.4}$$

Dittus-Bolter correlation gives

$$h_i = 0.023 \frac{k_m}{d_i} Re_m^{0.8} Pr_m^{0.4} \text{ where } Re = \frac{\rho_m V_m d}{\mu_m} \text{ and } Pr = \frac{\mu_m (C_p)_m}{k_m}. \tag{5.5}$$

$$(C_p)_m = x(C_p)_g + (1-x)(C_p)_l \tag{5.5a}$$

$$\frac{1}{\mu_m} = \frac{x}{\mu_g} + \frac{1-x}{\mu_l} \tag{5.5b}$$

$$A_i = \pi d_i * Height\ of\ the Test\ section$$

$$\Delta T_i = T_{wi} - T_m$$

ii) ETEM

ETEM=1: Liquid and Vapor phases are maintained at equal temperature.

ETEM=0: The vapor phase is maintained equal to saturation temperature at the local pressure.

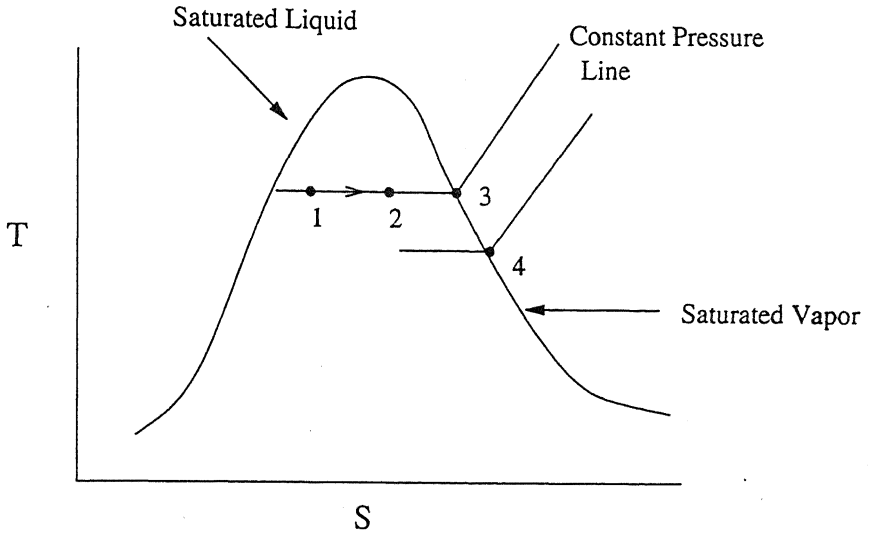

Figure 5.19: Phase equilibrium diagram on T-S coordinate.

$T_l = T_g$ essentially means it can be at state 1 or 2.

$T_g = T_s$ means it can be at 3 or 4.

When inventory is very large and void fraction is less, then the large heat content of the liquid phase keeps the liquid temperature nearly invariant. For such case $T_l = T_g$ or $T_g = T_s$ makes little difference. For low flow and low pressure condition with sufficiently large void $(\alpha > 0.5)$ the two phases move with a very small speed. Hence the interaction time between the two phases is large. Therefore the possibility of attaining equilibrium is bright. On the other hand, in the case of high pressure, high void with turbulent flow condition (High Reynolds number), is a highly non-equilibrium state. Here the assumption of saturated vapor at local pressure will fit well.

iii) Number of Bubbles per unit Volume

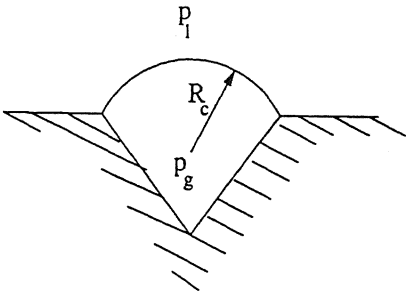

Figure 5.20: Vapor Bubble Nucleus

If R_c=Radius of curvature of the nucleus surface, then surface tension creates a pressure within the nucleus such as

$$p_g = p_l + \frac{2\sigma}{R_c} \tag{5.6}$$

Clausius-Clapeyron equation gives $\frac{dp}{dT} = \frac{h_{evap}}{T\left(\frac{1}{\rho_g^0} - \frac{1}{\rho_l^0}\right)}$ (5.7)

Assuming that the steam behaves like an ideal gas, $\frac{1}{\rho_l^0} << \frac{1}{\rho_g^0}$. Hence $\frac{1}{\rho_l^0}$ is neglected.

Therefore $\frac{dp}{dT} = \frac{\rho_g^0 h_{evap}}{T}$ (5.8)

Integrating and using equation (1) we have $R_c = \frac{2\sigma}{\rho_g^0 h_{evap}} \frac{T_s}{T_g - T_s}$ (5.9)

R_c is also known as active nucleus radius; that is only after reaching R_c, nucleus will be activated and can lead to a bubble.

From equation (2) it is clear that with increasing wall superheat $(T_g - T_s)$, the active bubble radius (R_c) will decrease. That means all nuclei of higher radii than R_c will be

activated. Thus the chances of formation of large nucleating site have enhanced. This is also confirmed by the following fact.

$$A_{1\phi} = 1 - n_b \pi \overline{R}_b^2$$

where $A_{1\phi}$ is the heating surface fraction which is bubble free and in direct contact with sub-cooled liquid. $\pi\overline{R}_b^2$ is the projection area of bubble on the heating surface. $\overline{R}_b$ will decrease as the radius of active nucleus R_c decreases. Therefore, for a constant $A_{1\phi}$, with decreasing $\overline{R}_b$, n_b will increase.

iv) ρ_l^0 AS A FUNCTION OF TEMPERATURE

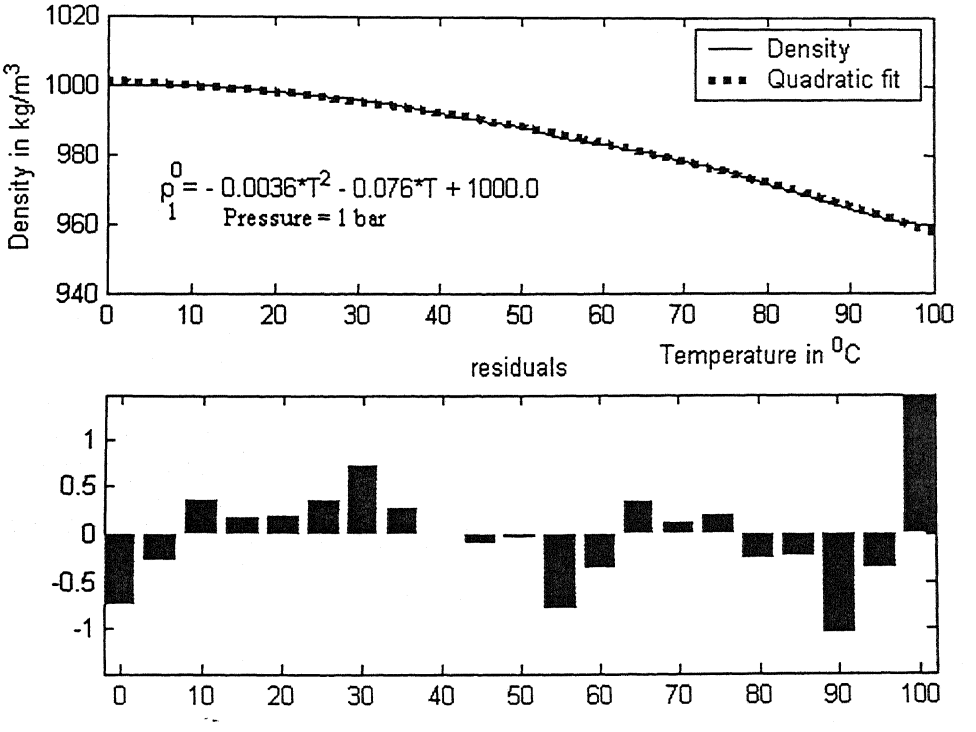

Figure 5.21: Variation of density with temperature and the residuals of quadratic fit.

The variation of liquid density with temperature has been plotted. Then a quadratic curve fitting has been performed to obtain the equation of dependence of density with temperature. The equation so obtained is found to be,

$$\rho_l^0 = -0.0036*T^2 - 0.076*T + 1000.0 \qquad (5.10)$$

5.4.3 Hydrodynamics

i) Relative Velocity Parameter

DFVEL is a program control parameter that determines whether the relative velocity is to be calculated or not. A value of DFVEL =1 calculates the drift velocity whereas DFVEL = 0 bypass the drift velocity subroutine.

Hence, a value of DFVEL = 0 and ETEM = 1 will convert the Drift Flux Model to a HEM (Homogeneous Equilibrium Model).

ii) Turbulence Parameter β_t

$$V = |\underline{V_r}| + \beta_t |\underline{V_m}|$$

$\underline{V_m}$ = Mass averaged mixture velocity

$\underline{V_r}$ = Average relative velocity

β_t = Parameter accounting for turbulent fluctuation

Generally β_t has a value of 0.1 or less because large turbulent velocity fluctuations often have magnitudes as large as 10% of the mean velocities. Nevertheless, the best value of β_t must be determined by comparison with experimental data.

A **sensitivity analysis** of β_t has been performed with respect to the mixture velocity. From the analysis it can be concluded that β_t has a very minute effect on the mixture velocity at high system pressure.

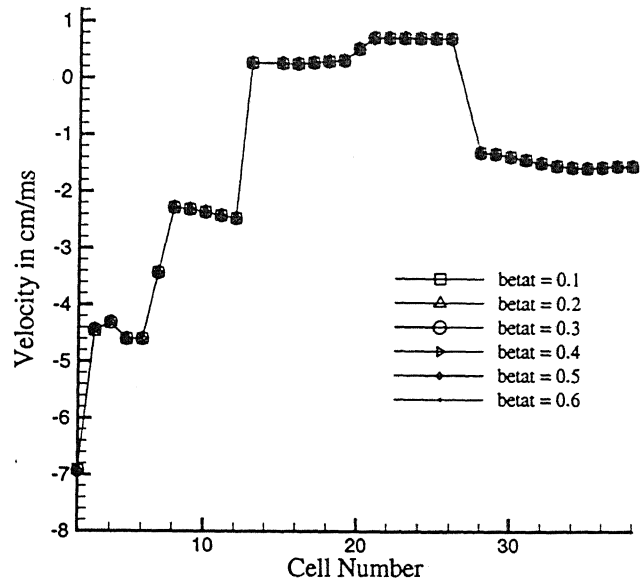

Figure 5.22: Variation of Mixture Velocity with β_t as a parameter.

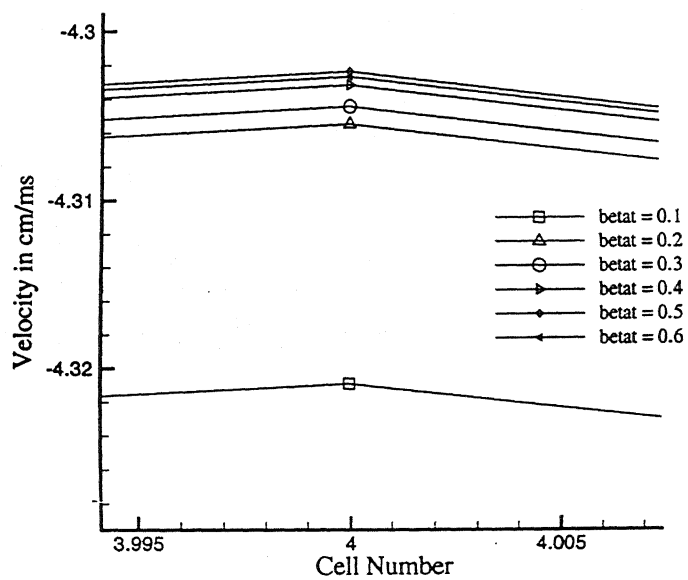

Figure 5.23: Enlarged View of the above figure.

Chapter 6

Conclusions and Scope for Future Work

6.1 Conclusion

A four equations Drift Flux model has been used for numerical simulation in the present work. The focus of the research is to bench-mark the geysering phenomenon. In the first stage of the present work the code has been tested to simulate small break LOCA condition. In the second stage, a vapor generation and bubble condensation model has been incorporated in the code. The model has been then validated with McMaster experimental test results on axial void fraction distribution. This model has been used to simulate geysering phenomenon in the same McMaster experimental set up. Finally the usefulness of the code has been studied while trying to validate the Apsara Loop experimental test data for void fraction at the two phase leg, pressure drop in the single phase leg and temperature of the liquid in the loop.

6.2 Scope for Future Work

The present work has opened up new areas of exploration. Following challenges are recommended for future researchers.

1. The simulation of Apsara Loop has been done by considering two sub-systems. One consisting of single phase leg and the other having two phase flow. The simulation of Apsara Loop as a whole is desirable to obtain more realistic solution.
2. A non-uniform initialization of all primitive variables (Pressure, Temperature, Velocity and Void fraction is expected. The code should have the provision for taking
   (a) initial condition as given and
   (b) initial condition as output of previous simulation.
3. Temperature dependent initialization of microscopic liquid density (ρ_l^0) should be incorporated.
4. The coalescence of bubbles has not been included. Therefore a model for the coalescence of bubble should be incorporated.
5. The model should be extended to two dimensional and three dimensional domains for better visualization.
6. Better estimation of momentum exchange function has to be made taking into account Basset, Virtual mass and Faxen forces.

References

1. Aritomi, M., J. H. Chiang and M. Mori, (1993).Geysering in parallel boiling channels, *Nuclear Engineering and Design,* **Vol. 141,** pp. 111-121.
2. Aritomi, M., T. Nakahashi, J.H. Chiang, M. Wataru and M. Mori,(1992).Fundamental study on thermo-hydraulics during startup in natural circulation boiling water reactors(I) *Journal of Nuclear Science and Technology,* **Vol. 29[7],** pp.631-641
3. Avdeev, A. A. (1986). The rate of growth (condensation) of vapor bubbles in a turbulent flow, *Thermal Engineering,* **Vol. 33 [1],** pp. 30-33
4. Bankoff, S. G., (1960). A variable density single-fluid model for two-phase flow with particular reference to steam-water flow, *Journal of Heat Transfer,* **Vol. 82,** pp.265-271.
5. Bankoff, S. G., and R. D. Mikesel, (1958). Bubble growth rates in highly sub cooled nucleate boiling, *Chemical Engineering.* , **Vol. 29,** pp.55-61.
6. Bergels, A. E., J.G. Collier, J.M. Delhaye, G.F. Hewitt and F. Mayinger,(1981) *Two-Phase Flow and Heat Transfer in the Power and Process Industries,* Hemisphere, Washington D.C..
7. Boure, J. A., A. E. Bergles and L. S. Tong, (1973). Review of two-phase flow instability, *Nuclear Engineering Design,* **Vol. 25,** pp. 165-192.
8. Bunsen, R., (1958).*Lib. Annalen der Physik and Chemie,* **Vol. 62.**
9. Chan, Y. L. and C. L. Tien (1985).A numerical study of two-dimensional natural convection in square open cavities, *Numerical Heat Transfer,* **Vol. 8,** pp.65-80.

10. Chatoorgoon, V., G.R. Dimmick, M.B. Carver, W.N. Selander and M. Shoukri, (1992). Application of generation and condensation models to predict sub cooled boiling void at low pressure, *Nuclear Technology*, **Vol. 98,** pp.366-378

11. Chen, Y. M., (1986). *Warmeubergang an der Phasengrenze kondensierender Blasen, Dissertation,* Technische Universitat, Munchen.

12. Chexal, V. K., A. E. Bergles, (1973). Two-phase flow instabilities in a low pressure natural circulation loop. *AIChe Symposium Series,* **Vol. 69**, pp. 37-45.

13. Chiang, J.H.,M. Aritomi, M. Mori, and M. Higuchi, (1994).Fundamental study on thermo hydraulics during startup in natural circulation BWRs(III).*Journal of Nuclear Science and Technology,* **Vol. 31[9]**,pp.883-893

14. Chiang, J.H., M. Aritomi, R. Inoue and M. Mori, (1992).Thermo hydraulics during startup in natural circulation boiling water reactors, *NURETH-5, September.*

15. Donevskin, B., and M. Shoukri, (1989). Experimental study of sub cooled flow boiling and condensation in annular channels, *McMaster University Rep. ME/89/TFRI*

16. Donald, D. Gray and Aldo Giorgini, (1976).The validity of the Boussinesq approximation for liquids and gases, *International Journal of Heat Mass Transfer,* **Vol. 19**, pp.545-551.

17. Duffey, R. B. and U. S. Rohatgi, (1994).Physical interpretation of geysering phenomena and periodic boiling instability at low flows. *International Conference on new trends in nuclear system thermo hydraulics, Proceedings,* **Vol. 1,** *May 30th –June 2nd,* Pisa, Italy.

18. Gartia M.R., A.K. Nayak, P.K. Vijayan, D.Saha, A. Khanna (2003).Simulation of geysering at start-up in a natural circulation loop, *International Symposium on Process Systems Engineering and Control, ISPSEC'03*, IITB, Mumbai.

19. Govier, G. W. and A. Aziz, (1972).*The Flow of Complex Mixture in Pipes.* Van Nostrand-Rheinhold Co., New York.

20. Griffith, P., J.A. Clark, and W. M. Rohsenow, (1958). Void volumes in sub cooled boiling systems, *ASME Journal of Heat Transfer,* **Vol. 19.**

21. Gunther, F. C. and Pasadena Calif, (1951). Photographic study of surface boiling heat transfer to water with forced convection, *Transactions of ASME, February.*

22. Hainoun ,A. , E. Hicken , J. Wolters ,(1996). Modeling of void formation in the sub cooled boiling regime in the ATHLET code to simulate flow instability for research reactors, *Nuclear Engineering And Design*, **Vol. 167,** pp.175-191

23. Hamit, F. G. (1980). *Cavitation and Multiphase Flow Phenomena*, McGraw-Hill, New York

24. Harlow, F. H. and Anthony A. Amsden, (1971).A numerical fluid dynamics calculation method for all flow speeds, *Journal of Computational Physics,* **Vol. 8,** pp.197-213.

25. Hewitt, G. F., F. Mayinger and J. R. Riznic, (1990). *Interphase Phenomena in Multiphase Flow,* Hemisphere, New York, pp.432-442.

26. Hirt, C. W., (1968). *Journal of Computational Physics*, **Vol. 2**, pp. 339.

27. Hughes, E. D. and L. J. Agee, (1981).A Drift-flux model of two-phase flow for RETRAN. *Nuclear Technology*, **Vol.54**, pp. 410-421.

28. Inada, F. and Y.Y. Yasuo, (1992). The boiling flow instability of a natural circulation BWR with a chimney at low pressure start up. *Proceedings of the International Conference on Design and Safety of Advanced Nuclear Power Plants,* **Vol. 3,** *October.*

29. Ishii, M. and K. Mishima, (1984). Two fluid model and hydrodynamic constitutive relations, *Nuclear Engineering and Design,* **Vol. 82,** pp. 107-126.

30. Ishii, M., (1975). *Thermo-fluid dynamic theory of two-phase flow,* Eyrolles, Paris.

31. Jaluria, Y. (1980). *Natural Convection Heat and Mass Transfer,* Pergamon Press, Headington Hill Hall, Oxford, England.

32. Liles, D. R. and W. H. Reed, (1978).A semi-implicit method for two-phase fluid dynamics, *Journal of Computational Physics,* **Vol. 26,** pp. 390-407.

33. Masuhara, Y., O.Yokomizo, Y. Bessho and T.Fukahori, (1993).Research on Geysering phenomena in natural circulation BWR. *Proceedings of the 2nd ASME and JSME nuclear engineering joint conference,* **Vol. 1**, *March.*

34. Meister, G., (1979). Vapor bubble growth and recondensation in subcooled boiling flow, *Nuclear Engineering and Design,* **Vol. 54**, pp. 97-114.

35. Moalem-Maron, D., and W.Zijl, (1978).Growth, condensation and departure of small and large vapor bubbles in pure and binary systems, *Chemical Engineering Science*, **Vol. 33**, pp.1339-1346.

36. Moalem, D. and S. Sideman, (1973).The effect of motion on bubble collapse. *International Journal of Heat Mass Transfer,* **Vol. 16**, pp.2321.

37. Nayak, A. K., P.K. Vijayan, D. Saha, V. Venkat Raj, M. Aritomi, (2002). Study on the stability behaviour of a natural circulation pressure tube type boiling water reactor, *Nuclear Engineering and Design,* **Vol. 215,** pp. 127-137.

38. Nayak, A. K., P.K. Vijayan, D. Saha and V. Venkat Raj, (1995). Mathematical modeling the stability characteristics of a natural circulation loop. *Mathematical and Computer Modeling,* **Vol. 22 [9],** pp. 77-87.

39. Nordman, D. and F. Mayinger, (1976). Experimental investigation of bubble growth and collapse during sub cooled boiling, *European Two-phase Group Meet.*

40. Paniagua, J. C., U. S. Rohatgi and V. Prasad, (1996a).Modeling of two phase flow instabilities during startup transients utilizing RAMONA-4B methodology. *International Mechanical Engineering Congress and Exposition, Atlanta, GA, Nov.17-22.*

41. Patankar, S. V. (1980). *Numerical Heat Transfer and Fluid Flow,* Hemisphere, New York.

42. Plesset, M. S., and S.A. Zwick, (1952). A non steady heat diffusion problem with spherical symmetry, *Journal of Applied Physics,* **Vol. 23.**

43. Rogers, J. T., M. Salcudean, Z. Abdullah, D. McLeod and D. Poirier, (1987). The on set of significant void in up-flow boiling of water at low pressure and velocities, *International Journal of Heat and Mass Transfer,* **Vol. 30,** pp. 2247-2260.

44. Saha, P. and N. Zuber, (1974). Point of net vapor generation and vapor void fraction in sub cooled boiling, *Proceedings 5th International Heat Transfer Conference,* Tokyo, Japan.

45. Stewart, H. B., (1979).Stability of two-phase flow calculation using two-fluid models, *Journal of Computational Physics,* **Vol. 33,** pp. 259-270.

46. Takemoto, T., M. Matsuzaki, M. Aritomi, K. Usui, M. Mori and Y. Yoshioka, (1999). The coalescence mechanism of multiple slug bubbles. *Journal of Nuclear Science and Technology,* **Vol. 36 [8],** pp.671-682.

47. Theofanous, T. G., T. Bohrer, M. Chen, and P.D. Patel, (1975).Universal solutions for bubble growth and influence of micro layers.*15th National Heat Transfer Conference,* San Francisco, CA.

48. Unal, H.C.,(1976).Maximum bubble diameter, maximum bubble growth time and bubble-growth rate during the sub cooled nucleate flow boiling of water up to 177 bar, *International Journal of Heat Mass Transfer*,**Vol. 19**,pp.643-649.

49. Wallis, G. B., (1969). *One dimensional two-phase flow,* McGraw-Hill, New York.

50. Zuber, N., S.A. Findlay (1965).Average volumetric concentration in two-phase flow systems, *Journal of Heat Transfer*, **Vol. 87a**, pp. 453.

Appendix

A.1 Void Fraction

The macroscopic densities for vapor and liquid are related to the microscopic quantities as,

$$\rho_g = \alpha\rho_g^0, \qquad \rho_l = (1-\alpha)\rho_l^0$$

$$\rho_m = \alpha\rho_g^0 + (1-\alpha)\rho_l^0$$

$$= \rho_g + \rho_l^0 - \alpha\rho_l^0$$

$$\alpha\rho_l^0 = \rho_g + \rho_l^0 - \rho_m$$

$$\alpha = \frac{\rho_l^0 - \rho_m + \rho_g}{\rho_l^0}$$

where ρ_g^0 = Microscopic vapor density or density of the pure vapor

ρ_l^0 = Microscopic liquid density or density of the pure liquid

A.2 Vapor Continuity Equation

The vapor mass balance equation is given by

$$\frac{\partial \rho_g}{\partial t} + \frac{1}{A}\frac{\partial}{\partial y} A\left(\rho_g V_m + \frac{\rho_g \rho_l}{\rho_m} V_r\right) = \Gamma_g \qquad \text{(A.1)}$$

Continuity equation is discretized at the cell centre j

Hence discretizing Equation (A.1) at j

$$\left(\frac{\partial \rho_g}{\partial t}\right)_j = \frac{(\rho_g)_j^{n+1} - (\rho_g)_j^n}{\Delta t} \tag{A.2a}$$

Also since $\rho_m V_m = \rho_g V_g + \rho_l V_l$ and $V_r = V_g - V_l$,

Now $\rho_g V_m + \frac{\rho_g \rho_l}{\rho_m} V_r$

$$= \rho_g \left(\frac{\rho_g V_g + \rho_l V_l}{\rho_m}\right) + \frac{\rho_g \rho_l}{\rho_m}(V_g - V_l)$$

$$= \frac{\rho_g{}^2 V_g}{\rho_m} + \frac{\rho_g \rho_l}{\rho_m} V_l + \frac{\rho_g \rho_l}{\rho_m} V_g - \frac{\rho_g \rho_l}{\rho_m} V_l$$

$$= \frac{\rho_g V_g (\rho_g + \rho_l)}{\rho_m} \tag{A.2b}$$

But $\rho_m = \alpha \rho_g^0 + (1-\alpha)\rho_l^0$ and $\rho_g = \alpha \rho_g^0$, $\rho_l = (1-\alpha)\rho_l^0$

That is, $\rho_m = \rho_g + \rho_l$

Hence $\rho_g V_m + \frac{\rho_g \rho_l}{\rho_m} V_r = \frac{\rho_g V_g \rho_m}{\rho_m} = \rho_g V_g$ (A.2c)

Now $\frac{1}{A}\frac{\partial}{\partial y} A\left(\rho_g V_m + \frac{\rho_g \rho_l}{\rho_m} V_r\right) = \frac{1}{A}\frac{\partial}{\partial y} A(\rho_g V_g)$ (A.2d)

Discretizing Equation (A.2d) at j

$$\left[\frac{1}{A}\frac{\partial}{\partial y} A(\rho_g V_g)\right]_j = \frac{1}{A_j}\frac{\partial}{\partial y}\left[A(\rho_g V_g)\right]_j$$

Applying central differencing scheme the RHS becomes

$$= \frac{1}{A_j} \frac{A_{j+\frac{1}{2}} (\rho_g V_g)_{j+\frac{1}{2}} - A_{j-\frac{1}{2}} (\rho_g V_g)_{j-\frac{1}{2}}}{\Delta y_j} \tag{A.3}$$

This is the form of equation reported in Equation (2.25).

A.3 Mixture Energy Equation

The Mixture energy balance equation is given as,

$$\frac{\partial \rho_m I_m}{\partial t}+\frac{1}{A}\frac{\partial}{\partial y}A\left[\rho_m I_m V_m+\frac{\rho_g\rho_l}{\rho_m}\left(I_g-I_l\right)V_r\right]=-\frac{p}{A}\frac{\partial}{\partial y}A\left[V_m+\frac{\rho_g\rho_l}{\rho_m}\left(\frac{1}{\rho_g{}^0}-\frac{1}{\rho_l{}^0}\right)V_r\right]$$

$$+KV_r{}^2+W_{vis}+Q \qquad \text{(A.4)}$$

The Mixture mass conservation equation is

$$\frac{\partial \rho_m}{\partial t}+\frac{1}{A}\frac{\partial\left(A\rho_m V_m\right)}{\partial y}=0 \qquad \text{(A.5)}$$

Multiplying Equation (A.5) by I_m gives

$$I_m\frac{\partial \rho_m}{\partial t}+\frac{I_m}{A}\frac{\partial\left(A\rho_m V_m\right)}{\partial y}=0 \qquad \text{(A.6)}$$

Subtracting Equation (A.6) from Equation (A.4) yields

$$\left\{I_m\frac{\partial \rho_m}{\partial t}+\rho_m\frac{\partial I_m}{\partial t}+\frac{I_m}{A}\frac{\partial\left(A\rho_m V_m\right)}{\partial y}+\frac{A\rho_m V_m}{A}\frac{\partial I_m}{\partial y}+\frac{1}{A}\frac{\partial}{\partial y}A\left[\frac{\rho_g\rho_l}{\rho_m}\left(I_g-I_l\right)V_r\right]\right\}$$

$$-\left\{I_m\frac{\partial \rho_m}{\partial t}+\frac{I_m}{A}\frac{\partial\left(A\rho_m V_m\right)}{\partial y}\right\}=-\frac{p}{A}\frac{\partial}{\partial y}A\left[V_m+\frac{\rho_g\rho_l}{\rho_m}\left(\frac{1}{\rho_g{}^0}-\frac{1}{\rho_l{}^0}\right)V_r\right]+KV_r{}^2+W_{vis}+Q \qquad \text{(A.7)}$$

$$\rho_m\frac{\partial I_m}{\partial t}+\rho_m V_m\frac{\partial I_m}{\partial y}+\frac{1}{A}\frac{\partial}{\partial y}A\left[\frac{\rho_g\rho_l}{\rho_m}\left(I_g-I_l\right)V_r\right]=-\frac{p}{A}\frac{\partial}{\partial y}A\left[V_m+\frac{\rho_g\rho_l}{\rho_m}\left(\frac{1}{\rho_g{}^0}-\frac{1}{\rho_l{}^0}\right)V_r\right]$$

$$+KV_r{}^2+W_{vis}+Q \qquad \text{(A.8)}$$

Dividing throughout by ρ_m in Equation (A.8) gives,

$$\frac{\partial I_m}{\partial t}+V_m\frac{\partial I_m}{\partial y}+\frac{1}{\rho_m A}\frac{\partial}{\partial y}A\left[\frac{\rho_g\rho_l}{\rho_m}(I_g-I_l)V_r\right]=-\frac{p}{\rho_m A}\frac{\partial}{\partial y}A\left[V_m+\frac{\rho_g\rho_l}{\rho_m}\left(\frac{1}{\rho_g{}^0}-\frac{1}{\rho_l{}^0}\right)V_r\right]$$

$$+\frac{1}{\rho_m}KV_r{}^2+\frac{1}{\rho_m}W_{vis}+\frac{1}{\rho_m}Q \qquad \text{(A.9)}$$

Mixture energy equation has to be discretized at the cell centre j.

Hence discretizing Equation (A.9) at j will give,

$$\left[\frac{\partial I_m}{\partial t}\right]_j=\frac{(I_m)_j^{n+1}-(I_m)_j^n}{\Delta t} \qquad \text{(A.10a)}$$

$$\left[V_m\frac{\partial I_m}{\partial y}\right]_j=(V_m)_j\left[\frac{\partial I_m}{\partial y}\right]_j=(V_m)_j\left[\frac{(I_m)_{j+\frac{1}{2}}-(I_m)_{j-\frac{1}{2}}}{\Delta y_j}\right] \qquad \text{(A.10b)}$$

$$\left[\frac{1}{\rho_m A}\frac{\partial}{\partial y}A\left\{\frac{\rho_g\rho_l}{\rho_m}(I_g-I_l)V_r\right\}\right]_j$$

$$=\frac{1}{(\rho_m)_j A_j}\frac{\left[A\left\{\frac{\rho_g\rho_l}{\rho_m}(I_g-I_l)V_r\right\}\right]_{j+1/2}-\left[A\left\{\frac{\rho_g\rho_l}{\rho_m}(I_g-I_l)V_r\right\}\right]_{j-1/2}}{\Delta y_j} \qquad \text{(A.10c)}$$

$$\left[\frac{p}{\rho_m A}\frac{\partial}{\partial y}A[V_m]\right]_j=\frac{p_j^{n+1}}{(\rho_m)_j A_j}\left[\frac{A_{j+\frac{1}{2}}(V_m)_{j+\frac{1}{2}}^{n+1}-A_{j-\frac{1}{2}}(V_m)_{j-\frac{1}{2}}^{n+1}}{\Delta y_j}\right] \qquad \text{(A.10d)}$$

$$\left[\frac{p}{\rho_m A}\frac{\partial}{\partial y}A\left[\frac{\rho_g\rho_l}{\rho_m}\left(\frac{1}{\rho_g{}^0}-\frac{1}{\rho_l{}^0}\right)V_r\right]\right]_j$$

$$=\frac{p_j^n}{(\rho_m)_j A_j\Delta y_j}\left\{\left[\frac{A\rho_g\rho_l}{\rho_m}\left(\frac{1}{\rho_g^0}-\frac{1}{\rho_l^0}\right)V_r\right]_{j+\frac{1}{2}}^n-\left[\frac{A\rho_g\rho_l}{\rho_m}\left(\frac{1}{\rho_g^0}-\frac{1}{\rho_l^0}\right)V_r\right]_{j-\frac{1}{2}}^n\right\} \qquad \text{(A.10e)}$$

$$\left[\frac{1}{\rho_m}KV_r{}^2+\frac{1}{\rho_m}W_{vis}+\frac{1}{\rho_m}Q\right]_j=\frac{1}{(\rho_m)_j}\left[KV_r{}^2\right]_j^n+\frac{1}{(\rho_m)_j}[W_{vis}]_j^n+\frac{1}{(\rho_m)_j}[Q]_j^n \qquad \text{(A.10f)}$$

The above Equations (A.9) to (A.10f) will give the updated value of mixture energy $(I_m)_j^{n+1}$ which can be used as a consistency check for the Equation (2.35).

A.4 Two Dimensional Equations for Junction Cell

$U = Velocity\ in the\ X-direction$

$V = Velocity\ in the\ Y-direction$

Total Mass Balance Equation

$$\frac{\partial \rho_m}{\partial t} + \frac{1}{A}\left[\frac{\partial (A\rho_m U_m)}{\partial x} + \frac{\partial (A\rho_m V_m)}{\partial y}\right] = 0 \qquad \text{(A.11)}$$

Vapor Mass Balance Equation

$$\frac{\partial \rho_g}{\partial t} + \frac{1}{A}\left[\frac{\partial}{\partial x}A\left(\rho_g U_m + \frac{\rho_g \rho_l}{\rho_m}U_r\right) + \frac{\partial}{\partial y}A\left(\rho_g V_m + \frac{\rho_g \rho_l}{\rho_m}V_r\right)\right] = \Gamma_g - \Gamma_c \qquad \text{(A.12)}$$

Mixture Momentum Equation in X-direction

$$\frac{\partial \rho_m U_m}{\partial t} + \frac{1}{A}\left[\frac{\partial}{\partial x}A\left(\rho_m {U_m}^2 + \frac{\rho_g \rho_l}{\rho_m}{U_r}^2\right) + \frac{\partial}{\partial y}A\left(\rho_m {U_m}^2 + \frac{\rho_g \rho_l}{\rho_m}{U_r}^2\right)\right]$$

$$= -\frac{\partial p}{\partial x} + \rho_m g_x + f_{vis} \qquad \text{(A.13)}$$

Mixture Momentum Equation in Y-direction

$$\frac{\partial \rho_m V_m}{\partial t} + \frac{1}{A}\left[\frac{\partial}{\partial x}A\left(\rho_m {V_m}^2 + \frac{\rho_g \rho_l}{\rho_m}{V_r}^2\right) + \frac{\partial}{\partial y}A\left(\rho_m {V_m}^2 + \frac{\rho_g \rho_l}{\rho_m}{V_r}^2\right)\right]$$

$$= -\frac{\partial p}{\partial x} + \rho_m g_x + f_{vis} \qquad \text{(A.14)}$$

Mixture Energy Balance Equation

$$\frac{\partial \rho_m I_m}{\partial t} + \frac{1}{A}\left[\frac{\partial}{\partial x}A\left\{\rho_m I_m U_m + \frac{\rho_g \rho_l}{\rho_m}(I_g - I_l)U_r\right\} + \frac{\partial}{\partial y}A\left\{\rho_m I_m V_m + \frac{\rho_g \rho_l}{\rho_m}(I_g - I_l)V_r\right\}\right]$$

$$= -\frac{p}{A}\left[\frac{\partial}{\partial x}A\left\{U_m + \frac{\rho_g \rho_l}{\rho_m}\left(\frac{1}{\rho_g{}^0} - \frac{1}{\rho_l{}^0}\right)U_r\right\} + \frac{\partial}{\partial y}A\left\{V_m + \frac{\rho_g \rho_l}{\rho_m}\left(\frac{1}{\rho_g{}^0} - \frac{1}{\rho_l{}^0}\right)V_r\right\}\right]$$

$$+ K\left[U_r{}^2 + V_r{}^2\right] + W_{vis} + Q \qquad \text{(A.15)}$$

A.5 Variables for Constructing the Junction and BC

KBOT (I): Number of junction connected to the bottom of pipe I. A zero value indicates an isolated end.

KTOP (I): Number of junction connected to the top of pipe I. A zero value indicates an isolated end.

LANG (I): Parameter that indicates the orientation of component I. Refer Figure 3.4 and Figure 3.5.

LBOT (I): Parameter that indicates the type of boundary conditions to be applied at the bottom of component I when it is an isolated end.

LTOP (I): Parameter that indicates the type of boundary conditions to be applied at the top of component I when it is an isolated end.

MBOT (I): Parameter that specifies the boundary data set for the bottom end of component I.

MTOP (I): Parameter that specifies the boundary data set for the top end of component I.

PROCEEDINGS OF

International Symposium on

Process Systems Engineering and Control

For Productivity Enhancement
through Design and Optimization

(ISPSEC'03)

January 3-4, 2003 Mumbai, India

ISA-The Instrumentation, Systems, and Automation Society

Organized by :
Indian Institute of Technology, Bombay
Co-sponsor :
Instrumentation, Systems
and Automation Society (ISA)

SIMULATION OF GEYSERING AT START-UP IN A NATURAL CIRCULATION LOOP

M. R. Gartia[a], A. K. Nayak[b], P. K. Vijayan[b], D. Saha[b], A. Khanna[a]

[a]*Indian Institute of Technology, Kanpur208016*
e mail: gartiamr@iitk.ac.in
akhanna@iitk.ac.in
[b]*Reactor Engineering Division, Bhabha Atomic Research Centre, Mumbai 400085*

Abstract: Geysering phenomenon is a type of unstable and periodic boiling occurring during start-up. Such phenomenon can induce instability in natural circulation system. It causes flow oscillations which can change the void fraction and reactivity. This makes the nuclear reactor difficult to control. Hence bench marking of the geysering is required. The present project involves development of a transient computer code based on second order finite difference technique considering a four equation drift flux model with appropriate model for subcooled boiling and condensation. The above phenomenon is considered in a two phase natural circulation boiling system and validated with the McMaster experimental data on axial void distribution.

Keywords: geysering, drift flux, subcooled boiling, condensation, natural circulation, bench marking, void distribution

1. INTRODUCTION

The current Light Water Reactors (LWR) achieves shut down through active safety systems. Passive safety systems have been proposed for advanced designs to enhance the reliability of safety functions. The advanced LWR would incorporate a number of passive safety features in its design. One of them is to adopt natural circulation core cooling during start-up, power raising, rated power conditions and accidental conditions. This concept is to eliminate the recirculation pumps which are normally present in conventional forced circulations BWRs. This is due to the reason that the forced circulation loop has the disadvantage of using a pump, which is costly. Again if by any reason the pump breaks down then the dissipation of fission heat is hampered. This results in tremendous accumulation of heat and may cause core melting in the reactor. Thereby it demands backup safety measures which will add to the cost of reactor.

However natural circulation systems require power to initiate the circulation through void generation. This mean the natural circulation reactor would be heated by fission energy from the startup under low temperature and low pressure condition. Thermal-hydraulic instabilities have been reported under low pressure conditions (Chiang *et al.*, 1994). If thermal hydraulic instabilities were to occur at startup then the reactor would not potentially continue operation during power up because the void fraction fluctuation in the reactor core would oscillate the reactivity. Therefore it is necessary to investigate and understand properly the thermal hydraulic instabilities during start up.

Aritomi *et al.* (1992, 1993) and Chiang *et al.* (1992, 1994) have conducted extensive research in the area of geysering under natural circulation. Masuhara *et al.* (1993) have also performed small scale experiment to demonstrate this phenomenon. These experiments illustrated that the geysering mode oscillation would occur at low pressures and low flow conditions. Aritomi *et al.*, (1992) had explained the driving mechanism of geysering as follows: When voids are generated in a heated channel, a large slug of bubbles forms, which grows due to decrease in hydrostatic pressure head as it moves towards the exit. The vapor then mixes with the liquid is the subcooled riser or upper Plenum and is condensed there. Due to bubble collapse and subsequent decrease in pressure, the subcooled liquid

enters the channels and restores the non-boiling nditions. This process repeats periodically causing w oscillations. Hence it is evident that the bubble mations, growth and collapse phenomenon are of portance to geysering instability.

lier attempts to model startup instabilities (Aritomi al., 1992)and (Paniagua *et al.*, 1996) indicate that, to dict the possible startup instabilities correctly, it is portant to accurately predicts the vapor generation e. In the present code the effect of the bubble mation as well as the condensation rate has been nsidered. Moreover, most of the models are visaged for system with high pressures (greater than bars) and thus are unsuitable for the simulation of rsering owing to the great influence of pressure on void content in the subcooled boiling regime. ally in the existing models there is no conclusive l physically well-defined description of the mass nsfer rate between the vapor and liquid phase, an ect which is of great significance for the lerstanding of phenomena in the subcooled boiling ime. In the present code a four equation drift flux del has been used which is numerically more stable n the five equation and six equation model.

2: FORMULATION AND SIMULATION SCHEME

e following code is based on the following thermal lraulic modeling features:

our fundamental balance equations – one liquid ss balance, one vapor mass balance equation, one ture momentum equation and one mixture energy nce equation.

econd order finite difference formulation.

rift flux model for phasic velocities

ppropriate vapor generation and vapor condensation odel.

h component has a one-dimensional representation a variable cross-sectional area. The equations are ed by a partially implicit method that can use erent time steps in different components. The ponents are discretized using staggered mess ngements. The momentum equation is advanced licitly that is, explicit updating of velocity has been e. The pressure has been updated implicitly. When transients are initiated, the system pressure changes assumed to be instantaneous and uniform ughout the individual computational cells. This s to a quasi-steady pressure distribution throughout system. The objective of our code is to determine void fraction in the subcooled regime with proper sideration of bubble formation rate and bubble lensation rate.

3. GOVERNING EQUATIONS

The basic one-dimensional, four equation drift flux model for two phase flows consists of the following conservation equations

Liquid mass balance:

$$\frac{\partial}{\partial t}\left((1-\alpha)\rho_l\right)+\frac{\partial}{\partial y}\left((1-\alpha)\rho_l V_l\right)=\Gamma_c-\frac{U_{he}}{A}\Gamma_g \tag{1}$$

Vapor mass balance:

$$\frac{\partial}{\partial t}\left(\alpha\rho_g\right)+\frac{\partial}{\partial y}\left(\alpha\rho_g V_g\right)=-\Gamma_c+\frac{U_{he}}{A}\Gamma_g \tag{2}$$

Mixture momentum balance:

$$\frac{\partial}{\partial t}\left(\rho_m V_m\right)+\frac{\partial}{\partial y}\left(\alpha\rho_g V_g^{\,2}+(1-\alpha)\rho_l V_l^{\,2}\right)=-\frac{\partial P}{\partial y}+\rho g_y+f_{vis} \tag{3}$$

Mixture energy balance:

$$\frac{\partial}{\partial t}\left(\rho_m I_m\right)+\frac{\partial}{\partial y}\left(\alpha\rho_g h_g V_g+(1-\alpha)\rho_l h_l V_l\right)=KV_r^{\,2}+W_{vis}+Q \tag{4}$$

Here f_{vis} is the distributed losses (pipe wall friction and local losses due to sudden change in area), U_{he} is the heated perimeter, I_m is the mixture specific internal energy:

$\rho_m I_m=\alpha\rho_g I_g+(1-\alpha)\rho_l I_l$; W_{vis} is the energy dissipation term, V_r is the relative velocity between phases: $V_r=V_g-V_l$ and Q is the heat source term in kW.

4. MODELLING OF VOID FORMATION IN THE SUBCOOLED BOILING REGIME

In the subcooled boiling regime, boiling occurs at the liquid cooled heating surfaces due to high heat flow densities, although the fluid has on average not yet reached the saturation temperature associated with the system pressure. In accordance with a suggestion by Griffith (Griffith *et al.*, 1958) four zones of heat transport and flow activity can be differentiated along a channel axis until saturation boiling has been reached. Zone I is referred to as single phase heat transfer zone, Zone II is onset of nucleate boiling (ONB) zone, Zone III is onset of significant Void (OSV) and Zone IV is the saturated core flow region. The equation of the following effect must be formulated in order to determine the void content in the subcooled boiling regime: (1) on set of nucleate boiling (ONB). (2) bubble formation and bubble growth (bubble generation rate) at the heating surface (3)onset of significant void (OSV) and bubble departure diameter (4)bubble condensation in the subcooled core flow.

4.1 *Onset of Nucleate boiling (ONB)*

It describes the point at which first boiling nuclei are activated at the boiling surface. A correlation by Bergels and Rohsenow (Bergels *et al.*, 1981) has been used to determine the wall superheating at which ONB will be activated.

$$\Delta T_{sat} = \frac{5}{9}\left(\frac{q''}{1100}P^{-1.156}\right)^{0.463P^{0.0234}} \qquad (5a)$$

$$T_w = T_{sat} + \frac{5}{9}\left(\frac{q''}{1100}P^{-1.156}\right)^{0.463P^{0.0234}} \qquad (5b)$$

The range of validity of the correlation is: channel diameter 2.4 and 4.6mm; flow velocity: 3-7ms^{-1}.Pressure: 1-36 bar.

4.2 *Onset of Significant Void (OSV)*

Assuming that the subcooled boiling occurs, the total heat Q supplied to the fluid from the heating surface per unit area can be arbitrarily partitioned into the following fractions:

$$Q = Q_{1\Phi} + Q_{GV}$$

Heat required to generate void is given by:

$$Q_{GV} = Q_{evap} + Q_{condensation}$$

$$q'' = q''_{1\Phi} + q''_{evap} + q''_{condensation} \qquad (6)$$

The heat flux associated with the single phase convection from the heating surface is given as:

$$q''_{1\Phi} = B_{1\Phi} h_{1\Phi}\left(T_w - T_l\right) \qquad (7)$$

Where T_w and T_l are the wall and liquid temperature respectively and $h_{1\Phi}$ is the heat transfer coefficient of the single phase liquid flow, which can be determined from the Dittus-Bolter correlation as:

$$h_{1\Phi} = 0.023\frac{k_l}{d_h}\mathrm{Re}^{0.8}\,\mathrm{Pr}^{0.4} \qquad (8)$$

The factor $B_{1\Phi}$ is dependent on the void and is intended to take into consideration the fact that with increasing with the wall superheating, the number of bubbles formed will increase. $B_{1\Phi}$ describes the heating surface fraction in direct contact with the subcooled liquid.

$$B_{1\Phi} = \frac{A_{eff}}{A_{he}} = \frac{A_{he} - A_b}{A_{he}} = 1 - \pi \sum_{i=1}^{n} R_{i,B}^2$$

$$= 1 - n\pi \bar{R}_B^2 \qquad (9)$$

Where A_b is the surface covered by bubbles, A_{he} is the heated surface n is the number of bubbles per unit area and $\pi \bar{R}_B^2$ is the projection area of a bubble on the heated surface, Although the bubbles have statistically different radii, the calculation has been carried out with average radius $\bar{R}_B$ for the sake of simplicity.

Hainoun(1994) has proposed $B_{1\Phi}$ as:

$$B_{1\Phi} \approx 1 - \frac{\pi}{16}\frac{\alpha}{\alpha_{osv}} \quad for\ \alpha \le \frac{16\alpha_{osv}}{\pi} \qquad (10)$$

$$B_{1\Phi} \approx 0 \quad for\ \alpha \ge \frac{16\alpha_{osv}}{\pi} \qquad (11)$$

where α_{osv} is the void fraction at the point when the bubbles become detached from the heating surface(OSV).Experimental data shows that α_{osv} may be about 5%-10%(Rogers *et al.*,1987)

Subcooling at OSV: The bubble will be detached from the wall only when the drag and buoyancy forces are greater than the holding force. The point at which the bubbles are first detached from the wall (this is OSV: Onset of Significant Void) is determined by the subcooling of the liquid at this location. The subcooling has been calculated using Saha and Zuber's model (Saha and Zuber, 1974) as follows:

$$\Delta T_{sub} = 0.0022 q'' \frac{d_h}{k_l} \qquad Pe \le 70000 \quad (12)$$

$$\Delta T_{sub} = 153.8 \frac{q''}{V_l \rho_l C_{p,l}} \qquad Pe \ge 70000 \quad (13)$$

where Peclet number can be found by the correlation $Pe=Re*Pr$.

Validity of the correlation:

P=0.1-13.8 MPa, m=95-2760 $kg.m^{-2}s^{-1}$,

q'' =0.28-1.9MWm^{-2}

Bubble Departure Radius: The radius at which the bubbles are detached from the wall after reaching their critical size and required subcooling is called the bubble departure radius. Bubble departure radius has been calculated using Unal's semi empirical model(Unal,1976)

$$R_{bd} = 1.21\times10^{-5} \frac{p^{0.709} S}{\sqrt{b\Phi}} \quad (14)$$

where

$$b = \frac{T_{sat} - T_l}{2}\left(1 - \frac{\rho_g}{\rho_l}\right)$$

$$\Phi = \left(\frac{V_l}{0.61}\right)^{0.47} \qquad for \quad V_l \not< 0.61 ms^{-1}$$

$$= 1 \qquad for \quad V_l < 0.61 ms^{-1}$$

$$S = \frac{T_w - T_{sat}}{2\rho_g h_{evap}}\left(\frac{k_w \rho_w C_{p,w}}{\pi}\right)^2$$

The range of validity of the correlation:

Pressure: 0.1-17.7 MPa

Heat flux: 0.47-10.64 MWm^{-2}

Velocity: 0.08-9.15 ms^{-1} and

Liquid sub-cooling: ΔT_{sub} =3-86 K

4.3 Bubble formation rate

The heat flux required for evaporation which is transferred from superheated boundary layer into the bubble can be calculated by:

$$q'' = nfV_{bd}\rho_g h_{evap} \quad (15)$$

f is the detachment frequency of the nucleation center at which bubbles are formed. n is the number of bubble nucleation center per unit area of heating surface. The heat flux required to reconstruct the superheated thermal boundary layer is given by:

$$q''_{GV} = nfQ_{recons} \quad (16)$$

Q_{recons} is the quantity of heat per nucleation centre withdrawn from the superheated wall to reconstruct the thermal boundary layer. To eliminate the unknown product *nf*, *a* parameter E is being defined as:

$$E = \frac{q''_{GV}}{q''_{evap}} = \frac{Q_{recons}}{V_{bd}\rho_g h_{evap}} = \frac{q'' - q''_{1\phi}}{q''_{evap}} \Rightarrow q''_{evap} = \frac{q'' - q''_{1\phi}}{E} \quad (17)$$

Also from Meister consideration for thermal boundary layer (Meister, 1979), the parameter E can be calculated as:

$$\frac{1}{E} = 2C_{evap}\left(\frac{T_w - T_{sat}}{T_w - T_l}\right)^2 \quad (18)$$

C_{evap} = evaporation parameter

≈ 0.5

Finally, evaporation heat flux is given by:

$$q''_{evap} = 2(q'' - q''_{1\Phi})C_{evap}\left(\frac{T_w - T_{sat}}{T_w - T_l}\right)^2 \quad (19)$$

Bubble formation rate:

$$\Gamma_g = \frac{q''_{evap}}{h_{evap}} \quad (20)$$

4.4 Bubble condensation rate

The condensation of bubble in a subcooled liquid is governed by two effects: (1) heat transfer at the phase interface; (2) inertia of the surrounding liquid. In the case of a large bubble formed with low subcooling and low flow rate, condensation proceeds very slowly. Hence the inertia of liquid surrounding the bubble can be neglected. In this case condensation is mainly governed by heat transfer at the phase interface. On the other hand, small bubbles, resulting in the case of considerable sub-cooling and high flow rate, condense very rapidly. Owing to the inertia of condensation, the surrounding fluid cannot flow fast enough to fill the space vacated by the condensed bubble. Hence it cannot compensate for the resulting underpressure. So, a large local pressure fluctuation may arise; this is termed as cavitation effect (Hamit, 1980). Mayinger and Nordman (1976) have showed that the pressure fluctuations in the vicinity of condensed bubbles increases greatly above Jacob number 100. This is an indication that condensation is predominantly controlled by inertia above Jacob number 100. Chen (1986) has demonstrated by measurements on bubble condensation with the aid of holographic interferometry that a thermal boundary layer exists in the vicinity of condensed bubble up to Jacob number of 60-80. Up to this boundary the pressure fluctuations at the end of condensation are slight which is an indication of heat transfer controlled condensation. Thus Jacob number can be used to differentiate different condensation regions. The Jacob number indicates the ratio between the energy that the liquid requires to reach the saturation state and the heat stored in the steam at the same volume.

$$Ja = \frac{\rho_l C_{p,l}(T_{sat} - T_l)}{\rho_g h_{evap}} \qquad (21)$$

(1) $Ja \leq 80$: condensation is largely determined by heat transfer at the phase boundary.
(2) $80 < Ja < 100$: transition region. Both the heat transfer and inertia effects are significant.
(3) $Ja \geq 100$: inertia effect is dominant.

Heat transfer controlled condensation
Heat transfer controlled condensation rate has been calculated using Hainoun *et al's* model (1996) as:

$$\Gamma_c = C_c 3.6 \frac{\alpha}{d_{bd}^2} \rho_g \upsilon_l Nu_1 Ja \quad for\ \mathrm{Re}_k < 10^4 \qquad (22)$$

$$\Gamma_c = C_c 3.6 \frac{\alpha}{d_{bd} d_h} \rho_g \upsilon_l Nu_2 Ja \quad for\ \mathrm{Re}_k > 3\times10^4 \qquad (23)$$

For $10^4 < \mathrm{Re}_k < 3\times10^4$, Γ_c is interpolated between the two regions.
where C_c is the condensation parameter and equal to 0.16. Nu_1 has been given by Hewitt *et al* (1990) as :

$$Nu_1 = 0.185\,\mathrm{Re}_B^{0.7}\,\mathrm{Pr}^{0.5} \qquad (24)$$

Re_B is the Bubble Reynold's number given by:

$$\mathrm{Re}_B = \frac{V_r d_{bd}}{\upsilon_l} \qquad (25)$$

$$Nu_2 = 0.228\,\mathrm{Re}_c^{0.7}\,\mathrm{Pr}^{0.5}\,Av^{0.25} \qquad (26)$$

Here Re_c is the channel Reynold's number. Av has been introduced by Avdeev (1986) which can be found from the correlation:

$$Av = 1 \quad \text{for } \alpha \leq 5\%$$
$$Av = (1-\alpha)^{-2.53} \quad \text{for } \alpha > 5\% \qquad (27)$$

Inertia controlled condensation
Inertia controlled condensation has been estimated by Hamit's correlation (1980) as follows:

$$\Gamma_c = C_c \rho_g \frac{\alpha}{\tau_c} \qquad (28)$$

τ_c is the condensation time (Hamit, 1980) which is given by:

$$\tau_c = 0.458 d_{bd} \left(\frac{\rho_l}{P_l}\right)^{\frac{1}{2}} \qquad (29)$$

Now the expressions for the evaporation rate Γ_g in $kgm^{-2}s^{-1}$ [equation (20)] and condensation rates Γ_c in $kgm^{-3}s^{-1}$ [equations (22), (23) and (28)] have been calculated. Finally Γ_g and Γ_c are put in the vapor mass balance equation [equation (2)] to find out the void fraction. The simulation has been

verified by comparing it with the McMaster
rimental data on axial void distribution.

5. RESULTS

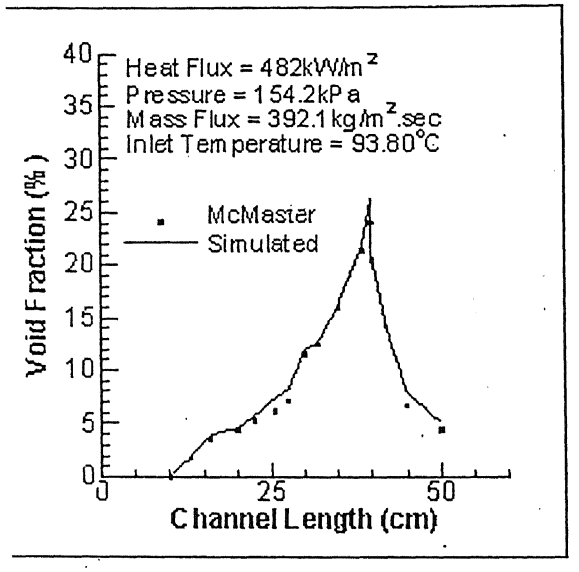

l Comparison of simulated results with McMaster test data for axial void distribution in sub-cooled boiling regime

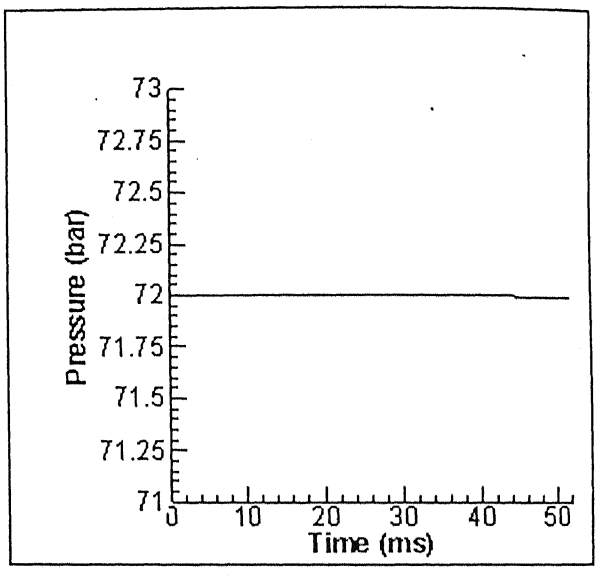

Fig. 3 Channel Pressure Variation with respect to time with initial pressure of 72 bar

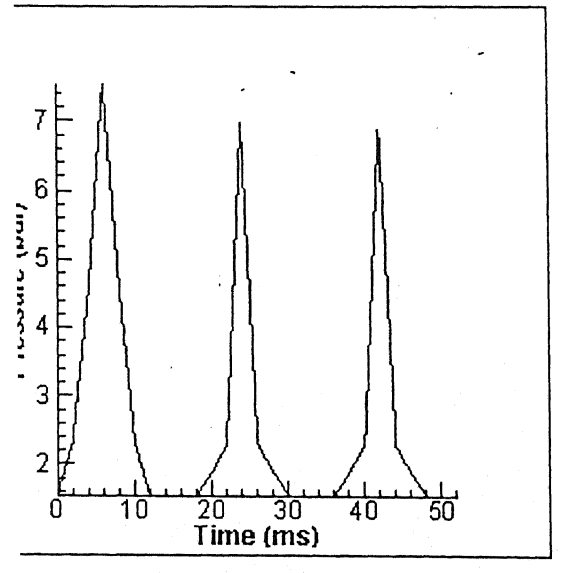

2 Channel Pressure Variation with respect to time with initial pressure of 1.542 bar

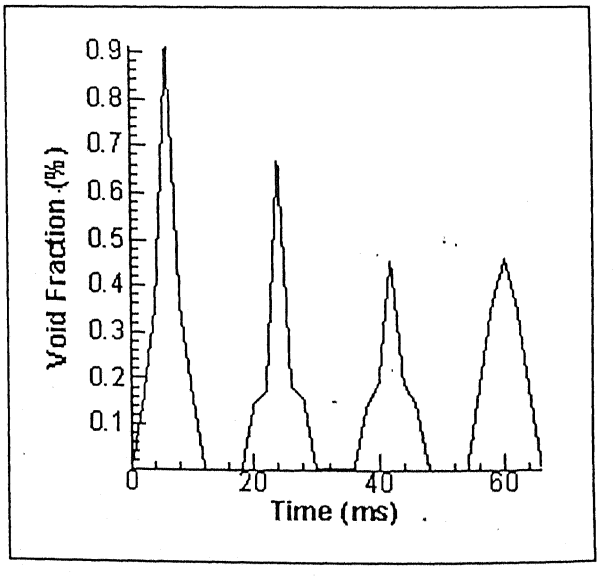

Fig. 4 Channel Average Void Distribution with respect to time with initial pressure of 1.542 bar

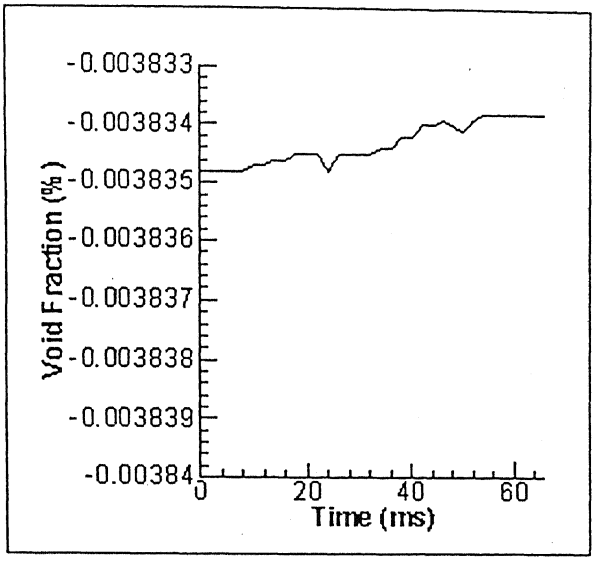

Fig. 5 Channel Average Void Distribution with respect to time with initial pressure of 72 bar

6. CONCLUSION

A computer code has been developed for the calculation of axial void fraction in the subcooled boiling regime using a four equation drift flux model with proper consideration of bubble formation and bubble condensation rates. The results obtained are in agreement with the McMaster experimental data on axial void distribution, as shown in figure 1. In figure 2, the variation of channel pressure with respect to time, with initial pressure 1.542 bar, is shown. The figure shows that at a low initial pressure during startup, boiling instabilities are prominent, which is a clear indication of geysering. The geysering period can also be determined from this figure, which is found to be about 20 ms for the case studied. Figure 3 shows that at a high initial pressure during startup, boiling instabilities are absent. The void fraction variation shown in figures 4 and 5 also confirm the above conclusion.

REFERENCES

Bergels,A.E., J.G. Collier, J.M. Delhaye, G.F. Hewitt and F. Mayinger,(1981) *Two-Phase Flow and Heat Transfer in the Power and Process Industries,* Hemisphere, Washington D.C.

Unal, H.C., (1976). Maximum bubble diameter, maximum bubble growth time and bubble-growth rate during the sub cooled nucleate flow boiling of water up to 177 bar, *International J Heat and Mass Transfer*, 19, pp.643-649

Bankoff, S. G., and R. D. Mikesel, (1958). Bubble growth rates in highly sub cooled nucleate boiling, *Chemical Engineering.* , 29, pp.55-61

Moalem-Maron, D. , and W.Zijl, (1978).Growth, condensation and departure of small and large vapour bubbles in pure and binary systems, *Chem. Eng. Sci.*, 33, pp.1339-1346

Plesset , M. S.,and S.A. Zwick, (1952). A non steady heat diffusion problem with spherical symmetry, *J.Appl. Phys.*, 23

Hamit, F. G.,(1980). *Cavitation and Multiphase Flow Phenomena,* McGraw-Hill, New York

Hainoun ,A. , E. Hicken , J. Wolters ,(1996). Modelling of void formation in the sub cooled boiling regime in the ATHLET code to simulate flow instability for research reactors, *Nuclear Engg. And Design*, 167, pp.175-191

Donevskin, B., and M. Shoukri, (1989). Experimental study of subcooled flow boiling and condensation in annular channels, *McMaster University Rep. ME/89/TFRI*

Chatoorgoon, V. ,G.R. Dimmick, M.B. Carver, W.N. Selander and M. Shoukri, (1992). Application of generation and condensation models to predict subcooled boiling void at low pressure, *Nucl. Tecnology* , 98 , pp.366-378

Aritomi,M.,T. Nakahashi,J.H. Chiang,M. Wataru and M.Mori,(1992).Fundamental study on themo-hydraulics during startup in natural circulation boiling water reactors(I).*Journal of Nuclear Science and Technology,* 29[7], pp.631-641

Chiang,J.H.,M.Aritomi,R.Inoue and M.Mori,(1992). Thermohydraulics during startup in natural circulation boiling water reactors,*NURETH-5,September*

Masuhara,Y.,O.Yokomizo,Y.Bessho and T.Fukahori,(1993). Research on Geysering phenomena in natural circulation BWR.*Proceedings of the 2nd ASME and JSME nuclear engineering joint conference.* 1, *March*

Chiang, J.H.,M. Aritomi, M. Mori, and M. Higuchi, (1994).Fundamental study on thermohydraulics during startup in natural circulation BWRs (III). *Journal of Nuclear Science and Technology,* 31[9], pp.883-893

Paniagua, J. C., U. S. Rohatgi and V. Prasad , (1996a). Modelling of two phase flow instabilities during startup transients utilizing RAMONA-4B methodology. *International Mechanical Engineering Congress and Exposition, Atlanta, GA, Nov.17-22*

Griffith,P., J.A. Clark , and W. M. Rohsenow. (1958). Void volumes in subcooled boiling systems. *ASME Journal of Heat Transfer,* 19